A Soft touch: wearable dielectric elastomer actuated multi-finger soft tactile displays

Hugh R. Boys

PhD Dissertation

Submitted in partial fulfilment of the requirements of the Degree of Doctor of Philosophy

School of Electronic Engineering and Computer Science

&

School of Engineering and Material Science

EPSRC funded.

Queen Mary University of London

2018

1st Supervisor: Dr Stefan Poslad, EECS

2nd Supervisor: Prof James Busfield

External Supporting Supervisor: Prof Federico Carpi

Abstract

The haptic modality in human-computer interfaces is significantly underutilised when compared to that of vision and sound. A potential reason for this is the difficulty in turning computer-generated signals into realistic sensations of touch. Moreover, wearable solutions that can be mounted onto multiple fingertips whilst still allowing for the free dexterous movements of the user's hand, brings an even higher level of complexity. In order to be wearable, such devices should not only be compact, lightweight and energy efficient; but also, be able to render compelling tactile sensations. Current solutions are unable to meet these criteria, typically due to the actuation mechanisms employed.

Aimed at addressing these needs, this work presents research into non-vibratory multi-finger wearable tactile displays, through the use of an improved configuration of a dielectric elastomer actuator. The described displays render forces through a soft bubble-like interface worn on the fingertip. Due to the improved design, forces of up to 1N can be generated in a form factor of 20 x 12 x 23 mm, with a weight of only 6g, demonstrating a significant performance increase in force output and wearability over existing tactile rendering systems.

Furthermore, it is shown how these compact wearable devices can be used in conjunction with low-cost commercial optical hand tracking sensors, to cater for simple although accurate tactile interactions within virtual environments, using affordable instrumentation.

The whole system makes it possible for users to interact with virtually generated soft body objects with programmable tactile properties. Through a 15-participant study, the system has been validated for three distinct types of touch interaction, including palpation and pinching of virtual deformable objects. Through this investigation, it is believed that this approach could have a significant impact within virtual and augmented reality interaction for purposes of medical simulation, professional training and improved tactile feedback in telerobotic control systems.

Funding acknowledgment

This work is supported by the Media and Arts Technology programme, funded by an Engineering and Physical Sciences Research Council (EPSRC) Doctoral Training Centre EP/G03723X/1 within Queen Mary University of London.

Acknowledgements

The last four years have been a perfect mix of intrigue, fun and difficulty. I've got to work on some truly fascinating and novel things, travel the world and spend my days with bright and talented people. For this opportunity, I am sincerely grateful.

Firstly, I would like to express my gratitude to Pippa Walker, William Brown and Prof Nobuoki Ohtani, without whom I would have never been inspired to pursue design. Secondly, thank you to my very special mix of supervisors. Prof Federico Carpi, Dr Stefan Poslad and Prof James Busfield. Their extensive knowledge, guidance and support over the years have kept me going. Ultimately, the interdisciplinary nature of this work would not have been possible without them. I really do not know how to thank them enough.

On top of this, a huge amount of gratitude goes to Dr Gabriele Fediani, a super interesting guy who is always working diligently on something new and exciting. He introduced me to the dielectric elastomer actuator concept with his early demonstrations of a tactile display using this principle. As soon as I saw it, I knew that it was something I had to work with. Without his initial research and collaborations thereafter, there is no way I could have done this work.

Also, thank you to my lab buddy Michele Ghilardi. He has made the last few years ridiculously fun and I count myself very lucky to have him as a friend. On top of this, he has provided me with great insights and workarounds on the numerous problems that I have faced over the years. Saluti!

Lastly, thanks to all of my friends and family; especially my parents and grandparents who have been supportive throughout it all. I promise that I will get a real job someday. Also, much love to Matt and Gerry, truly great friends that have made living in London tremendously fun.

Thanks again!

Statement of originality

I, Hugh Boys, confirm that the research included within this thesis is my own work or that where it has been carried out in collaboration with, or supported by others, that this is duly acknowledged below and my contribution indicated. Previously published material is also acknowledged below.

I attest that I have exercised reasonable care to ensure that the work is original, and does not to the best of my knowledge break any UK law, infringe any third party's copyright or other Intellectual Property Right, or contain any confidential material.

I accept that the College has the right to use plagiarism detection software to check the electronic version of the thesis.

I confirm that this thesis has not been previously submitted for the award of a degree by this or any other university.

Signature:

Date:

Details of collaboration and publications:

Conference paper: "Enabling wearable soft tactile displays with electroactive smart elastomers" By Gabriele Frediani, Hugh Boys, Stefan Poslad, Federico Carpi.

Haptics: Perception, Devices, Control, and Applications. Volume 9775 of the series Lecture Notes in Computer Science pp 326-334. (included in appendix).

Conference paper: "A dielectric actuator-based tactile display for multiple fingertip interaction with virtual bodies." By Hugh Boys, Gabriele Frediani, Stefan Poslad, James Busfield, Federico Carpi.

SPIE Smart Structures and Materials + Non-destructive Evaluation and Health Monitoring. Proceedings of the SPIE, Volume 10163, pp 12-24.

Conference paper: “Soft wearable non-vibratory tactile displays”. By Hugh Boys, Gabriele Frediani, Stefan Poslad, James Busfield, Federico Carpi.

Published, RoboSoft 2018.

Table of figures

List of tables

List of symbols and abbreviations

% : Percent

~ : Approximately

ΔI : Change in stimulus intensity

2D : Two Dimensional

3D : Three dimensional

A : Amps

AR : Augmented reality

C : Capacitance

CSV : Comma-separated values

dA : Change in area

DC : Direct current

DE : Dielectric elastomer

DEAs : Dielectric elastomer actuators

DOF : Degrees of freedom

dQ : Change in charge

dU : Change in electrostatic energy

dW : Mechanical work

E : Electric field

EAP : Electroactive polymer

g : Grams

HC-DEA : Hydrostatically coupled - dielectric elastomer actuator

Hz : Hertz

I : Baseline stimulus

JND : Just noticeable difference

K : Webbers constant

kHz : Kilohertz

kV : Kilovolt

LED : Light emitting diode

mA : Milliamp

MJ/m³ : Megajoules per meter cubed

ml : milliliter

mm : Millimeter

ms : Millisecond

MR : Mixed reality

MΩ : Megaohm

N: Newtons

p : Electrostatic pressure

PWM : Pulse width modulation

Q : Charge

R : Resistance

SDK : Software development kit

SMA : Shape memory alloys

SWCNT : Single-walled carbon nanotubes

U : Electrostatic energy

USB : Universal serial bus

V : Volts

Vcap : Volume of spherical cap

Vgel : Volume of gel

VHB

Vin : Voltage before low-pass filter

vol : Volume

Vout : Voltage after low-pass filter

VR : Virtual reality

W : Watt

z : dielectric elastomer membrane thickness

δQ : Change in heat energy of system

ϵ_0 : Dielectric permittivity of a vacuum

ϵ_r : Relative dielectric constant

μF : Microfarad

μm : Micrometer

$\Phi(\lambda)$: Voltage-stretch curve

$\Phi B(\lambda)$: Breakdown voltage-stretch curve

Ω : Ohm

1 Introduction

1.1 Motivation

Virtual, augmented and mixed reality is starting to gain significant traction in the consumer market. This is primarily due to the prevalence of low-cost headsets that can deliver responsive high-resolution graphics and audio at the high framerates and low latencies required. Moreover, these devices are becoming increasing less tethered, and no longer require the user to be connected to external static computing systems. Through these means, virtual environment interaction is becoming an increasingly more wearable and untethered experience. But although there has been significant progress in wearable technologies capable of rendering virtual environments visually and aurally; the same cannot be said for the haptic modality. One reason for this is the difficulty in rendering realistic touch sensations in a wearable solution.

Rendering touch sensations to the user's hand have been demonstrated to increase presence and immersion in virtual environments and teleoperation scenarios (Kim et al., 2017; Ramsamy et al., 2006). Furthermore, touch is thought to increase performance and dexterity within these contexts (Kong et al., 2016; Sarakoglou et al., 2012). In particular, rendering mechanical pressure sensations to individual fingertips relating to the compliance of virtual tissues has a number of applications in medical training and telerobotic operating systems (Coles et al., 2011; Culjat et al., 2008); but is yet to be achieved in a truly wearable untethered system.

The wearability of such systems is typically limited due to the size, weight and power requirements of the actuation technologies employed. To the best of our knowledge, there is not a wearable system that can render interactions with soft compliant objects to multiple fingertips simultaneously in a wearable and portable device. In this work, such a system will be explored.

1.2 Haptic rendering overview

To date, there has been a number of approaches in generating haptic stimuli to the user's hand. The most prevalent is grounded or exoskeletal kinaesthetic solutions. Kinaesthetic haptic devices aim to replicate the experience of force/ torque applied to the body. To do this, these devices use a series of actuated mechanical linkages, either grounded to a desktop ("Force Dimension," 2018, "Geomagic Touch," 2017; Massie and Salisbury, 1994) or through an exoskeletal frame ("CyberGrasp," 2017, "Dexta Robotics," 2017). Typically, this genre of haptic device tends to restrict the working area of the user; or limit the free dextrous movements of the user's hand. Additionally, due to weight, size and power requirements, they cannot be considered for use in wearable untethered portable systems (Pacchierotti et al., 2017).

An approach that lends itself to wearable systems is the rendering of cutaneous/ tactile information through actuators placed on the fingertips. Cutaneous or tactile sensations concern stimuli perceived at the level of the skin, such as mechanical force and temperature (Erp and Dobbelsteen, 1998). Although there have been tactile devices that used heat (Jia et al., 2015) and also electrical stimulus (Kaczmarek et al., 1991), tactile devices are typically concerned with providing mechanical pressure and vibrational stimuli (Erp and Dobbelsteen, 1998). Mechanical cutaneous forces applied to fingertips can enable users to deduce contact pressure and compliance of virtual objects. Furthermore, mechanical forces delivered through soft compliant interfaces have been shown to be useful in medical training simulations (Coles et al., 2011; Li et al., 2013) and teleoperation scenarios (Culjat et al., 2008); as they are capable of mimicking the interaction with soft organic tissues.

So far there have been a number of approaches that have experimented with different types of actuation technologies placed on the fingertips. To date, all these approaches appear to have limitations. These limitations either manifest themselves in their ability to be incorporated into wearable multi-finger systems, or in being able to render compelling tactile interactions.

A common approach is the placement of vibrating motors on individual fingertips. Vibrotactile devices, as they a commonly referred to, are typically limited in their tactile expression to vibrational stimuli only. This limits their ability to render naturalistic touch interactions. Other techniques that have aimed to address this issue

have used complex arrays of servo motors or DC (Direct Current) motors located on the fingertips. But these approaches tend to be large, burdensome and noisy; making them unsuitable to be placed on multiple fingers for extended periods of time. Pneumatic actuated systems offer several advantages, primarily in their ability to generate high forces through soft compliant interfaces; but a system architecture of pumps valves and regulators limit their use in portable untethered systems.

Smart materials where the mechanical properties can be electronically modulated offer exciting new avenues for wearable tactile devices. Shape Memory Alloys, for example, have been shown in relatively compact and light in weight multi-finger wearable solutions. But due to slow actuation response speeds, they are not able to recreate compelling tactile interactions with virtual models (Gabardi et al., 2016). Dielectric Elastomer Actuators (DEAs) on the other hand appears to be the most promising actuation technology for wearable tactile devices. The advantages of DEAs over other actuation methods include peak force generation, weight, compact design, low power consumption, ease of manufacture and organic actuation similar to that of natural muscle (Carpi et al., 2008). The primary issue afflicting this technology is the typically high driving voltages required, making isolation and the controlling circuitry more complex and expensive. Although there have been a number of tactile devices that have used DEAs as their actuation technology; to best of our knowledge there is yet to be developed a device for multi-finger tactile interaction, nor has there been a device incorporated into a virtual environment for the purpose of facilitating interaction with virtual soft objects. A system capable of achieving this feat could have significant advantages.

1.3 General challenges in rendering multi-finger tactile interactions with virtual compliant objects

Rendering realistic touch sensations to individual fingertips as a response to virtual compliant object interaction requires the following general steps: track the 3D positions of the user's fingertips; determine where the user's fingertips are in relation to a virtual model; if a collision between the user's fingertips and the virtual model occurs, compute relevant haptic response. Update the tactile device to apply relevant tactile response. Update virtual model. To achieve this there are a number of challenges. These can be split into four distinct categories: the wearable fingertip mounted display itself, the hand tracking system, the electronic controlling system and the virtual environment.

The primary focus of this work is to create a wearable fingertip mounted tactile display that uses dielectric elastomer actuation. To this means, an actuator capable of generating significantly perceivable force sensations has to be developed and made compact enough as to be placed on multiple fingertips simultaneously. The device should ideally fit within the width of the user's fingertip, as to allow for the natural movement of the user's fingers.

To track where the fingertips are in 3D space; the wearable system should be able to integrate with existing hand tracking systems. To these means, a device placed on the fingertips should not impede recognition and tracking of the fingertips.

Typically, the power supply and controlling circuitry are too large to be placed upon the fingertip; and therefore, has to be placed on another location on the body. Connecting wires should not impede finger dexterity; and the driving electronics should be wearable and therefore have minimal power consumption, be light in weight and as compact as possible. As stated previously, Dielectric Elastomer Actuators typically require high driving voltages within kilo Volt range. Therefore, extra consideration has to be taken in isolating the user from the potentially hazardous voltages.

A virtual environment has to be constructed. This is a programme that takes the user's fingertip positions as inputs and then computes the corresponding haptic response. Graphical outputs are also typically required, as to help the user locate where their

hand is in relation to the virtual object. The virtual model then has to updated based upon this interaction. This should all occur at a frame rate that is as high as possible, as to reduce the delay between actions of the user and the response of the system.

The last challenge concerns validating the system. Firstly, the mechanical performance of the actuator proposed should be validated against existing actuation methods used for tactile stimulation; and secondly, the psychophysical performance in terms of users being able to use the device to perceive between different tactile sensations generated by the device needs to be assessed.

1.4 Thesis specific challenges

The challenges tackled in this thesis are interdisciplinary by nature, as this research stems across material science, computer science, electronic engineering and system design. Here the research investigations are outlined and referenced to the corresponding chapter:

- Research and development for compact higher force generating DEA soft actuators. (chapter 4)
- Investigation of wearable multi-finger device that incorporates the higher force generating soft actuator and that can also be used in conjunction with a low cost optical tracking system. (chapter 4)
- Investigation, development and testing of a multi-channel DEA soft actuator control unit for the purpose of electronically controlling individually addressable DEA driven tactile displays located on different fingers. (chapter 5)
- Access the electromechanical performance tactile display system in terms of force output, actuation stroke and frequency response. (chapter 6)
- Develop a user testing environment for the psychophysical evaluation of the tactile display system proposed, for single finger and multi-finger virtual soft object interaction. (chapter 7)

1.5 Research Objectives

The primary objective of this work is to develop and access a wearable multi-fingertip tactile display for the purpose rendering interactions with soft compliant virtual objects. Currently, there is not a device that can be worn on multiple fingertips that can also render variable electronically controlled forces through a soft tactile actuation technology.

1.6 Novel contributions

Improved design configuration to enable compact high force generating Hydrostatically Coupled- Dielectric Elastomer Actuators (HC-DEA)

Dielectric Elastomer Actuator's (DEAs) have been highlighted as a promising technology for soft, lightweight and compact actuators (Carpi et al., 2008). Hydrostatically Coupled – DEAs offer a safe configuration in order to apply soft tactile stimuli to the user's fingertip (Carpi et al., 2010a) and have been shown in a single finger tactile device (Frediani et al., 2014b). But due to the size of previous devices, it has not been able to be incorporated into a multi-finger approach. This work reduces the size of the HC-DEA enabling wearability on multiple fingertips, whilst developing a construction technique to increase the overall force output at a reduced driving voltage. The described displays have a soft bubble-like interface with the fingertip that can render electrically tuneable displacements of up to 3.5 mm and forces of up to 1N. The displays have a volume of 20 x 12 x 23 mm and a weight of 6g. Due to the shape and material selection of the wearable device, the tactile display can also be used in conjunction with a low-cost optical hand tracking system ("Leap Motion," 2017).

Design and evaluation of a multi-channel control unit for portable DEA systems

A multi-channel DEA (Dielectric Elastomer Actuator) driving system has also been investigated, as to enable individual control of up to four DEA devices simultaneously. The system proposed makes use of an Arduino microcontroller with a custom developed high voltage shield, capable of generating DC (Direct Current) control singles ranging from 0.7 to 5kv. The system has been used to drive four fingertip-mounted soft displays simultaneously but has also found applications in a

novel laser positioning system, a multi-chamber bioreactor and a multi-segment tuneable lens system.

Psychophysical assessment of a wearable multi-finger soft tactile display for four different types of touch interaction within a VR environment

To access how the multi-fingertip system can be used to render interactions with virtual compliant objects of programmable soft tactile properties; A custom developed virtual environment, which allows users to access the tactile properties of virtual compliant objects in four different modes of touch interaction is created. This environment is used to present users with soft compliant objects that have programmable tactile properties relating to pressure sensations rendered through a fingertip-mounted device. In effect, users can differentiate between compliant objects using the system proposed in four different types of touch interaction. These touch interactions relate to a single finger touch, multi-finger touch, a pinching gesture between the thumb and the index finger on a compliant virtual ball object, and a vertical multi-finger palpation gesture on a deforming virtual box. Through user tests aimed at determining a common psychophysical performance metric known as the Webbers ratio; the psychophysical performance of the device is accessed for the four different modes of touch interaction.

1.7 Outcomes

Conference paper: “Enabling wearable soft tactile displays with electroactive smart elastomers” By Gabriele Frediani, Hugh Boys, Stefan Poslad, Federico Carpi.

Haptics: Perception, Devices, Control, and Applications. Volume 9775 of the series Lecture Notes in Computer Science pp 326-334. (included in appendix).

Conference paper: “A dielectric actuator-based tactile display for multiple fingertip interaction with virtual bodies.” By Hugh Boys, Gabriele Frediani, Stefan Poslad, James Busfield, Federico Carpi.

SPIE Smart Structures and Materials + Nondestructive Evaluation and Health Monitoring. Proceedings of the SPIE, Volume 10163, pp 12-24.

Conference paper: “Soft wearable non-vibratory tactile displays”. By Hugh Boys, Gabriele Frediani, Stefan Poslad, James Busfield, Federico Carpi.

IEEE International Conference on Soft Robotics (RoboSoft), 2018, pp 270-275

1.8 Outline of report

The rest of this report is structured as follows; firstly, a background is presented composed into three sections: an introduction to the physiology of the haptic sensory system, an introduction to haptic rendering devices and evaluation methods. The last part consists of an introduction into dielectric elastomer actuation (DEA). (Chapter 2)

A literature review concerning the different approaches in tactile rendering is conducted. From this DEAs are identified as a promising actuation technology for multi fingertip mounted soft tactile rendering displays. (Chapter 3)

In chapter four, a design is developed based upon an existing approach in DEA tactile rendering technologies. But as identified in the initial part of the chapter, there are several areas of improvement required to make the device suitable for a more compact higher force generating multi-finger approach. The last part of this chapter introduces a new configuration for the construction of soft DEA actuators to address these issues.

Mechanical testing of the new actuator design is conducted in chapter five. In this chapter, various parameters of the actuators design and construction are experimentally tested to access how this influences the uniaxial force output, displacement and frequency response. The parameters tested in this chapter concern, initial stretching of the dielectric material, the lateral size of the actuating device and the number of layers of dielectric material used. A design to be used in the experimental psychophysical performance tests is then presented.

The sixth chapter concerns an investigation into the psychophysical performance of the device. For this, user tests are constructed and performed that evaluate the perceptual performance of the tactile display proposed within four different modes of tactile interaction. These four modes relate to a single finger and multi-finger static object interaction, index finger and thumb pinch of a soft virtual ball of programmable soft properties, and lastly, multi-finger vertical palpation of soft tissue.

Conclusions made from this work are presented in chapter 7.

2 Fundamental concepts of haptic sensory system and dielectric elastomer actuators

In this chapter, the fundamental concepts on which this work relies upon are discussed. Rather than including this within the literature review chapter, it is thought that this chapter will serve those who are not familiar with in the field of haptics, as well as those not familiar in dielectric elastomer actuation.

The first part (2.1) will focus on the haptic sensory system, in which the physiology behind the sense of touch is discussed. This should give the reader a basic knowledge of the biological mechanisms related to haptic perception. Within this section, A widely-used metric for psychophysical evaluation of haptic devices will also be introduced. This will enable the reader to see how such systems can be compared and assessed through user testing.

In the latter part of this chapter (2.2), Dielectric Elastomer Actuator's (DEAs) will be introduced. This section will start with the underlying concepts behind the technology but will then shift into the more complex topics. It is important the reader has a knowledge of these concepts, as it informs many of the design choices made within this work.

2.1 Physiology of haptic sensory system and psychophysical evaluation

This subchapter covers the basic physiology of the haptic sensory system. The goal of this thesis is to create a device capable of rendering cutaneous soft touch sensations to multiple fingertips for the purpose of enabling users to distinguish between different virtual objects of varying soft tactile properties. To these means, the basic physiological mechanisms behind these sensory systems are described.

2.1.1 Haptic Sensory System

The haptic sensory of the hand enables fine dextrous control of objects in active manipulation tasks, hence why it has been a core focus in telerobotic and VR interaction scenarios (Hurmuzlu et al., 1998; Kim et al., 2017). In literature concerning haptic devices, it common for haptic experiences and thus haptic rendering devices to be grouped into two modalities; these are kinaesthetic haptic interactions and cutaneous haptic interactions, also referred to as tactile interactions.

2.1.2 Kinaesthetic haptic system physiology

Kinaesthetic haptic interactions concern the sensations experienced due to force/ torque acting upon the human body. It is experienced not only by receptors within the skin, but also by receptors within muscles, tendons and joints (Jones and Lederman, 2006). The other haptic modality, cutaneous haptic interactions, are haptic experiences triggered by receptors within the skin. This cutaneous haptic modality is attributed to a wider range of haptic perceptions, and these are typically broken down into three groups: cutaneous pain perception, temperature perception and mechanical tactile perception (van Jan, 2006). The kinaesthetic haptic perceptual system is comprised of four types of receptors, commonly referred to as mechanoreceptors (Jones, 2000):

Golgi Endings: These are located in the joint ligaments, the fibrous connective tissues that surround joints. They help us identify joint movement, especially in cases of extreme flexion and extension.

Ruffini Endings: These are located in joint capsules, which make up the synovial lining surrounding a joint. Similar to Golgi endings, Ruffini endings detect joint movement particularly in cases of end of range motion and extreme flexion and extension.

Golgi Tendon Organs: These are found in tendons and give active position sensations of limbs in comparison to each other. Tendons typically act as the mechanical link between muscle and bones.

Muscle Spindles: These are found in muscles and help us perceive muscle movement. This is one of the predominant receptors that help create our awareness of body movement and position. These receptors also play a key role in informing our perceptual system of the force exerted on a limb.

The feedback loop frequencies for kinaesthetic receptors typically range between 0.5 and 1.7 Hz. Although this might appear to be slow, the human body can produce precise and accurate motions that exceed these frequencies. It has been proposed that motor and cognitive haptic systems which initiate and direct active movement create a memory motor trace of the predicted movement, which acts as a comparison trace for receptor feedback when such a trace is not available at higher motor actuation frequencies (Hale and Stanney, 2004).

When we move a leg or an arm, we can sense that the position of the limb has changed. This gives us the ability to perceive the movement and position of our limbs. But different joints afford different sensibilities in movement and position sensing. For example, studies have suggested that position resolution varies from proximal to distal limbs, with proximal joints having a higher angular position resolution than distal ones (Clark et al., 1995). For example, the Just Noticeable Difference (JND), the minimum increment at which movement is perceived, of angular position change of the shoulder has been reported to be 0.8 degrees, for the wrist and elbow it has been shown to be 2 degrees, and for a finger joint its 2.5 degrees (Tan et al., 1994).

2.1.3 Cutaneous haptic system physiology

Tactile haptic interactions sometimes referred to as cutaneous interactions are perceptual interactions that occur at the level of the skin. Unlike the kinaesthetic haptic perceptual system, tactile haptic receptors are only found in the skin and not within joints, tendons, muscles et cetera. Sensations perceived by the skin can be broken down into three groups; pain, temperature and mechanical tactile (van Jan, 2006). Although there have been tactile haptic devices that use heat (Jia et al., 2015) and electrical stimulus as a method for tactile haptic interaction (Bach-y-Rita et al., 1998); tactile haptic devices are typically concerned with providing stimuli of

pressure or vibrational forces upon the skin. Similarly, to the kinaesthetic haptic perceptual system, the tactile sensitivity of an area of skin varies with the densities and types of receptors. Typically, there are two main types of skin which have varying concentrations and types of receptors; these are glabrous skin, as found on parts of the body that are typically bald such as the palm of the hands and bass of the feet; and hairy skin, as found on the forearm, legs et cetera. In tactile interactions concerning vibrotactile and pressure stimulus, there are four predominant types of receptors which provide tactile information in the form of electrical impulses sent to the central nervous system. Again, these are commonly referred to as mechanoreceptors as they respond to mechanical pressure or distortion upon the body (Hale & Stanney, 2004). The four types mechanoreceptor units used for classifying mechanoreceptors are: Rapidly adapting type I and II (RAI & RAII) and slowly adapting type I and II (SAI and SAII). Rapidly adapting mechanoreceptors typically respond with bursts of impulses at the onset and removal of stimulus, and slow adapting mechanoreceptors typically have a sustained discharge of impulses and are therefore good at sensing sustained and static forces upon the skin. Whether a receptor is grouped into a type I or type II is dependent on the properties of their receptive fields (Vallbo and Johansson, 1984). For example, type I fast acting and type I slow acting mechanoreceptors have a higher spatial resolution than type II receptors. This is because the receptors are triggered by forces applied to smaller areas. The four main types of mechanoreceptors are listed below (Hale and Stanney, 2004).

Pacinian Corpuscles can be found in glabrous and hairy skin. They are categorised into the fast-acting type II (FAII) group as they have a very poor spatial resolution of 2cm and are only triggered on the onset and removal of the mechanical stimulus. The stimulation frequency range is between 100 – 1,000Hz. They typically relay information about the roughness of surfaces and vibrational oscillations.

Ruffini Endings can also be found within both glabrous and hairy skin. They are categorised as slow acting type II receptors as they have a poor spatial resolution of about 1cm and send impulses over the duration stimuli actuation. The stimulation frequency range is between 0.4 – 100Hz. They convey sensations of skin stretch and static forces.

Meissner Corpuscles are only found in glabrous skin such as the palms of the hands and bass of the feet. They are categorised as fast-acting type I as they have a spatial resolution of around 3-5mm and only send impulses at the onset and removal of a mechanical stimulus. The stimulation frequency range is between 2 – 40Hz. They are responsible for sensations of flutter, slip and grip control.

Merkel Disks are also only found in glabrous skin and are categorised as slow acting type 1 as the spatial resolution is extremely good at 0.5 mm and they send continuous impulses over stimuli duration. The stimulation frequency range is between 0.4 – 10Hz. Skin curvature, pressure, form, texture and sharpness of edges are the proposed sensations caused by these receptors.

Hair follicles are also thought to play a role in sensing some cutaneous tactile interactions, as they provide a mechanical link to the epidermis. But the hairy skin that covers the majority of the body is thought to have a lower spatial resolution than compared to glabrous skin (Johansson and Vallbo, 1983). Therefore, hairy skin is not the best suited for discriminating between different textual information of two-dimensional form perception (Hale and Stanney, 2004). Although it has been shown that vibrotactile information can be conveyed effectively in areas of hairy skin (Bach-Y-Rita et al., 1969). As mentioned previously different types of mechanoreceptors are sensitive to distinct physical parameters such as stimuli frequency and contact area, but it is widely thought that majority of tactile experiences is the result of multiple mechanoreceptor responses (Johansson, 1978; Johansson and Birznieks, 2004; van Jan, 2006).

The glabrous skin of the hand, in particular, the fingertips have been identified as a prime location for tactile stimulation, as this the typical contact area used for object manipulation tasks. This has led the design of many tactile haptic devices that focus on the actuation of this region of the hand (Pacchierotti et al., 2017). The glabrous skin of the hand contains one of the most densely populated areas of mechanoreceptors, especially Meissner corpuscles and Merkel cell-neurite complexes. Theses specific mechanoreceptors enable high resolution and sensitivity in defining edge contours due to the indentation of the skin. Spatial resolution, the ability to distinguish between two give points, is at a maximal at the fingertips and decreases

towards the wrists, therefore, indicating higher concentrations of mechanoreceptors within these areas (Johansson, 1978).

2.1.4 Just Noticeable Difference (JND) psychophysical metric

Just Noticeable Difference (JND) is a widely-used metric in the assessment of haptic rendering systems. In essence, JND is a quantitative measure for perceptual resolution. It is defined as the minimum increment of a stimulus that enables a user to detect a change or a difference between two stimuli (Faimagne, 1986). A metric used to quantify JND for different types of stimuli is known as Weber's constant, named after the psychophysicists Ernst Heinrich Weber (1795–1878). Webbers constant (K), sometimes referred to as the Weber fraction, can be deduced by dividing the stimulus intensity change needed in order for a difference to be perceived (ΔI) by the original baseline stimulus (I) (Fechner, 1860).

$$\Delta I/I = K$$

The Weber constant is the result of Weber's law, which states that the size of the JND is a constant proportion of the original stimulus value. Faimagne (1986) has discussed that JND is intrinsically ambiguous due to the lack of definition of just noticeable. For example, in a trail where the change in stimulus ΔI is perceived only 65% of the time, does that mean that the original intensity plus ΔI is bigger than the original intensity? Faimagne discusses that an empirical criterion of 75% should be enforced in psychophysical tests concerned with JND, so that:

$$I + \Delta I(0.75) > I$$

A good exploration and summary of the current haptic evaluation research that focuses on JND have been conducted by Feyzabadi et al (2013). Below is a table compiled by Feyzabadi et al listing the JND metrics discovered in experiments using haptic rendering systems on the actuation of different body parts:

Table 2-1 Table illustrating JND metrics discovered in experiments using kinaesthetic haptic devices on different sections of the body.

Reference	Test Point	No. Subjects	Weber Fraction %	Application
Doerrer et al. 2002	Fingertip	20 (18m, 2f)	5	Push Button Design
Brewer et al. 2005	Index Finger	23m (11m, 12f)	19.7 - 46	Fine Motor Control
Pang et al. 1991	Two Fingers	5m	7	Grasping
Jones 1989	Elbow	14 (7m, 7f)	5.2 – 8.8	General Experiment
Vicentini et al. 2010	Hand	17 (11m, 6f)	15	Robot Tele-operation
16 Newberry et al. 2007	Both Hands	12m	11.5 – 16.5	Car Industry
2 Tan et al, 1994	Whole Arm	3 (1f, 2m)	1 - 2	General Experiment
17 Abbink et al, 2004	Foot	8 (4m, 4f)	30 – 50	Car Industry

2.2 Dielectric Elastomer Actuators

2.2.1 Fundamental principles of Dielectric Elastomer Actuators/ Transducers

The working principle that underpins Dielectric Elastomer Actuators (DEAs), deformation of a solid material through the application of a voltage, has been observed since the 18th century (Carpi et al., 2010b). But the topic has gained significant further investigation since the late 1990s (Pelrine et al., 1998, p. 199). What makes DEAs such an exciting actuation technology is that they offer: large area strains (of up to 100%), high energy densities (up to 1 MJ/m³) and fast actuation response times (< ms)(Carpi et al., 2008, p. 200). A DEAs configuration resembles that of a capacitor; a dielectric insulating material sandwiched between two opposing electrodes. The differentiation being that the dielectric is comprised of a soft flexible elastomeric material with the electrodes are compliant and bonded to the surface of the dielectric. When a voltage is applied, the opposing charges induced on the electrodes creates an electrostatic pressure. This is due to opposing charges between the electrodes attracting each other and the like charges that gather on each of electrodes repelling each other. As the dielectric is made from an elastomeric material with an assumed constant volume, a thinning occurs in a plane perpendicular to the applied electrodes and expansion in the plane parallel (see Figure 2-1).

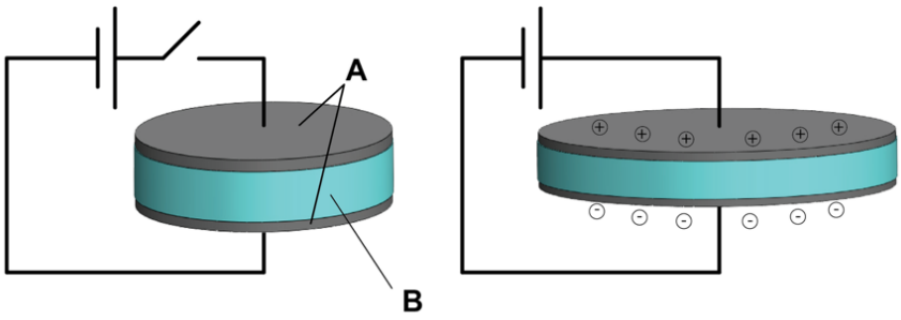

Figure 2-1 Illustration of the DEA principle of operation: compliant electrodes (A) connected to a voltage source which supplies electrical charges that deform the layer of elastomeric dielectric material (B), by squeezing its thickness and expanding its surface.

The electrostatic pressure p which causes this deformation is known as the Maxwell Stress. For planar configurations of DEAs this is outlined by the following equation (Pelrine et al., 2000b):

$$p = \epsilon_r \epsilon_0 E^2 = \epsilon_r \epsilon_0 \left(\frac{V}{z}\right)^2 \tag{1}$$

where ϵ_0 is the dielectric permittivity of vacuum, ϵ_r is the elastomer's relative dielectric constant, E is the electric field, V is the voltage and z is the membrane's thickness. This equation proposed by Pelrine et al (2000b) is determined as follows:

As stated previously, a planar DEA is essentially a capacitor. If we assume the electrodes have a resistance of zero and the elastomeric dielectric material is perfectly insulating, hence an infinite electrical resistance and lastly the system is perfectly elastic, meaning no disruptive mechanical losses during deformations of the system. The electrostatic energy U of our deformable perfect capacitor is:

$$U = \frac{1}{2} CV^2 \tag{2}$$

where C is the Capacitance and V is the voltage across the capacitor. Based on these assumptions, C can be written as:

$$C = \varepsilon_r \varepsilon_0 \frac{A}{z} \tag{3}$$

where ϵ_0 is the dielectric permittivity of vacuum, ϵ_r is the elastomer's relative dielectric constant. The electrostatic energy U of a capacitor can be written as:

$$U = \frac{1}{2} \varepsilon_r \varepsilon_0 \frac{A}{z} V^2 \tag{4}$$

Following this, the change in electrostatic energy dU of this capacitive system is:

$$dU = VdQ + U\left\{\left(\frac{1}{z}\right)dz - \left(\frac{1}{A}\right)dA\right\} \tag{5}$$

where dQ is a change in charge of the system. The first term on the right-hand side of the equation VdQ is the electrical energy supplied externally to the elastomeric capacitor system. The second term on the right is the conversion of electrical energy into mechanical energy/ work. This can in visualised in the in flowing the illustration:

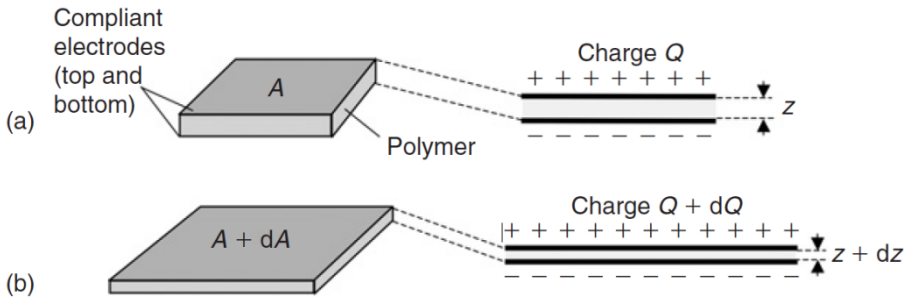

Figure 2-2 The two working states of our elastomer capacitor system, a) non-actuated, b) actuated. (Pelrine and Kornbluh, 2008)

Another assumption is that our elastomeric capacitor operates with a constant volume and therefore described as an incompressible system, which is typically true for elastomeric materials, thus:

$$Az = vol = constant \tag{6}$$

which can be expressed as:

$$A\,dz + z\,dA = 0$$

or:

$$\left(\frac{1}{z}\right)dz = -\left(\frac{1}{A}\right)dA \tag{7}$$

If we substitute equation (7) into equation (5) we end up with either of the following:

$$dU = VdQ - 2U\left(\frac{1}{A}\right)dA$$

or: (8)

$$dU = VdQ + 2U\left(\frac{1}{z}\right)dz \tag{9}$$

Again, the first term on the right-hand side of each of these equations VdQ is the electrical energy supplied to the elastomeric capacitor system. And the second term on right is work done on the electric field. These equations (8, 9) highlight the two potential uses of dielectric elastomers: firstly, as in actuator. For example, if we see an increase in the overlapping electrode area of the system, dA>0, indicating the

electrical energy of the system is decreasing, therefore electrical energy is being converted to mechanical work. Therefore, any increase in the overlapping electrode area whether due to the application of an electric field pressure (Voltage) or as the result of an external force, causes electrical energy to be converted to into mechanical work, providing, of course, there is a charge on the elastomer sheet. And secondly, if the area is decreasing, dA<0, for example, the elastomer sheet is contracting from a previously stretched position, mechanical energy is being converted to electrical energy, and therefore the system is acting as a generator. The same can be said to be true for a change in thickness, but with an inverse relationship, as denoted by the difference of the sign in equation (9).

Considering the actuator mode of the system described, an application of a voltage across the elastomeric material results in a Maxwell stress of *p,* which is sometimes referred to as the effective pressure or actuation pressure. This can be defined by the following the equation:

$$-Ap\,dz = dW \tag{10}$$

p is the compressive pressure applied over the area A through a displacement of dz which provides the mechanical work dW equal to the actual work on the polymer.

The first law of thermodynamics states that within a closed system the change in internal energy dU is equal to amount of heat added to that system δQ, minus the amount of work done dW by the system:

$$dU = \delta Q - dW \tag{11}$$

If no heating of the system is assumed, so that:

$$\delta Q = 0 \tag{12}$$

dU can be written as:

$$dU = pAdz$$

or:

$$p = \left(\frac{du}{Adz}\right) = \left(\frac{1}{A}\right)\frac{dU}{dz} \tag{13}$$

The Maxwell stress induced from the electric field is only valid if the Area A and the charge Q remained fixed. Due to our constant volume assumption, equation (6), there can be considered only one relevant spatial variable, either A or z at a time. Therefore, differentiating U in respect of Z when U is changed according to constant volume assumption, the Maxwell Stress can be derived from equation (9), again considering that the charge remains constant so that:

$$dQ = 0 \tag{14}$$

Therefore, the Maxwell stress can be written as:

$$p = \left(\frac{1}{A}\right)\frac{dU}{dz} = 2U\left(\frac{1}{Az}\right) = \frac{2U}{vol} \tag{15}$$

Considering electrostatic energy U of a capacitor, equation (4), the Maxwell Stress can be determined as:

$$p = \epsilon_r\epsilon_0 E^2 = \epsilon_r\epsilon_0\left(\frac{V}{z}\right)^2 \tag{16}$$

2.2.2 Dielectric Elastomer Materials

There are a number of dielectric materials that have been explored for DEA applications. These range from synthetic elastomers such as acrylics, silicones, fluoroelastomers, polyurethane, polybutadiene (Pelrine et al., 2000a, 2000b) to even natural rubber latex compositions (Jaaoh et al., 2018). Typically, applications that have used DEAs have opted for acrylics and silicones. These materials have related benefits and disadvantages as discussed.

One of the most commonly used acrylic dielectric materials used for the construction of DEA devices is VHB (3M, USA). It is a commercially available adhesive tape that has a thickness ranging from 500μm to 1mm. It has been shown that a pre-strain applied to the material enables actuation strains greater than 100% (Pelrine et al., 2000b). Manufacture of DEAs is simplified with VHB film due to its adhesive properties. Although the high strains and ease of manufacture are desirable, the materials main limitations concern its high viscoelastic properties. The viscoelastic properties of VHB effects response time and reliability (Liu et al., 2014). Viscoelastic behaviour of elastomeric materials is shown as a time-dependant permanent deformation due to instantaneous, constant stress. Therefore, viscoelasticity of a material relates to the material demonstrating both viscous and elastic characteristics under stress and deformation (Yousefzadeh, 2017). This phenomenon in pre-strained VHB film results in a stress relaxation of the membrane causing a performance drop in electromechanically induced strain over time. Therefore, VHB films cannot be considered as a suitable candidate for long life, consistently performing actuators.

A material that does not exhibit this viscoelastic behaviour to such a high degree is silicone elastomers. Indeed, they have been shown in a number of situations demonstrating fast actuation speeds (Kornbluh et al., 2000; Maffli et al., 2015), actuation life's over a million cycles (Saint-Aubin et al., 2018) and temperature stability (Michel et al., 2010). The issue with this dielectric material is that strains are significantly lower than the VHB acrylic counterparts, with typical strain performance being around 10% at comparable voltages (Michel et al., 2010). Although there is a number of approaches in the formation of elastomer films into various thickness and dimensions; there are also commercial suppliers of silicone films, such as Elastosil (Wacker, Germany) specifically developed for use in DEAs which range in thickness from 20μm to 400μm. The low thickness can result in significantly reduced actuation

voltages, but all present significant challenges in the handling and fabrication. One issue with silicone elastomer approaches is the difficulty in bonding silicone elastomers to rigid support frames or to other silicone layers. Potential ways to address this is with Kapton adhesive tape (DuPont, USA) and with oxygen plasma bonding techniques.

2.2.3 Compliant electrodes for DEAs

As with dielectric elastomer membrane material selection, there have been a number of approaches in the application and formulation of compliant electrodes. The two main criteria for compliant electrodes are high conductivity/ low sheet resistance, even at high stains; and minimal mechanical stiffening to the dielectric membrane when applied.

To these means the most common approach is the use of a carbon powder, such as Vulcan XC72 (Carbocrom, Italy) (Carpi et al., 2007), Black pearl 2000 (Cabot, USA) (this work) or Ketjenblack EC-600JD (AkzoNobel polymer chemistry, The Netherlands) (Kovacs and Düring, 2009); typically mixed with another material such as an oil/grease or an uncured elastomeric matrix such as silicone in order adhere the carbon powder to the surface of dielectric membrane; although, loose carbon powders have also been shown (O'Brien et al., 2007). The advantage of loose powder is that it has a negligible stiffing effect, but however this method is not robust and is easily damaged. Other approaches have used an oil/ grease to adhere the carbon particulate to the surface (Frediani et al., 2014b; Huang et al., 2012). These are usually applied by hand with a brush and stencil, therefore uniform thickness is hard to achieve. This approach is prone to smudging, therefore controlling and maintaining the electrodes pattern on the actuating dielectric membrane is difficult. This approach is also not suitable for multi-layer actuator designs as there is no mechanical bonding between the alternating electrode and dielectric membrane layers.

A robust method to adhere a conductive particulate to the surface of a dielectric elastomer membrane is to add it to an uncured/ non-polymerized elastomer such as a silicone, then curing this mixture to the surface of the dielectric, forming a conductive rubber layer. The primary issue with this approach is that the mixture can add a non-negligible stiffening to the membrane material. Therefore, the focus has to be paid to applying the mixture in thin layers, but this, in turn, can increase the sheet resistance of the applied electrodes (Rosset and Shea, 2013). The thickness of the cured conductive rubber layer should be negligible to the thickness of the DEA membrane (Pelrine et al., 1998); to these means, there are a number of methods developed in the application of these electrodes.

A common approach is to use a stencil applied to the surface of the dielectric membrane, and then by using an air-brush, spraying a low viscosity uncured conductive rubber mixture to the exposed surfaces (Matysek et al., 2009). This approach has been used in creating more complex multilayer stacked actuators. Where both the dielectric and conductive layers are sprayed and cured in an alternating fashion (Araromi et al., 2011). The advantage of the later is extremely thin layers of dielectric can be created (μm range), reducing the driving voltages required.

Screen printing has been shown as an effective way to apply uncured conductive elastomer mixtures. The advantage of this approach is that it offers good control of the electrode pattern features, controlled line widths of ~5μm (Hyun et al., 2015), as well as being suitable for mass manufacture processes (Fasolt et al., 2017).

Pad printing processes, another common mass-printing approach, has also been demonstrated to create thin compliant electrode layers. This process has also been used to deposit extremely thin dielectric membrane layers (~3μm), creating DEAs with extremely low driving voltages (<300V)(Poulin et al., 2015). For this approach to work, the viscosity of the mixtures involved has to be carefully controlled.

Inkjet printing is another approach that offers serval advantages, primarily in the ability to digitally control the pattern of the electrode, allowing for quick design iterations and optimisations of the electrodes profile. A difficulty in this approach is the control of the print mixtures physical parameters, such as viscosity and surface tension which are vital for consistent printing results (Rosset and Shea, 2013).

A comprehensive review of compliant electrodes and application processes for DEA devices, that includes approaches such as metal electrodes and other flexible conductive compounds has been conducted by (Brochu and Pei, 2010). Furthermore, a discussion of these techniques with regard to commercial processes and current limitations in the field has been conducted by (Rosset and Shea, 2013).

2.2.4 DEA Breakdown failure and electromechanical instability

There are a number of mechanisms that can lead to failure of DEAs. The predominant failure mode is referred to as dielectric breakdown. Effectively this is a short-circuiting that occurs between opposing electrode layers. This short-circuiting occurs when there are conducting channels present in the dielectric (DE) membrane. The charge that leaks through these channels can cause localised heating, potentially leading to greater charge leakage and permanent damage to the dielectric membrane. These conducting channels typically develop around flaws and inconsistencies of the DE membrane (Anderson et al., 2012). An approach to address this issue is the use of self-healing/ self-clearing electrodes. These electrodes use the heating effect caused through the flowing charge to burn away the conducting channels. This self-healing characteristic has been observed with single-walled carbon nanotubes (SWCNT)(Yuan et al., 2008), electrolessly deposited silver (Lau et al., 2011) and doped conductive polymer electrodes (P3DOT) (Yuan et al., 2007). These approaches typically require expensive materials and are hard to achieve due to the interplay of the controlling circuitry, electrode surface resistance and properties of the dielectric membrane itself. Also, a defect or hole that develops within the dielectric membrane that is typically under a pre-strain often leads to catastrophic rupturing regardless of the ability of the electrode to electrically isolate these defects.

Electro-mechanical (Pull-in) instability is a common cause of dielectric breakdown and mechanical failure of certain types of DE membranes. As stated previously, the Maxwell stress on the DE membrane is proportional to the square of the applied electric field (Pelrine et al., 2000b). As DE membrane thins due to an application of a voltage, the electric field will grow, resulting in a further increase in the Maxwell stress. If this rate of increase is greater than resisting elastic stress, failure of the DE membrane can occur (Anderson et al., 2012; Carpi et al., 2008). This effect is typically observed in softer DE membranes, as stiffer dielectrics will only endure smaller deformations before an electrical breakdown limit is reached. In this case, the applied electric enables electrical pathways to be formed within the dielectric without the large deformations/ instability range observed with softer DE membranes. Typically, before dielectric breakdown or mechanical failure occurs in the softer DE membranes prone to pull-in instability, a complex wrinkling pattern can be observed on the surface membrane (Plante and Dubowsky, 2006), this effect is particularly

observed in over actuated acrylic VHB membranes. The third type of DE is proposed that suggests an elastomer can reach stable deformation state before electrical breakdown down occurs (Zhao and Suo, 2010). The three types of DE can be distinguished according to their voltage induced stretch curves (fig 2-4).

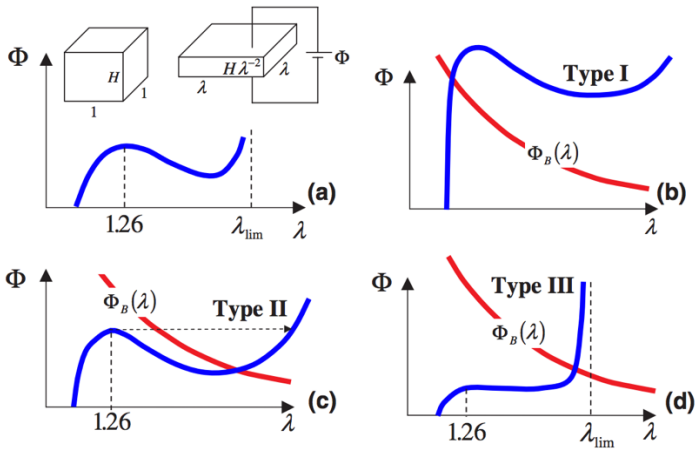

Figure 2-3 Voltage-stretch curves of three different types of DE Φ(λ) (Blue lines), with respect to electrical breakdown voltage-stretch curve ΦB(λ) (Red lines). (a) Shows generic DE voltage stretch curve, (b) Type I, aka the stiffer DE, where electrical breakdown happens before the instability/ large deformation phase, (C) Type II that demonstrates pull-in instability and large deformations before electrical breakdown, (d) Type III that demonstrates large deformations and stable stretch state before electrical breakdown (Zhao and Suo, 2010).

2.2.5 Pre-stretch

Applying a pre-stretch/ pre-strain to a DE membrane before actuation tends to improve the elastomers actuation performance. This is widely attributed to two main effects. Firstly, the pre-strain reduces the thickness of the DE membrane, therefore increasing the Maxwell stress (Pelrine et al., 2000a); secondly, an increase in the electrical breakdown strength of the DE is observed (Kofod et al., 2003; Plante and Dubowsky, 2006; Zhao and Suo, 2010). Other advantages of pre-strain include improved mechanical efficiency (Palakodeti and Kessler, 2006), increased response speed (Choi et al., 2005) and directionally controlled actuation strain through applying the pre-strain along certain axes (Pelrine et al., 2000b). It has been shown that pre-stretch can reduce or remove the pull-in instability mechanism of certain DE's, shifting voltage-stretch response curve of the material. This is particularly prevalent with acrylic VHB membranes (Koh et al., 2011a) illustrated in the figure below (2-5).

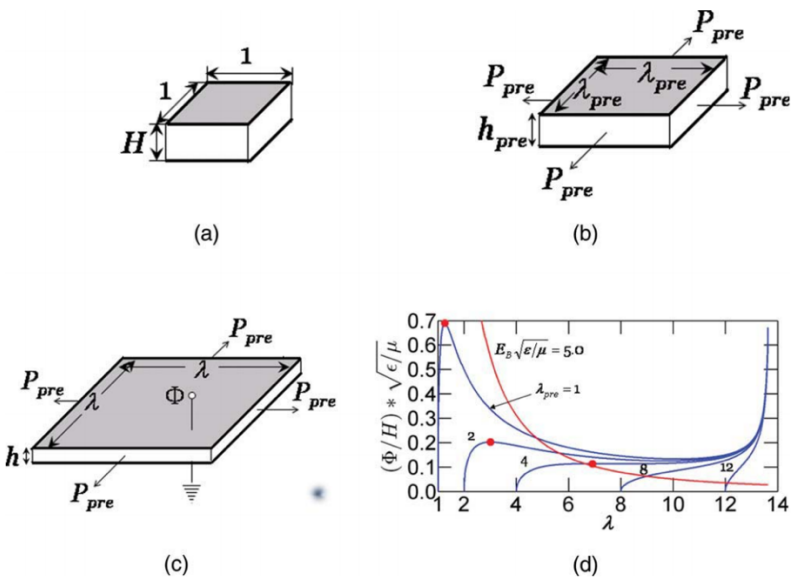

Figure 2-4 (a) DE at rest, (b) DE with applied pre-strain, (c) DE with pre-strain and applied electric field, (d) Graph illustrating voltage-stretch curves for the differently pre-strained DE membranes. A 400% prestretch is shown to be optimal for acrylic VHB film, as this pre-strain generates large stable strains and demonstrates an increase dielectric breakdown strength. The red dots of the 100% and 200% denotes the electrical breakdown points for these pre-strained samples. (Koh et al., 2011a).

The primary limitation with pre-stain is that a ridged support frame is required to maintain the stretch position. The support frame can significantly increase the total mass of DEA device, decreasing the effective work density and power to mass ratio (Brochu and Pei, 2010).

2.2.6 DEA configurations and existing applications

There have been a number of actuator configurations presented that utilizes the electronically controlled expansion and contraction of a DE membrane. In-depth reviews of some of these configurations have been presented by Carpi et al. (2008) and Kornbluh et al. (2002). Here, a few of these configurations are discussed along with applications of.

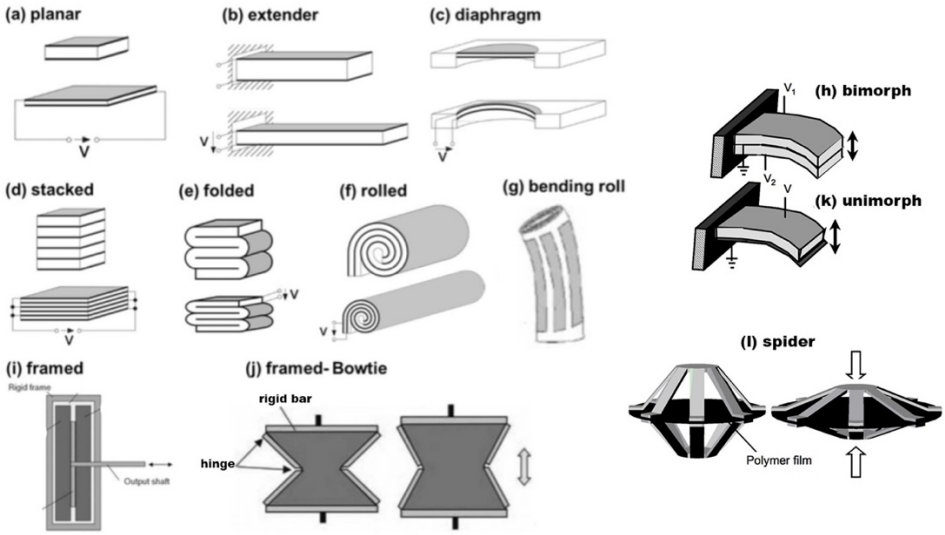

Figure 2-5 Diagram showing a variety of DEA configurations, collected by (Carpi et al., 2008; Kornbluh et al., 2002).

The above figure (2-6) shows various DEA configurations as compiled by Carpi et al. (2008) and Kornbluh et al. (2002). These configurations have been used in several experimental and commercial applications. A planar annular configuration has been used to expand and contract a soft deformable lens for the purpose of changing focus length in optical systems (Federico Carpi et al., 2012; Maffli et al., 2015). An array of planar DEAs applied to a single membrane have been used to reduce laser speckle effects (Blum et al., 2012). A rolled actuator (2-6f) has been developed that can generate 200N of uniaxial force, an array an array of such had used in an arm wrestling robot (Kovacs et al., 2007). Multiple two-DOF (Degrees Of Freedom)bending rolled actuators (fig. 2-6g) have been used to create a walking robot (Pei et al., 2003). Stacked actuators that generate a contractive force due to the thinning of multiple stacked DEA membranes have been shown in low-power analogue control pneumatic valves (Giousouf and Kovacs, 2013). An array of diaphragm actuators (2-6c) have been used in a wearable tactile display (Koo et al., 2008). Typically to gain higher degrees of freedom, multi-segmented DEA devices

have been developed where serval sections can be simultaneously electromechanically controlled to achieve different types of actuation motion. A nine segment conical device has been devolved that can potentially control up to six DOF (Conn and Rossiter, 2012).

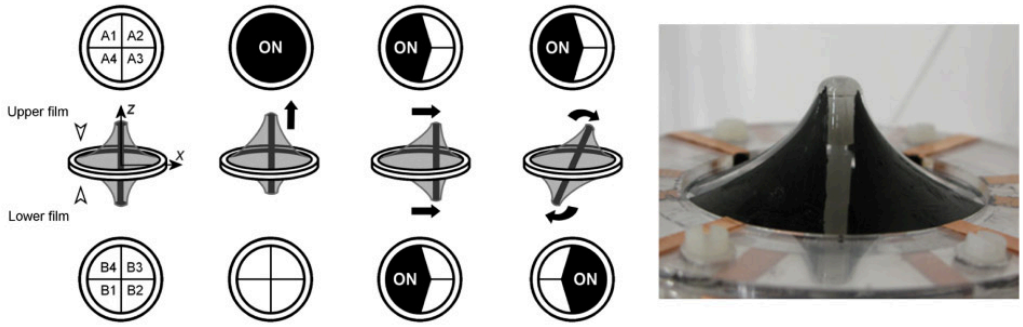

Figure 2-6 Multi-segment conical dielectric elastomer actuator diagram showing five degrees of freedom, with photo of configuration on right (Conn and Rossiter, 2012).

Due to the high voltage nature typically associated with DEA (Dielectric Elastomer Actuator) devices, there have been a number of configurations presented to separate the user from the potentially hazardous high voltage components. This is typically achieved by coupling the DEA membrane to a passive non-conductive component. One such device uses an array of non-conductive cantilevered pins to transfer forces generated by a DEA membrane for laterotactile "tickle" stimulation purposes (Knoop and Rossiter, 2015). Another approach is the use of an electrically insulating incompressible fluid to transfer forces, commonly referred to as hydrostatically coupled DEAs. This design has been demonstrated for a contractile rigid surface device and bubble like device illustrated in figure (2-8).

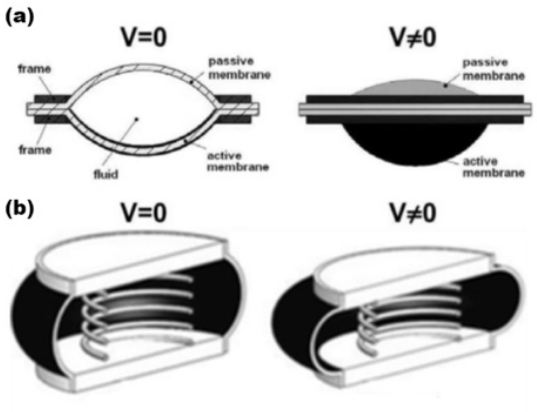

Figure 2-7 (a) diagram of hydrostatically coupled "Bubble-like" DEA configuration (Carpi et al., 2010b), and contractile hydrostatically coupled DEA configuration (F. Carpi et al., 2012)

2.3 Chapter conclusion

This chapter has discussed the core prerequisites to which this work relies on. Firstly, it has introduced the fundamental concepts behind the haptic sensory systems, then moved onto to general approaches in rendering these sensations in human-computer interfaces with a brief discussion of validation methods. Lastly, it has focused on the fundamental concepts of DEA technologies, to which this work employs for achieving its objective, building a compact wearable multi-finger soft tactile display.

In the next section, a literature review focusing on the state of art in actuation technologies and approaches for wearable tactile displays will be presented.

3 Literature survey

The goal of this thesis is to create a wearable tactile haptic device that can be worn on multiple fingers in order to allow for multi-finger tactile rendering of virtual soft objects. To these means, a literature investigation examining actuation technologies in wearable tactile devices will be conducted.

3.1 Scope of survey

In this survey, the focus will be on wearable actuation technologies for the purpose of stimulating the cutaneous mechanoreceptors. Particular focus will be paid to actuation technologies that can be mounted directly to the fingertip. The definition of wearable in this survey concerns the ability of the system to worn. An ideal wearable system is where the actuator, driving circuitry and supporting components can all be located on the user's body (Pacchierotti et al., 2017). But fingertip mounted tactile devices that are tethered due to power requirements, such as to the pumps and valves required in pneumatically actuated systems will also be considered. As stated, this survey will pay particular focus on the stimulation of mechanoreceptors located on the fingertips. That is to say, tactile sensations due to temperature, chemical reaction and electric current will be ignored; although it is considered that in order to make realistic tactile rendering possible, these tactile sensations should ideally be considered.

3.2 Mechanical actuation methods in fingertip mounted haptic devices

Five different actuation technologies that have been used to create wearable fingertip mounted tactile displays have been reviewed. These are: vibratory motors, DC (Direct Current) motor/ servo motor, Shape Memory Alloys (SMA), pneumatic/ microfluidic and Dielectric Elastomer Actuator (DEA).

3.2.1 Vibratory motor

Vibratory motors placed upon the skin can activate various types of cutaneous mechanoreceptors which generate vibrotactile sensations. To these means there are several vibratory actuator types used, such as: offset mass motors, voice coil and solenoids. Vibrotactile actuators offer a number of advantages for use in wearable tactile interfaces, such as lightweight and compact form factor, typically low driving voltages and relatively simple control circuitry. The predominant drawbacks concern:

noise, vibrational induced discomfort with continuous use and limited to rendering vibrotactile stimuli only.

(Cheng et al., 1996) presented one of the early incarnations of a wearable haptic device that used vibrational motors to provide vibrotactile feedback for VR interactions. The device enabled users to determine the amount of pressure applied to a virtual grape though proportional vibrotactile stimuli applied to the fingertip. The device consisted of two offset mass DC (Direct Current) motors secured to the fingertip via a gloved interface.

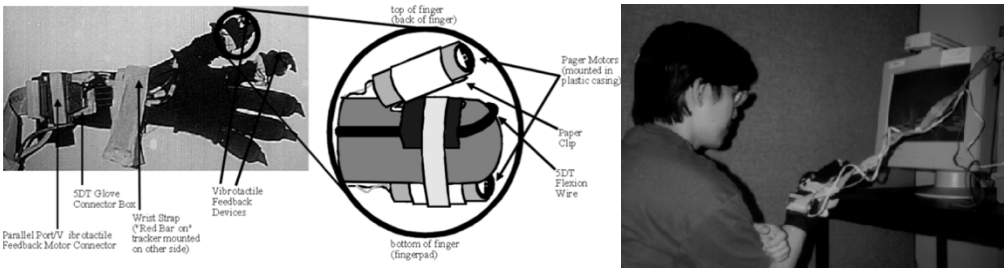

Figure 3-1 Right: Labelled diagram of the vibrotactile device proposed by (Cheng et al., 1996), Right: participant using the device to interact with a virtual scene displayed on a 2D monitor .

CyberTouch systems (2018) released a commercially available vibrotactile wearable device, that again uses a glove to locate offset mass DC motors upon the fingertips. Each motor can be addressed individually to convey continuous or pulsed vibrations of different durations and intensities.

There have been a number of research projects that have researched potential applications of wearable vibrotactile devices. (Murray et al., 2003) placed voice coil actuators on fingertips to improve telerobotic control of a robotic hand performing manipulation tasks. (Bial et al., 2011) embedded vibratory coin cell motors, typically found in mobile devices, into the fingertips of motor cycle glove to supply navigational information to the rider. (Mazzoni and Bryan-Kinns, 2016) placed vibratory motors on the back of the hand, in order to convey mood of music in films to hearing-impaired users. (Uchiyama et al., 2008) created glove with a 3 by 3 array of coin cells motors located to the back of the hand, to convey directional information to visually impaired wheelchair users.

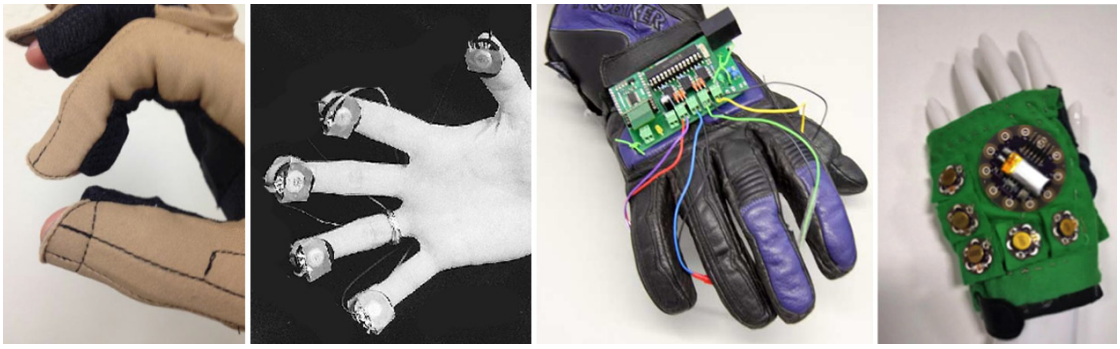

Figure 3-2 Left to right: Cybertouch, Voice coil vibrotactile telerobotic feedback device by(Murray et al., 2003), vibrotactile motor bike navigation aid (Bial et al., 2011), Mood-glove (Mazzoni and Bryan-Kinns, 2016).

Although this approach lends itself to wearable multi-finger systems, the sensations rendered by vibrotactile actuators are limited to vibrational sensations. A more naturalistic tactile sensation is the application of continuous pressure applied directly to the fingertip, rather than a vibration intensity that is used represent a contact pressure.

3.2.2 DC motor/ servo finger pad moving platform devices

There have been a number of haptic devices that use small DC (Direct Current) or servo motors located on the fingertip to render varying types of mechanical forces. Forces are transferred from the motors to the pulp of the fingertip typically through a compliant fabric, wire or rigid platform interface. This approach can offer serval advantages, such as high degrees of freedom, relatively high force generation and non-tethered wearable systems. These devices tend to be intended for single finger only and typically do not lend themselves to multi-finger configurations due to size and weight on the fingertip. The size and weight of these devices vary, typically due to the degrees of freedom in which the tactor can move. Other limitations concern noisy operation, particularly with servo motor approaches; and jittery sensations due to motor and gearing limitations.

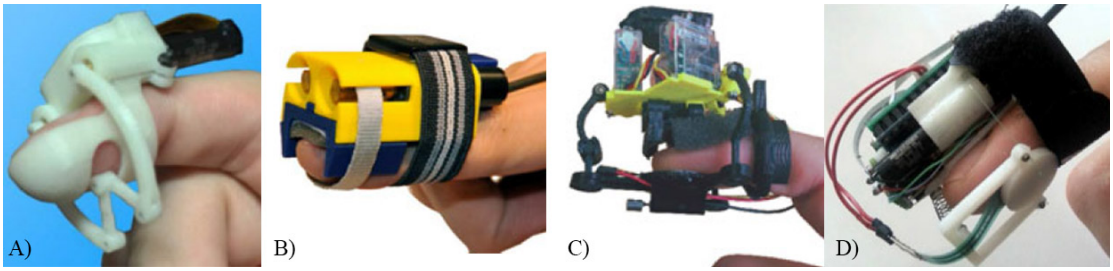

Figure 3-3) (A) Link-Touch two-DOF device (Tsetserukou et al., 2014b), (B) Gravity grabber (Minamizawa et al., 2007), (C) 3 DOF servo based system (Chinello et al., 2015), (D) 2-DOF wired device (Kim et al., 2016).

There have been a number of designs proposed in this category. (Tsetserukou et al., 2014b) proposed a two DOF device that can provide indentation and shear forces upon the fingertip, as well as simulating contact and release with virtual objects. A similar DOF device is created by (Minamizawa et al., 2007), but uses a fabric interface between the finger pulp and motors. The authors state that this device can render tactile sensations upon the fingertip that simulates the gravity induced shear forces from holding an object between the thumb and finger. (Chinello et al., 2015) have created a version composed of three servo motors. The servo motors used are capable of moving a plate in three DOF against the fingertip pulp in order to simulate indentation, curvature and slip tactile sensations. (Kim et al., 2016) developed a two DOF device that uses wires to move a similar tactile plate against the fingertip, but have incorporated Inertial Measurement Unit (IMU) for position tracking purposes. (Kawasaki et al., 2010) created a device based upon a 0.8g brushless DC motor that is used to drive one DOF screw pin which applies pressure to the user's finger. The device weighing only 4.3g on the fingertip is capable of generating forces up to 2.6N over a displacement range 4mm. According to a psychophysical study conducted with ten participants, although the device generated perceivable forces on the finger pad, the sensations were reported to be unrealistic and not in keeping with the virtual object being rendered.

Although these devices can be made into compact lightweight form factors, the location of a servo and motor on the fingertip typically results in bulky burdensome designs, which limits finger dexterity and multi-finger placement. Another issue with these devices is that they do not lend themselves to rending soft tactile forces, as the interface in which the force is delivered to the fingertip, the tactor, is rigid. Forces delivered through a soft interface could have serval advantages over a ridged tactor. For example, locating and fitting of the device to the user's fingertip could be

improved with a compliant soft interface. Another advantage, especially considering medical simulation, is that a soft interface would be more suited to delivering tactile forces associated with interacting with soft deformable objects/ tissues.

3.2.3 Pneumatic/ hydraulic actuation

Pneumatic haptic actuation typically involves the controlled inflation of an expandable cavity, such as a piston or a balloon. This expanding cavity then applies a mechanical pressure to the user. To these means, these systems are reliant on a series of electronically controlled pumps, regulators and valves. Due to the compressible nature of air, and that these systems are typically formed from soft expandable silicones; pneumatic haptic devices are particularly suited to rending soft/ compliant mechanical forces. This makes them particularly suited to simulating soft tissue interaction, as is required in medical training simulators. Primary limitations of this actuation technology concern the difficulty in miniaturising the driving systems required.

(Moy et al., 2000) created a pneumatically actuated array of inflating silicone cavities for stimulating a single fingertip. The device consists of a square 5 by 5 array of 1mm in diameter inflating cavities, with 2.5mm of spacing separation. According to the authors, the device can render tactile information relating to texture, shape and local compliance. The device appears to be limited in its force output at 100mN, but has a relatively high cavity actuation stroke of 0.6mm. The main limitation with this approach is that it is benchtop limited, as each of the 25 cavities requires its own regulated air-line feed, therefore making a completely wearable system difficult. (Kim et al., 2006) adopted a similar design for rendering push button sensations in augmented-reality, but again is limited to benchtop operation. There have also been attempts at using soft pneumatics in wearable configurations. (Sonar and Paik, 2016) created soft pneumatic actuator skin with embedded force feedback sensors; and (Raitor et al., 2017) created a wrist-mounted device that delivers motion guidance for teleoperation purposes. One of the main issues with these wearable devices, as with pneumatic actuation in general, is that they are reliant on a system of pumps, regulators, valves and controlling circuitry; which is difficult to make wearable too. Therefore, pneumatic wearables are typically tethered to a control unit via airlines, which limits the working area.

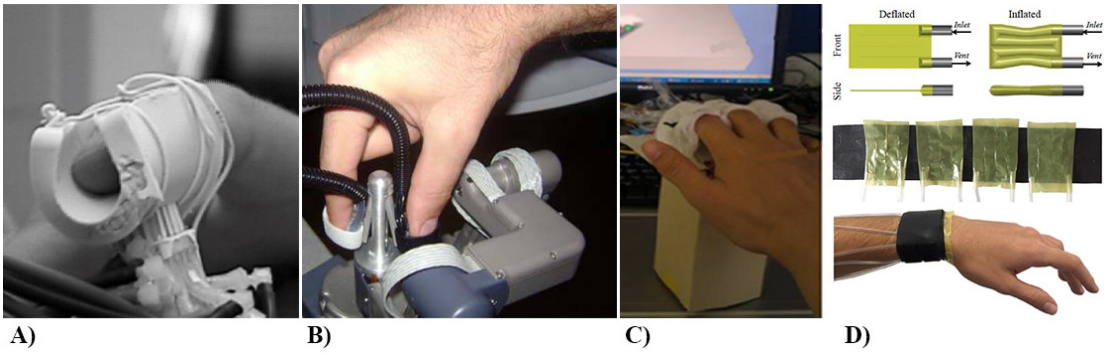

Figure 3-4) A) Fingertip array consisting of 25 individually controllable silicone tactors (Moy et al., 2000). B) Pneumatically actuated fingertip tactors for Da Vinci teleoperation system (Culjat et al., 2008). C) Multi-fingertip tactile display to simulate locating tumours in virtual tissues (Li et al., 2013). D) Four chamber wrist mounted navigation aid (Raitor et al., 2017).

Other notable applications of soft pneumatic haptic devices are as follows. (Li et al., 2013) created a multi-finger benchtop palpation device for training physicians to locate tumours, within virtual soft tissues. (Culjat et al., 2008) attached inflating tactors to the controls of a telerobotic operating system to provide soft tactile feedback to the operator during telerobotic surgery. (Coles et al., 2011) made a pulsating pneumatic system in order to simulate locating the femoral artery for needle insertion training.

Although not technically a pneumatic approach, there have been a number of attempts of using hydrolytic actuation which is reliant on a similar system architecture of pumps and valves. In these devices, a fluid is used to inflate a cavity or chamber as opposed to air. (Ninomiya et al., 2009) created a desktop mounted an array of hydraulically filled silicone balloons that exert a pressure against the user's fingertip, intended to be used as a brail display. This approach has also been adopted for use by a commercial enterprise known as HaptX (USA), who have created a wearable version of the device. Little is published about this system. But as seen with pneumatic systems, this approach tends to be tethered to a driving system of pumps and valves ("HaptX | Haptic gloves for VR training, simulation, and design," 2018).

Pneumatic/ hydraulic actuation appears to have several advantages for delivering tactile stimuli. Forces delivered through a soft compliant interface are not only better suited at simulating interaction with soft tissue as is required in medical simulation and teleoperation scenarios, but inherently soft interfaces could also provide a more comfortable approach for the transmission of tactile pressure forces to the user's fingertip. The primary limitation of this approach though is difficulty in miniaturising

the systems needed to drive multiple pneumatic or hydraulic chambers/ cavities. Therefore, fully wearable multi-finger devices would be difficult with this approach.

3.2.4 Shape Memory Alloy (SMA) actuation

SMA actuation relies on a wire that expands and contracts due to a change in temperature. The temperature of SMA wires and the resultant extension can be increased through the application of a current. Contraction occurs due to cooling of the system. Advantages of this approach for wearable tactile actuators is that can generate high forces and displacements in a lightweight and compact form factor, with relatively simple controlling circuitry. The primary issue with these devices is the low response speed due to the difficulty in dissipating heat from such systems.

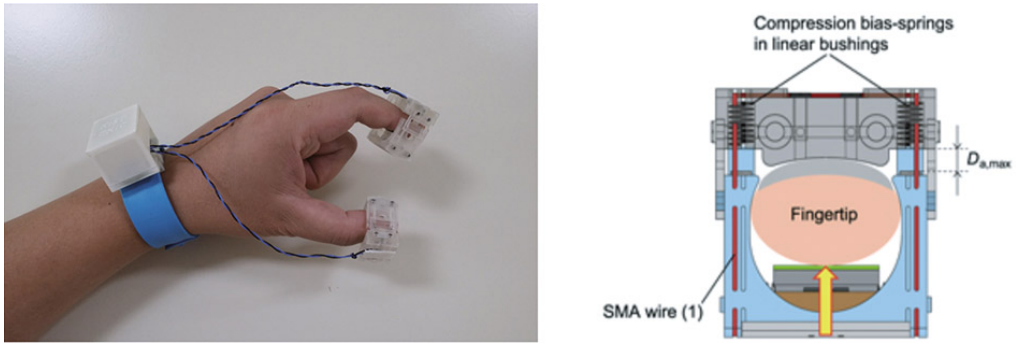

Figure 3-5 Right: SMA actuated lightweight, multi-finger wearable tactile system, Left: schematic of operation. The Red wire represents the expanding and contracting SMA wire (Hwang et al., 2017).

Hwang et al. (2017) created a wearable multi-finger device using shape memory alloys in a ring configuration around the fingertip. The contracting and expanding wires of the SMA move a rigid platform in a uniaxial motion against the fingertip. The developers of this device experimented with two configurations; one which could render shear forces by moving the tactor platform laterally against the fingertip; and a version that created a vertical intentional force. The device generates relatively high forces of up to 6N with corresponding displacements of 5mm. The weight of the device is around 7.2g. Retraction of SMA devices, full actuation to zero (6 to 0N), is reported to be around 4.9 seconds, limiting the frequency of operation.

SMA offers the ability to create large forces and displacements within compact lightweight form factors, as well having simple, compact and wearable driving circuitry. But the primary limitation is the slow response speed of the devices, making it suitable to deliver response naturalistic tactile interaction with virtual objects.

3.2.5 Dielectric elastomer actuation

There have been presented many different actuator designs for DEAs. (Carpi et al., 2008; Kornbluh et al., 2002) have conducted a detailed overview of different DEA configurations. The advantages of DEAs over other actuation methods include peak force generation, weight, compact design, low power consumption, ease of manufacture and organic actuation similar to that of natural muscle. The primary issue with this technology is the high-voltages required, typically in kilo Volt range, making isolation and the controlling circuitry more complex and expensive.

(Koo et al., 2006) presented a flexible wearable tactile display based on a 4x5 array of individually controllable dielectric elastomer dots. The device is inherently soft and flexible as it is formed from a soft silicone elastomer. In theory, the device can be wrapped around a user's fingertip to render tactile stimulus. The main issue facing this device is that it requires high driving voltages. This is common for most DEAs, but within this actuator configuration, only a thin silicone protective film protects the voltages from the user. If the film thickness is increased, mechanical properties of the actuator such as actuation height and force output are further reduced. Current force output from each of the individually addressable actuators is ~14mN at 3.5kV with a corresponding unblocked vertical displacement of 0.5mm. The diameter of each of the dots is 2mm with 3mm spacing. So far there has been no published psychophysical testing data pertaining to this device, potentially due to the electrical isolation issue; although the authors claim the low current of <0.1mA is too minute to afflict electrical damage.

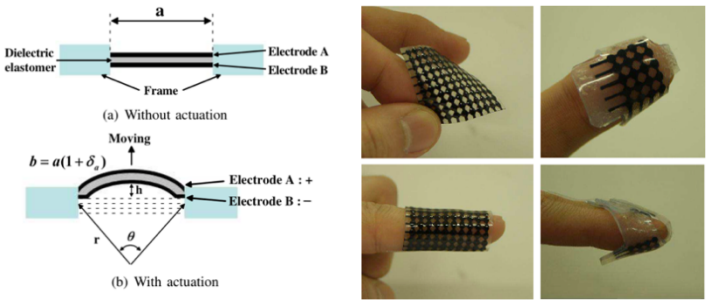

Figure 3-6 DEA buckling Actuator diagram and device placed on finger (Koo et al., 2008).

(Zhang et al., 2006) have presented a haptic force feedback device that employs a rolled DEA. The device is capable of applying forces of up to 7.2N and has a maximum actuation displacement of 8mm. The dimensions of the cylindrical device

are 12x45 mm and weigh ~38g. The operating voltages of the device range from 0 to 3.5kv. The researchers who developed this device also implemented a safety mechanism of a 25mA circuit breaker. In the event of a failure, the circuit breaker would prevent electric shock to the user. The researchers also concluded the power flowing through there DEA is not sufficient to cause harmful physiological effects to their user. The main limitations with this device seem to be its bulkiness, this is due to the high forces the authors intended to generate from this configuration. For use as an actuation method for a fingertip tactile rendering device, this actuator, although produces high forces, appears to be too cumbersome.

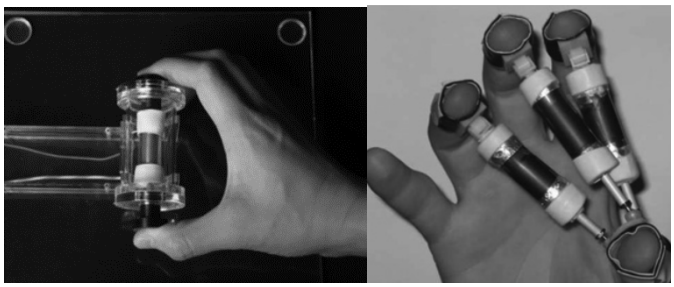

Figure 3-7 Static and portable force feedback haptic devices based on miniature rolled actuators (Zhang et al., 2006).

(Carpi et al., 2010b) propose a DEA design that has been demonstrated in a single finger tactile rendering device (Frediani et al., 2014b). An interesting feature is that it couples an active high voltage membrane with a passive safe to touch membrane through a coupling fluid. The main disadvantage of this type of device is the low force output of <0.6N at a relatively high driving voltage of 5kV.

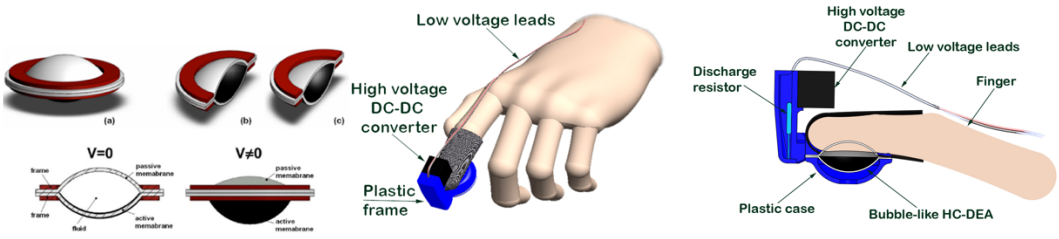

Figure 3-8 Left: Hydrostatically Coupled DEA diagram (Carpi et al., 2010a), Right: HC-DEA actuator embedded into a wearable haptic display (Frediani et al., 2014b).

An approach focused on providing laterotactile stimulation of a localised area of skin (Knoop and Rossiter, 2015). By coupling an active DEA membrane to the user's skin through an array of non-conducting cantilevered pins, they could create areas of lateral stretch and compression. Results from a psychophysical study demonstrated that users of the device were highly sensitive to this mode of tactile stimulation for

frequencies up to 100Hz. This design presents an effective method to separate the user from the high voltage areas of the DEA. The main limitation with this approach is that it can only deliver laterotactile stimulation at small forces. The pins deliver a max force of up to ~90mN over a 0.6mm displacement range, with a peak driving voltage of 3.5kV.

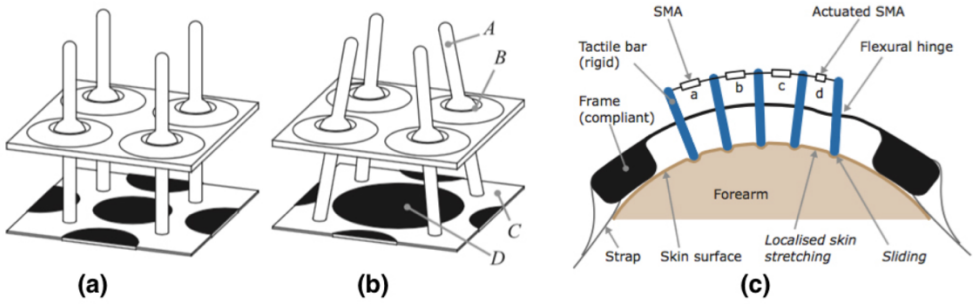

Figure 3-9 Laterotactile display. Left: unactuated. Right: Actuated. A) Stimulating pin, B) Ball joint, C) Dielectric membrane, D) DEA active area (Knoop and Rossiter, 2015).

DEAs appear to be a promising actuation technology for wearable fingertip mounted devices. In effect, they make it possible to create electromechanically generated forces in a compact, lightweight and compliant form factor. DEAs have been shown to apply forces up to 0.6N transmitted through a soft compliant membrane (Frediani et al., 2014b) but are yet to be formed into a wearable multi-finger system. As identified with the soft interface pneumatic systems reviewed, the transmission of forces to the user's fingertips has a number of advantages relating to comfort and suitability in rendering interactions with soft compliant virtual objects, as for medical simulation scenarios. The primary limitation with this technology is typically high driving voltages required, which make circuit design and placement more of a difficulty; but this approach still appears suitable for completely wearable multi-fingertip systems.

3.3 Discussion

In this survey, a number of actuation technologies have been reviewed. Each of the technologies appears to have advantages and disadvantages when considered for use in a multi-fingertip wearable tactile display system. The table presented below classifies these actuation technologies with respect to the following dimensions: related mechanical induced tactile sensation, core advantages/ disadvantages for use

in a wearable multi-fingertip system, weight on the fingertip, max force output, associated reference.

Table 3-1: Actuation technologies used in fingertip mounted wearable tactile display with state of the art example.

Actuation technology	Induced tactile sensations	Core advantages	Core limitations	Weight on fingertip (g)	Max force out (N)	Reference
Vibratory motor	Vibrational	Compact form factors, light weight, simple and compact wearable controlling circuitry.	Limited to rendering vibrational sensations, noisy, discomfort over long periods of use.	1.7	NA	(Murray et al., 2003)
DC motor/ servo	Pressure, indentation, shear.	Can apply forces with high degrees for freedom to simulate more complex tactile interactions. Compact wearable driving circuitry.	Noisy operation, can be large and bulky depending on DOF complexity and servo/ DC motor choice.	4.3	2.6	(Kawasaki et al., 2010)
Shape Memory Alloy (SMA)	Pressure, indentation, shear.	High forces, light weight, compact form factor, simple and compact wearable controlling circuitry.	Slow response speeds.	7.2	6	(Hwang et al., 2017)
Pneumatic/ microfluidic	Pressure, indentation.	High forces, low weight, compact form factor. Can be used to render forces through a soft compliant interface. Conforms to user's fingertip pad.	Non-wearable and complex driving system.	0.65	2	(Culjat et al., 2008)
Dielectric elastomer actuator (DEA)	Pressure, indentation.	Low weight, compact form factor. Can be used to render forces through a soft compliant interface. Conforms to user's fingertip pad.	High driving voltages required, Low forces.	~20	0.6	(Frediani et al., 2014b)

From table (3-1), it is clear there is currently no ideal multi-finger wearable system capable of rendering soft forces to induvial fingertips. Vibrotactile actuators are easy to embed into wearable gloves, and the controlling circuitry is relatively simple and

wearable too. The primary issue is that these devices are limited to rending vibrational sensations. Although vibrational intensity can be used to represent contact pressure, or any another scalar value; the realism of the tactile interaction is constricted to vibrational sensations. The more complex, higher degrees of freedom devices that use various configurations of servo or DC motors address this issue. But these devices tend to be too large as to be worn on multiple fingertips simultaneously. Plus, they have other limitations concerning noise of operation and jittery un-naturalistic tactile feedback sensations. Pneumatics that can delivery forces through a soft compliant interface offer this realism and have been shown to be useful in medical simulation contexts and also within telerobotic control scenarios. But due to the requirements of pumps, regulators, valves and the powering system needed to drive these components; these devices are typically tethered to a grounded control unit. SMA's appear to the ultimate solution with regards to compactness and wear-ability of the entire system, as well being able to generate high forces on the fingertip. But the slow response speed of the actuator is a major limiting factor, limiting its suitability for rendering dynamic virtual interactions in a realistic fashion. Lastly, DEAs can have fast response speeds, generate significant forces and have been demonstrated in a single fingertip wearable system. But currently there is not a compact and lightweight design proposed that can be worn on multiple fingertips for the purpose of rendering soft tactile force interactions in VR/AR scenarios.

3.4 Summary

In this survey, a number of actuation technologies have been reviewed. DEAs appear to the most promising technology in rendering forces to multiple fingertips through a soft compliant fingertip mounted interface. The ideal system will be as follows:

1. Be as compact as possible, as to fit within the dimensions of the finger pad area
2. Be as lightweight as possible, as to not burden the user when worn on the fingertip
3. Be able to be worn on multiple fingertips of the same hand simultaneously
4. Be able to render significantly perceivable forces to the user in a comfortable fashion
5. Be able to be used in conjunction with a low cost optical tracking system, such as the Leap Motion sensor, as to be easily integrated with VR/AR environments
6. Be electronically driven by a lightweight and compact wearable system.

The next chapters will focus on the design and fabrication of such a device.

4 Development of multi-finger soft tactile display

The primary objective of this thesis is to develop a wearable tactile haptic device that can be worn on multiple fingertips for the purpose of rendering soft tactile force interactions in VR/AR scenarios. To these means, DEAs have been identified as a promising actuation technology. Previous work by (Frediani et al., 2014b) have shown the use of this technology for a single finger tactile display; but there are apparent limitations concerning size, weight on fingertip, force output and integration with optical hand tracking systems; which make it unsuitable for a multi-finger approach as required in this work.

In this chapter, DEAs, more specially HC-DEAs, will be reviewed further with a particular focus on Frediani et al (2014) original single finger haptic device, which represents the state of the art in wearable tactile devices using DEA technology. From this, several areas of investigation will be conducted to improve the design and construction methods for a wearable multi-finger soft tactile display system.

4.1 HC-DEA structure

The Hydrostatically Coupled-DEA (HC-DEA) configuration enables a safe transmission of forces generated from electromechanically active dielectric elastomer membranes, which typically have high driving voltages within the kV range. Effectively, a planner DEA membrane, as described in section 2.3, is coupled to a passive membrane through a liquid medium. The electromechanically active membrane, or active membrane, is clamped to the passive membrane with the coupling fluid sandwiched between to form a bubble shape as illustrated below:

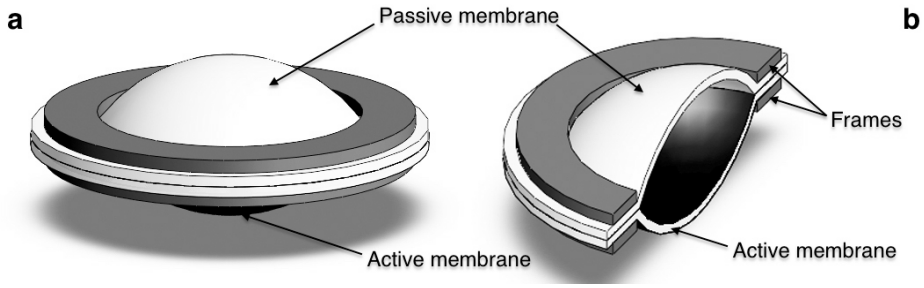

Figure 4-1 HC-DEA configuration

The membranes are held in place by two rigid support frames which have serval functions. Firstly, they help maintain the optimal prestretch of the elastomer

membranes. Secondly, they act as a lateral constraint to maximize actuation in the axis perpendicular to the frames. The coupling liquid, typically a silicone gel, is ideally incompressible and insulting as to transfer the electromechanically generated forces from the high voltage active membrane to the passive membrane.

4.2 HC-DEA operating principles

As mentioned previously, the HC-DEA couples an electromechanically active membrane to a passive membrane through an incompressible insulting gel. When a voltage is applied across the active membranes compliant electrodes, a resulting Maxwell stress occurs, resulting in an expansion of the surface area. As this membrane has a pre-curvature, due to the aforementioned bubble configuration, as well as being constrained by the rigid support frame, the active membrane buckles outwards, effectively forming a larger spherical cap. As the coupling medium is incompressible and thus of fixed volume, the expansion of the active membrane region causes the passive membrane to decrease in area to compensate, forming a proportionally smaller spherical cap on the passive region (Carpi et al., 2010b). When the voltage across the membranes is ceased, the active membrane transitions back into a relaxed state, thus causing the active membrane to decrease in area and passive membrane to increase to compensate.

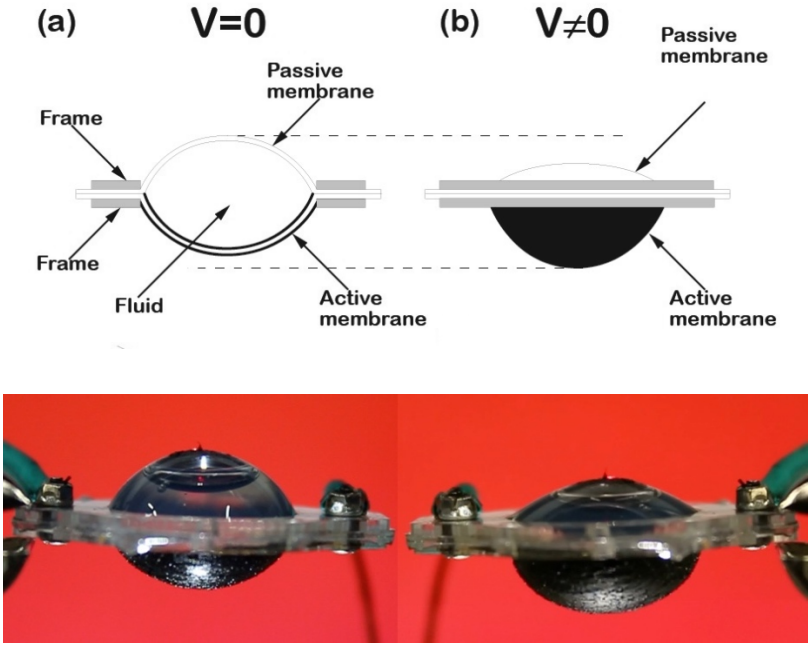

Figure 4-2 Schematic and photographic illustration HC-DEA actuation states. (a) Left show the actuator at rest with no voltage applied to active membrane, (b) Right shows expansion of the active membrane due to the application of a voltage and the corresponding reduction in the passive membranes area.

The hydrostatically coupled DEA configuration caters for two desirable features for wearable tactile displays. Firstly, the aforementioned way to protect the user from the potentially high voltages applied across active membrane; and secondly, the hydrostatic coupling transfers the forces, which can be applied to the passive region by the user's finger, evenly across the active membrane surface area. Reducing the risk of localised thinning caused by perturbation, which can lead to premature electrical breakdown (Frediani et al., 2016).

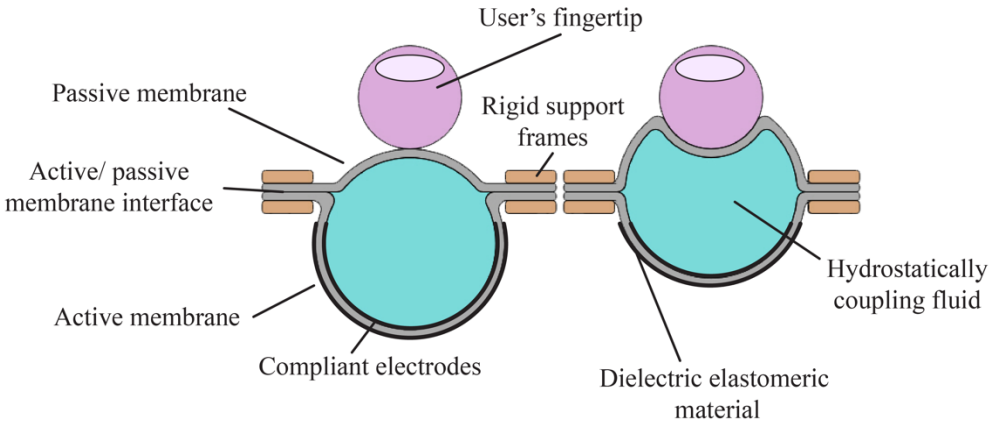

Figure 4-3 Schematic illustration of HC-DEA transferring force to user's fingertip. Left voltage is applied across active membrane, reduced force applied to user's fingertip; Right, voltage reduced, increased force applied to fingertip.

One of the disadvantages of this configuration, is that the maximum force is applied to the user's fingertip when the voltage is zero, and thus the minimum force is applied when the voltage highest. It would be preferable for the minimum force to applied when the voltage is zero, as to allow the best fitting and removal of the device to the user's fingertip when the voltage is off. If the device was also capable of rendering forces that are higher than the comfortable limit of the user, maximum force when the voltage is off could also be a safety concern.

4.3 General HC-DEA construction method

The general construction process of the HC-DEA is as follows.

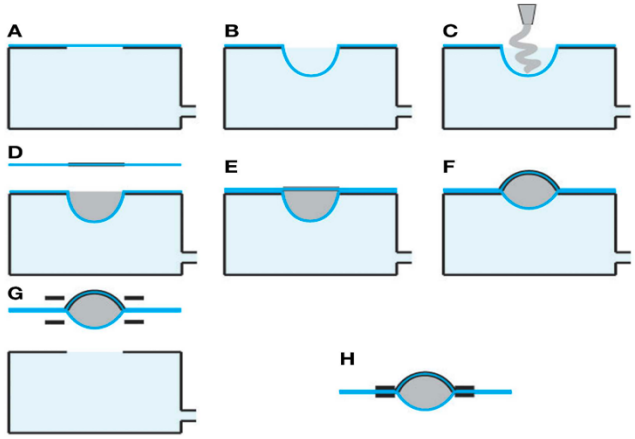

Figure 4-4 Frediani et al (2014) HC-DEA Fabrication process, described in detail below.

A sheet of the film used for the passive region of the HC-DEA is placed over a vacuum and deformed into a cavity due to a vacuum pressure (illustrated in A-B in fig 4-4). A liquid is then injected into this cavity (C). The active membrane, which consists of a dielectric film with compliant electrodes on opposing sides, is then placed over the top to seal the cavity and enclose the liquid (D-F). The layers are typically held together by the adhesion properties of the films used. After the bonding of the active and passive membranes occurs, the vacuum is released. The now formed bubble is then sandwiched between two rigid support frames (G) to form the final HC-DEA configuration (F).

4.4 Design review of current state of the art HC-DEA fingertip tactile device

Frediani et al (2014) proposed the design shown in figure (4-5) as a system to render soft tactile forces to a single fingertip. Its composed of HC-DEA encased within a 3D printed housing that also contains a low-to-high voltage DC converter and load resistor. Power is supplied via a low voltage (0-5V) cable from a wrist-mounted control unit. The device is held to the fingertip with the use of a stretchable fabric.

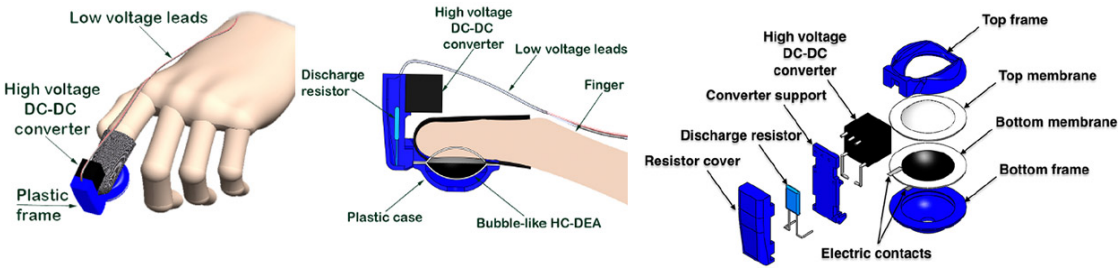

Figure 4-5 Design of single finger tactile display with labelled components. Left: Render of the device placed on index finger. Middle: cut view of HC-DEA stimulating fingertip. Right: Exploded actuator (Frediani et al., 2014b)

4.4.1 Construction process of existing HC-DEA for single finger device

The active and passive membranes for the existing HC-DEA device consist of 1mm VHB film stretched. VHB film is a commercially available material typically used as adhesive tape (VHB 4910, 3M, USA). The reasons for this choice are that the 1mm thick film offers more durability and deformation resistance as opposed to thinner VHB films.

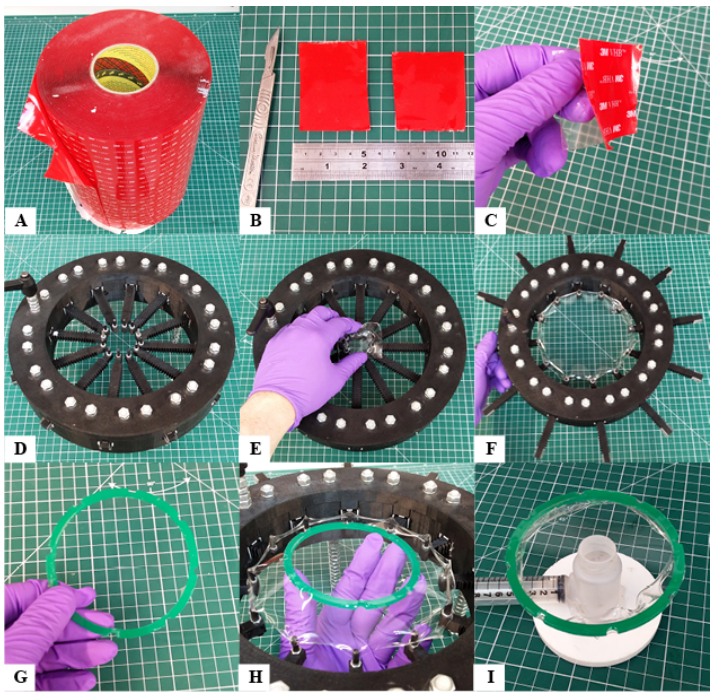

Figure 4-6. Bi-axial prestretch process of VHB 4910 dielectric film, highlighting how the commercial grade material transitions from roll to the acrylic circular support frame.

In the above figure, the pre-stretching of VHB film onto a circular frame is demonstrated. The film is cut into 50mm square tiles. The un-stretched VHB film is then placed onto a radial pre-stretcher and stretched by a factor of four, a pre-stretch amount that has been shown to demonstrate the optimal electromechanically generated strain (Koh et al., 2011a).

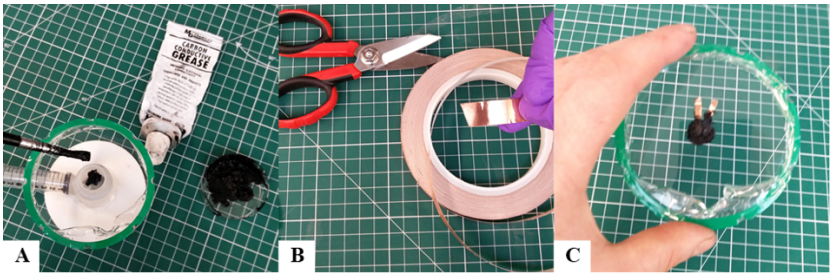

Figure 4-7 Steps to create the active membrane

The figure above outlines how the active membrane is constructed. In step A) a circular electrode is painted with conductive carbon grease. This is done by hand and applied with a fine-tipped paintbrush. The top diameter of the vacuum cavity is used as a guide to make sure carbon grease is not applied outside of the active area, this is because the carbon grease will affect the adhesion characteristics of the VHB film in an adverse fashion, which in turn will affect how well the active membrane bonds to the passive membrane. Caution has to be taken to apply the carbon grease neatly, as this will affect how the active membrane deforms. The frame is then flipped and carbon grease is applied to the opposite side to form the opposing electrode. B demonstrates copper foil cut into (approx.) 3mm by 12mm strips. These strips are then placed in the configuration demonstrated in C, this completes the construction of the active membrane part of the HC-DEA.

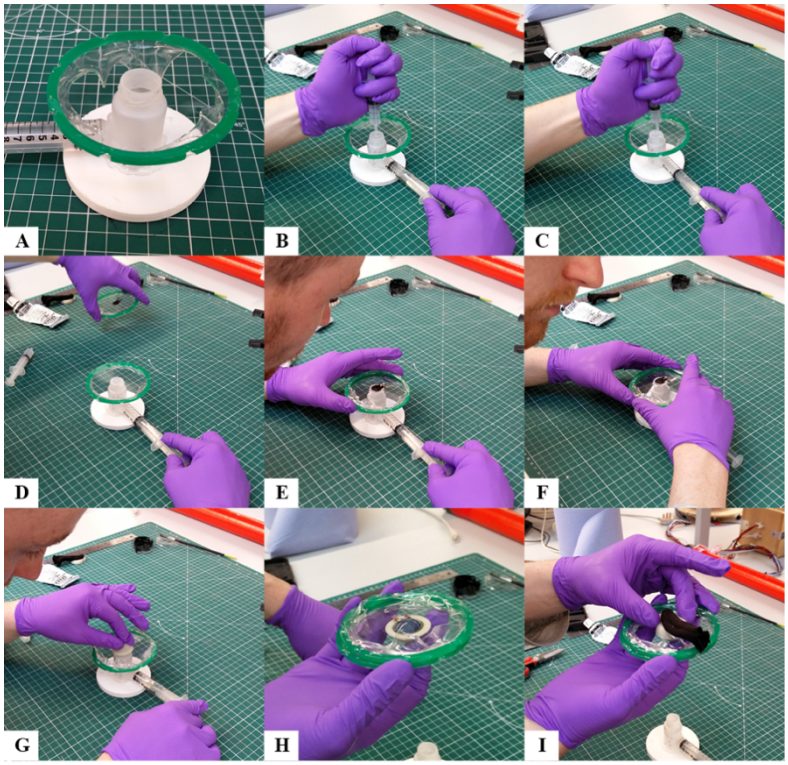

Figure 4-8 Process of forming the HC-DEA bubble

The next stage is to create the passive membrane. Here the same steps are followed as shown in figure (4-8). The frame with the pre-stretched VHB, which will form the passive side, is then placed over the cavity of the vacuum chamber as shown above in A. The next step is to create a cavity in the VHB film by creating a vacuum pressure by drawing out the syringe plunger of the negative pressure chamber. 1ml of a non-conductive silicone gel is then deposited into the cavity by use of a syringe. In this case, Transil 40A is used as it is a low viscosity silicone gel. The active membrane created previously is then placed over the top and held in place (D-F). The bottom half of the actuator frame is then placed over the active side and pressure is applied (G). The syringe that created the negative pressure is then gradually released until it is possible to withdraw the now formed bubble from the vacuum chamber. The top half of the actuator frame which also has the fabric finger attachment is then placed on top of the passive side. Speed has to be taken in this step as the bubble tries to increase to a size larger than that of the diameter of the cavity of the vacuum. This is due to the bubble trying to find the equilibrium state between the adhesion of the VHB layers and the pressure created by the elastic properties of the VHB film.

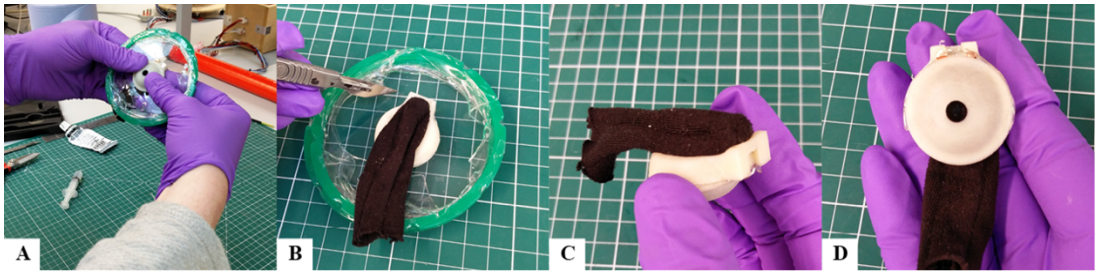

Figure 4-9 Final steps to create a HC-DEA fingertip tactile device

Before the device can be cut out of the frame, a pressure is applied by hand to increase the adhesion between the layers of the HC-DEA and the outer frame. Once the excess VHB is trimmed away the device is now ready to be mounted to the low-to-high voltage unit placed at the end of the of the device where the copper contacts can be seen in (D).

4.4.2 Review and possible improvements of existing HC-DEA construction process for single finger device

The existing fabrication process requires a significant amount of skill and patience, and thus is incredibly difficult to reproduce in a consistent and timely fashion. Considering how much time is required to make each actuator with this process (~>1 hour), and the amount of failure that can occur at each step; a new process and design is to be developed. Several areas have been identified to these means:

Stretching error

A bi-axial pre-stretch of 400% has been demonstrated to be optimal for VHB 4910 films (Koh et al., 2011a), as this is the point where optimal electromechanical induced strain is achieved without risking material rupture due to overstretching and premature electrical breakdown. The proposed HC-DEA configuration has effectively two prestretch stages during fabrication. One where the membrane is initially radially stretched, and the other when the membrane is formed into a spherical cap. Electromechanical tests need to be conducted in order to determine the correct ratio of initial radial prestretch, volume of inner coupling fluid and diameter of bubble/ support frame.

Controlled bubble diameter

In the current method to produce a HC-DEA, the size of the diameter of the bubble is initially formed by the cavity diameter of the vacuum chamber. The support frames of

the HC-DEA, that have a larger diameter than that of the vacuum chamber, are then used to sandwich the HC-DEA membranes. To get the volume of gel into the bubble, the VHB film has to be deformed into the smaller diameter of the negative pressure chamber cavity. Considering that the vacuum cavity diameter is 16mm and the outer support frame is 21mm, the membrane that forms this cavity, in which the coupling gel is inserted, has to be over-stretched by a significant amount, which can sometimes lead to mechanical failure. A way to address this is to have a support frame that matches the diameter of the vacuum cavity and perhaps have a frame that can be placed in-between the VHB and negative pressure chamber itself as to maintain the diameter.

Application of compliant electrode

Currently, the carbon grease is applied with a paintbrush using the negative pressure cavity diameter as a guide. This process is the most time-consuming aspect. Care has to be taken not to paint outside of this diameter as it will negatively affect the adhesion between the different layers of VHB film. One possible method to improve the neatness as well as improving the time it takes to apply the electrodes could be to use a stencil made from a non-stick grease proof paper, and experiment with a cured compliant electrode, that will not have significant effects on the adhesion of the VHB membranes.

Rigid circuitry to soft DEA interface

Frediani et al (2014) current design uses the support frame of the HC-DEA actuator as the fingertip attachment method and as the shielding casing to the high voltage active membrane of the actuator. As the HC-DEA bubble actuator is sandwiched between these two layers, VHB spreads outside of the diameter of the frame. This also causes the copper electrical contacts to move from their original positions. It is then possible for the copper electrical contacts to not be fully encapsulated within the device, which could be potentially hazardous as well as leading to a temperamental electrical contact.

Compression of the VHB layers

In the current design, the support frame of the HC-DEA is also the outer casing of the device. To improve the adhesion and bonding between the different layers of VHB,

the outer casing could be designed to provide an additional clamping force between the layers.

4.4.3 Summary of existing HC-DEA fingertip tactile device limitations for multi-finger adaptation

As identified from the design study of the construction process of Frediani et al (2014) HC-DEA fingertip tactile device; there seems to be a number of areas of development that could potentially improve the performance of the device in areas such as safety, robustness and manufacturing consistency. The text below outlines some of the physical issues with the current design which makes it unsuitable for use within a multiple fingertip system:

A) Due to the diameter of the device (~30mm) it is currently only possible to use this system on one finger.
B) The high voltage circuitry placed on the fingertip adds weight and size affecting dexterity.
C) The method for attaching the device to the finger currently requires multiple free fingers and is not adaptable for differently sized fingers, nor does it locate the device to a consistent fingertip position.
D) The device is only held together by the adhesion characteristics of VHB film that form the HC-DEA.
E) The shape of the device impedes its uses with optical hand tracking systems.

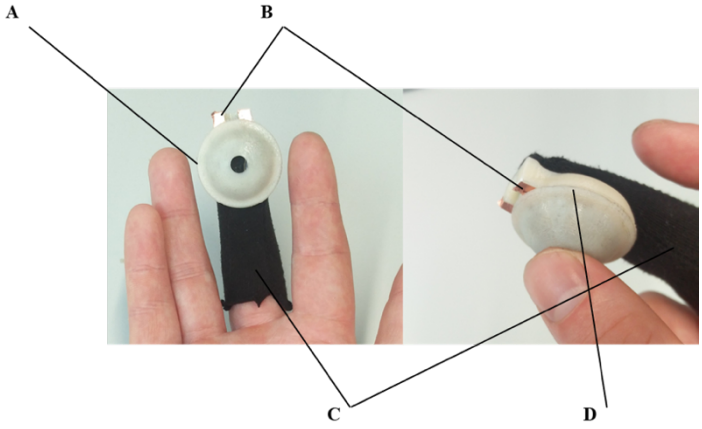

Figure 4-10 demonstrating some of the physical flaws of the device which makes it unsuitable for a multiple fingertip device. A) Highlights a diameter larger than the lateral width of the fingertip. B) Risk of exposure to electrical contacts. C) Non-adjustable fingertip attachment. D) Device reliant on adhesion properties of VHB film.

4.5 Design and fabrication of a compact higher force generating HC-DEA for a multi-finger tactile display

Here the design and construction methods of the HC-DEA proposed in this work are presented. One of the key design features of this work is that the HC-DEA is produced separately to the encapsulating outer casing. This is beneficial for several reasons. Firstly, it enables the actuator to be easily changed and replaced in case of failure. Secondly, this approach enabled better containment of the high voltage components of the actuator. Lastly, this approach simplified manufacturability of actuator, which resulted in less failure and more consistency during production.

The requirements for the development of this actuator are as follows:

1. Be safe for the user to interact with
2. Be as compact as possible
3. Provide a secure method in which to attach high voltage transmission cables
4. Generate as high as possible electromechanically controlled uniaxial forces
5. Be robust
6. Be consistent in performance and manufacturability

To this means, the following design is presented:

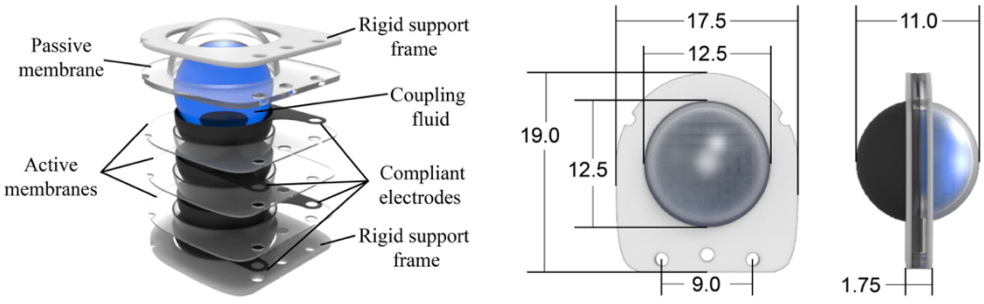

Figure 4-11 Left: Exploded rendering of the proposed HC-DEA in this work, with labels identifying the key components. Right: Dimensions of the final actuator given in mm.

The design and fabrication of some of the key features, such as the rigid support frame, application of compliant electrodes, formations of multi-layered membranes and final formations into HC-DEA are discussed in the following sections.

4.5.1 Rigid support frame

The support frame serves two main tasks: maintain the lateral diameter of HC-DEA during actuation and maintain prestretch of the dielectric. For the design in this work, it also serves a third purpose, which is to act as a rigid fixation point in order to secure the high voltage signal transmission cables which are discussed later on. Below demonstrates some of the key dimensional considerations in the support frame design.

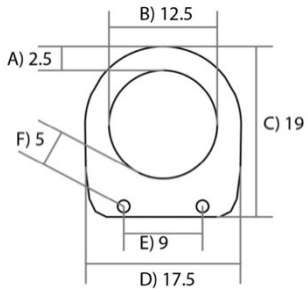

Figure 4-12 Support frame schematic with dimensions in mm.

In figure (4-12), a schematic illustration shows the key considerations in the design of the support frame which are outlined below:

A) Dictates the radial adhesion area of the passive and active membranes. If higher forces are to be generated, by using stiffer active and passive membranes; the adhesion between the layers needs to be strong enough to cope with the increased pressure on this seam
B) This dimension sets the lateral diameter of the actuating HC-DEA bubble
C) Length of the actuator placed on the fingertip
D) The lateral width of actuator across fingertip
E) The voltage applied across the actuator is supplied through these holes. If the holes are too close together, it is possible for sparking to occur due to the electrical breakdown limit of air (~3kV/mm)
F) Again, if this distance is too small sparking can occur

The support frame is laser cut from a 0.5mm acrylic sheet (Plexiglas, Evonik, Germany) with a layer of double-sided Kapton tape (DuPont, USA) applied to one side, see figure (4-13). This is to increase the addition between the VHB film and the rigid support frame.

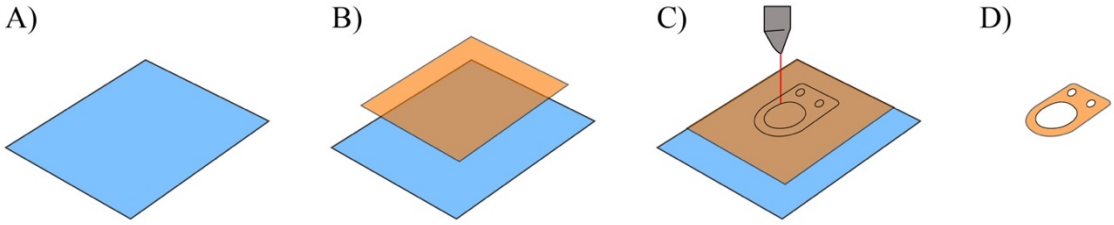

Figure 4-13 A) 0.5mm acrylic sheet (Plexiglas, Evonik, Germany) B) Addition of double sided Kapton (DuPont, USA) tape C) Layers cut using a laser cutter, D) Final support frame.

As the support frame is effectively flat, it can then be placed on both the active and passive membranes before the cavity and fluid insertion steps. This means the lateral bubble diameter better maintained at the diameter of the support frame.

4.5.2 Compliant electrode and application

To improve the neatness and speed of compliant electrode application, a mixture of silicone and carbon black was applied to dielectric membranes using an airbrush and laser cut stencil. The mixture is formed from carbon black powder (Black pearl 2000, Cabot, USA) added to an uncured silicone pre-polymer with its accompanying curing agent (CF19-2186, Nusil, USA) at a ratio of 1:10 by weight. To ensure a more homogenous mixture; a planetary mixer was used to mix the components. A vacuum was then employed to remove air bubbles from the mixture. The stencil was laser cut out of a greaseproof paper to the shape and dimensions as illustrated below.

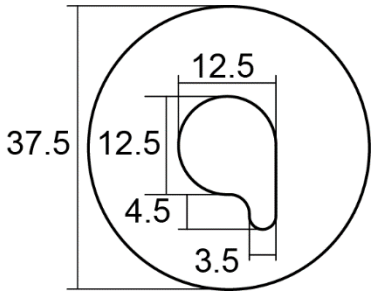

Figure 4-14 Layout of the stencil mask for the application of the sprayed-on compliant electrode.

The larger 12.5mm circle represents the overlap area of the electrodes in the HC-DEA. The smaller protruding tabs are used to provide electrical contact between the voltage supplying cables and compliant electrode surfaces. Once the mixture was sprayed onto the dielectric membranes using an airbrush and fume cupboard. The mixture was cured at room temperature for 10 mins. The resulting compliant electrodes had an average sheet resistance of 45 kΩ/sq as measured according to the procedure described by the standards for DE transducers (Carpi et al., 2015).

4.5.3 Construction of the multi-layered active and passive membranes

To increase the force output of the HC-DEA, a multi-layer structure for the active and passive membranes, consisting of dielectric elastomer layers intertwined with opposing compliant electrode layers was developed. The process to form the multilayer active membrane is illustrated below.

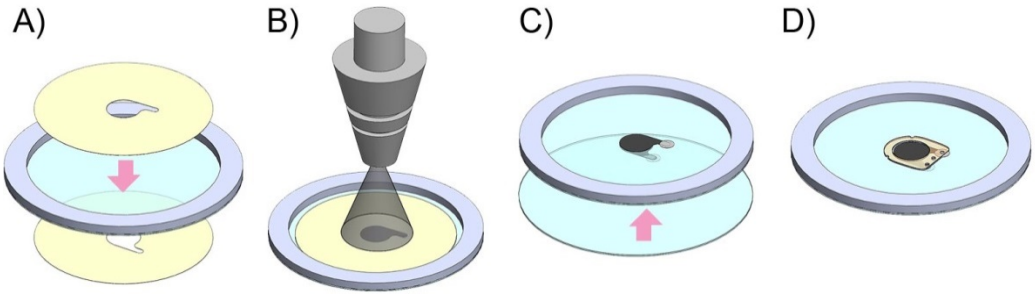

Figure 4-15 Fabrication of the active membrane. A) Addition of laser cut stencils to membrane material. B) Spraying of the compliant electrode. C) Addition of another pre-strained membrane. D) Support frame added to one side. Steps A to C is repeated depending on the number of layers required for the membrane.

Firstly, 1mm thick VHB film (VHB 4910, 3M, USA) which had been pre-strained in the process described previously, is applied to a laser cut 3mm thick acrylic ring. The aforementioned stencils are applied to either side of the film (A). The compliant electrode mixture is then sprayed on to either side and cured at room temperature for 10mins (B). Once the stencils are removed, aluminium foil cut into 4mm circles is then placed at the end of the electrical connection tabs of the compliant electrodes. The aluminium improves the connection reliability of the electrical contacts which is discussed later on. Pre-strained layers are added carefully as to avoid trapping air between the layers (C). The passive membrane is formed in a similar fashion, except compliant electrodes and aluminium are not applied. Support frames are then attached to one side of the now formed active or passive multilayer membranes (D).

4.5.4 Formation into HC-DEA Bubble configuration

Here, the formation of the HC-DEA bubble is discussed as illustrated below.

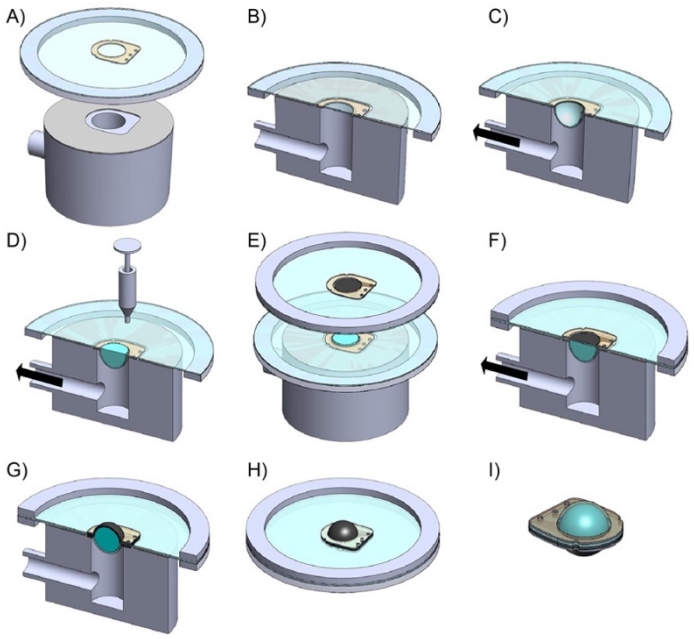

Figure 4-16 Illustration of the process to construct the HC-DEA design presented in this work. Black arrow illustrates the application of negative pressure.

Once the active and passive membranes are constructed as outlined previously; the passive membrane is then placed on a specially designed negative pressure chamber so that the support frame is in-between the top part of the negative pressure chamber and membrane material (B). The top part of the chamber is covered by a laser cut PTFE sheet (Teflon, Chamours, USA), this prevents adhesion to the VHB membrane. Negative pressure is created by a vacuum pump, which causes a cavity to be created in the central region. A predetermined volume of coupling fluid is inserted into this cavity using a syringe (D). For a 12.5mm in diameter bubble actuator, this is calculated to be 0.8ml. In this work dielectric silicone grease (8462, M.G. Chemicals, Canada) is used as the coupling fluid. The silicone grease was chosen as there is a chemical incompatibility with the acrylic-based VHB film, this prevented the grease defusing through the film and also prevented premature rupturing along active and passive membrane bonding interface. The active membrane is then placed over the cavity and aligned using the support frame (E). A pressure is then applied to increase the bonding between the active and passive membrane interface (F). After a period of 5 minutes, the negative pressure is realised (G). The frames can now be released from

the top of the chamber (H). The last step is to use a scalpel to cut out the now formed HC-DEA (I).

4.6 Design of outer casing for multi-finger HC-DEA tactile display

Here the design of the outer casing is presented. The general role of the outer casing is to protect the user from the high voltage areas of the HC-DEA, allow the actuator to move freely in a motion perpendicular to the support frames and provide a method of attachment to the user's fingertip. For the multi-finger system developed in this work there are some additional requirements which are described as follows:

1. Provide a secure and insulated method to attach the supplying high voltage transmission cables to the HC-DEA.
2. Provide an additional clamping pressure to the HC-DEA to hold layers together and prevent leakage of the coupling fluid, as well as shield high voltage areas.
3. To not impede tracking of the fingertips by a low cost optical tracking device.
4. Be able to be worn on multiple fingers of differed shapes and sizes.

For these means, the following design is presented.

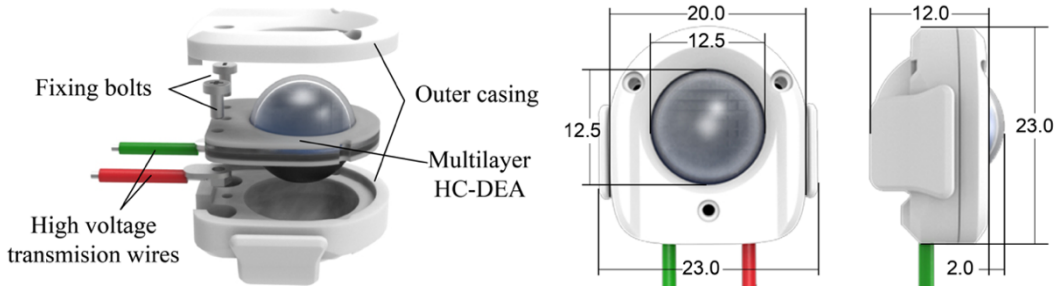

The design considerations and fabrication processes of some of the key features; such as the high voltage transmission wires, additional clamping of the HC-DEA, fingertip attachment method and integration with the optical tracking system are discussed in the subsequent sub sections.

4.6.1 Voltage supply cable to compliant electrode interface

To lessen the weight and bulk from the fingertip, the low-to-high voltage unit is no longer placed on the fingertip. This enables less weight on the fingertip and the ability to encase the HC-DEA in a more compact package. The high voltage required to drive

the HC-DEA is thus supplied high voltage transmission cables. To these means a method to securely attach these cables to the different layers of the multi-layered HC-DEA has to been developed, as the detachment of these wires could be potentially hazardous.

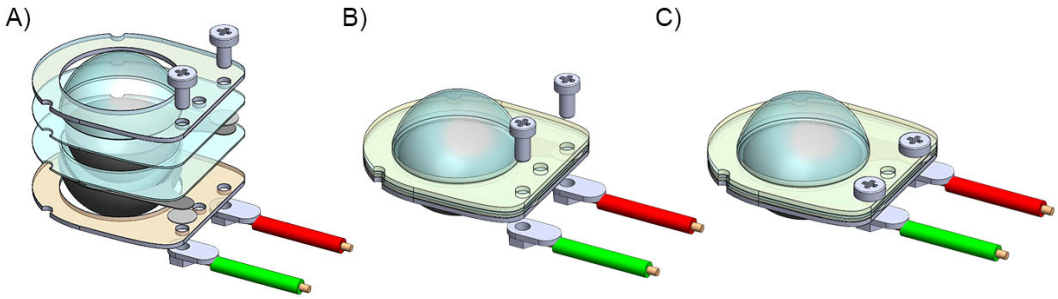

Figure 4-17 Schematic illustration of the attachment of the high voltage transmission cables. A) shows an exploded view of the different layers of the HC-DEA which have to connect to the wires. B) shows the bolts that penetrate the different layers of the HC-DE. C) Final attached configuration.

The above figure (4-17), shows this attachment method. As can be seen, bolts penetrate the layers of the HC-DEA and are connected to a custom-made solder tab with an M1 screw thread. The transmission wires are then soldered onto to these tabs. In this work, 2mm thick coaxial cable is used as it provides added electromagnetic shielding as well as being relatively thin and flexible to allow for the movements of the fingertip. One of the main advantages of this penetrating bolt method is that increasing the number of layers used in the construction of the HC-DEA does not increase the complexity in connecting the electrode surfaces.

4.6.2 Additional clamping pressure to the support frame of HC-DEA

A specially designed outer casing that further clamps the layers of the HC-DEA together, locks the cables in place and also prevents the high voltage areas from being exposed to the user has been developed. The final casing was produced by a 3D printing process, in this case, an Object30-Pro (Stratasys, USA) printing a translucent resin (VeroClear-RGD810, Stratasys, USA).

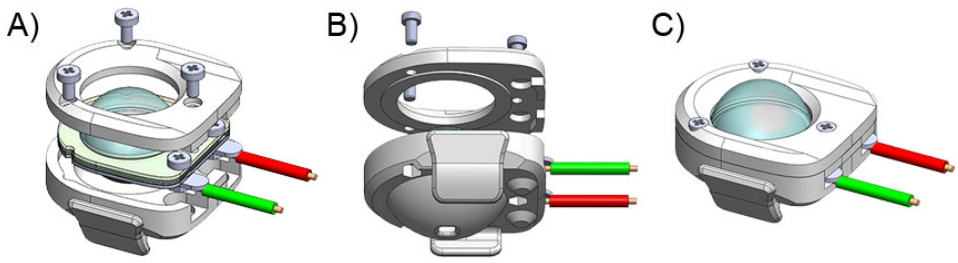

Figure 4-18 Schematic of the outer casing clamping the HC-DEA and connecting cables in place.

The casing uses three m1 screws to radially clamp the HC-DEA together. As seen in (B) above, there is a 0.5mm protruding ring around the bottom of the top frame which evenly distributes this clamping pressure around the top frame of the HC-DEA.

4.6.3 Fingertip attachment method

To attach the casing to the user's fingertip, a variety of differently sized silicone straps with a thickness 1.5 mm were produced using a transparent silicone elastomer (Transil 40-1, Mouldlife, UK) cured in laser-cut acrylic moulds. The transparent elastic strap allowed for securing the device to the fingertip easily, without precluding optical tracking, see fig (4-19).

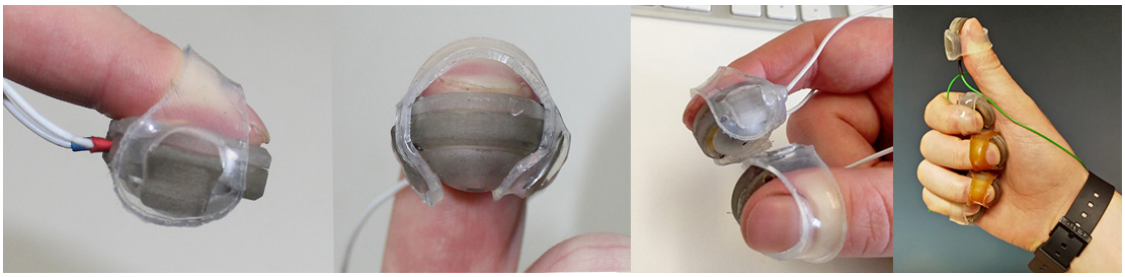

Figure 4-19 Photographs shows the tactile display secured to the fingertips.

4.6.4 Integration with the optical hand tracking system

One of the key requirements of this design is that it has to be compatible with low-cost optical tracking devices, such as the Leap Motion (Leap, USA). Therefore, the device when placed on the fingertip should not occlude or prevent the fingertip from being tracked. To these means, shape and material considerations have been made in the design. Firstly, the dimensions of the device have been made as compact as possible as to fit within the width of the fingertip. The device measures 20mm across the fingertip and 23mm in length and protrudes 12mm in height away from the fingertip. The bottom and top parts of the casing have a domed contour as to be similar in profile to a fingertip.

Several 3D printed materials have been tested in the form proposed to see which works best in conjunction with the optical tracking system. From these tests, it was discovered that VeroClear-RGD810 (Stratasys, USA) appeared to perform the best. From analyses of the stereoscopic infrared images taken from the Leap motion, it appears that VeroClear-RGD810 has similar infrared reflective properties to the skin of the fingertips. Further investigation needs to be conducted to confirm this result.

4.7 Design and development chapter conclusion

In this chapter, a design and manufacturing process for a multi-finger HC-DEA driven tactile display has been presented. This design has delivered a significantly smaller encumbrance to the device (20x23x12mm) as compared to Frediani's initial approach (30x45x20mm) (2014). Therefore, the device is capable of being placed on multiple fingertips simultaneously whilst minimising impedance to fingertip dexterity. The design also makes it possible to increase the number of layers used in the formation of the active membrane, therefore making stiffer higher force generating HC-DEAs possible. The containment of the HC-DEA on a rigid support frame also enables greater control of the actuators' dimensional properties, as well as providing a robust method in which to attach penetrating electrodes. The penetrating electrode design proposed appears to be a robust method in order to connect up the corresponding electrode layers of the multi-layered HC-DEA. The movement of the low-to-high voltage circuitry from the fingertip reduces significant bulk, minimising the weight and size of the device upon fingertip. The device with the silicone strap weighs a total of 6g. Due to the dimensional properties of the device, and the material selection, the device can be used in conjunction with a low-cost optical tracking system without modification of the software.

In the next chapter, a multi-channel high-voltage control unit, capable of driving multiple HC-DEAs simultaneously is presented.

5 Development of a low-cost multi-channel DEA Control system for a multi-finger tactile display

One of the main issues facing EAP devices is the typically high driving voltages required for actuation, within the kV range. Therefore, there is added complexity in the generation, control and containment of such voltages. On top of this, if we want devices for a wearable context, or just to compete with existing actuation technologies, such as coin cell DC vibrator motors; compact and lightweight circuitry is required. Furthermore, to actuate multiple actuators simultaneously with differing voltages, as is required for a multi-fingered DEA tactile display, a system capable of generating the voltages required for each actuator within the system has to be developed. This chapter explores the development of such a system.

5.1 Existing high voltage driving systems for DEA devices

Within the EAP field, they are two primary commercial suppliers of High voltage driving equipment. Firstly, we have the bench top driving solutions from Trek (USA, 2017), and then we have the miniaturised low-to-high voltage components by Emco (USA, 2017). This section discusses the advantages and limitations of both.

5.1.1 Trek benchtop solution

Figure 5-1 Trek 615-10 10kV high-voltage AC/DC generator (source: http://www.trekinc.com/images/products/AMPLIFIERS/615_10.png)

The model 615-10 is a large cumbersome workbench machine. On top of this, it costs within the region of £10,000. What is good about this unit is the great performance in terms of consistent high voltage output, and also embedded control features such as high frequency (within kHz) sinusoidal, square wave or sawtooth high voltage signal generation. It can also be proportionally controlled by remote low voltage DC signal. It also has a feature which caters for high voltage and current monitoring with a 0-5V signal output. But as this device is a 15 kg, plugged into the mains workbench

solution, it not really suitable for wearable portable solutions. Also, as this device is capable of generating up to 10 kV at tens of mA, it is completely overpowered considering the context of use, and therefore can be considered as a potentially hazardous machine, unsuitable for applications involving human users.

5.1.2 Emco miniaturised component solution

Figure 5-2 Emco low-to-high voltage DC-DC converter to convert a 0.7-5V input signal to 0.7-5kV. (source: http://www.emcohighvoltage.com/images/EMCO_Q_Series.jpg)

This 2cm^3 component weighing only 4 grams is capable of turning a low voltage analogue DC signal into a high voltage signal, adequate for driving DEA devices. For the particular model used in this work, model Q50-5, linear conversion of a 0.7-5V input voltage is translated to a 0.7-5kV output signal, with a maximal input power consumption of 0.7W.

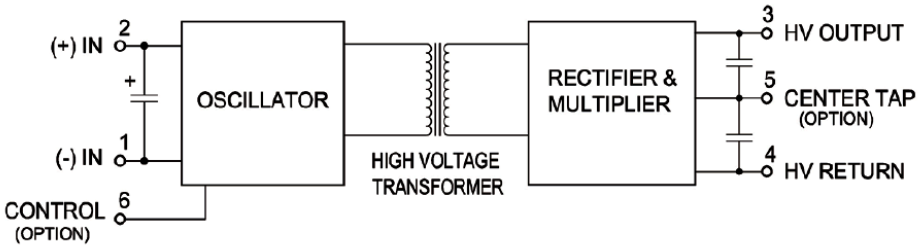

Figure 5-3 Block diagram of Emco DC/DC converter. The Q50-5 model does not have the control pin 6, nor the centre tap pin 5 (source: http://www.emcohighvoltage.com/datasheets/qseries.pdf).

As can be seen in the block diagram above, the device delivers a high-voltage conversion by turning the low voltage input signal into an oscillating signal which is then passed through a step-up transformer coil. The AC higher voltage signal induced in the secondary coil is then rectified to a DC high voltage output.

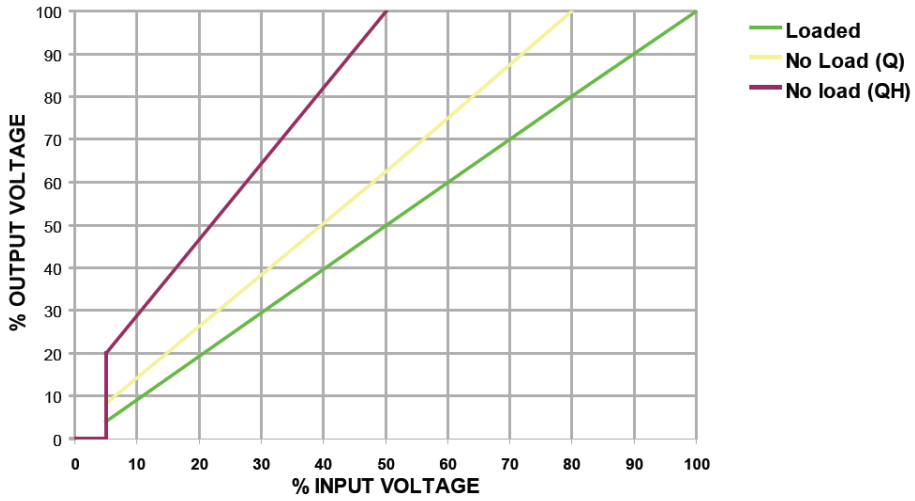

Figure 5-4 Graph showing the input to output voltage conversion ratio for the Loaded and non-loaded Emco converters. The green line represents the performance of the component used in this work (source: http://www.emcohighvoltage.com/datasheets/qseries.pdf)

The loaded component has a linear conversion of input to the output voltage, once an activation threshold voltage has been achieved. For the model used in this work, this input threshold is 0.7V; therefore, only voltages of >700V can be generated controlled with this component. By loaded and unloaded, a load resistance between the two high voltage output pins is required for a loaded system. The load resistor serves two purposes: firstly, for the rectifying circuitry of the converter, enabling the maximum output current available and keeping a stable 1 to 1000 (in the case of the Q50-5 model) input to output voltage ratio. And secondly, as the DEA is effectively a capacitive system, it allows for the rapid discharge of the capacitor when the voltage applied across the DEA electrodes is decreased. This basic circuit is illustrated below.

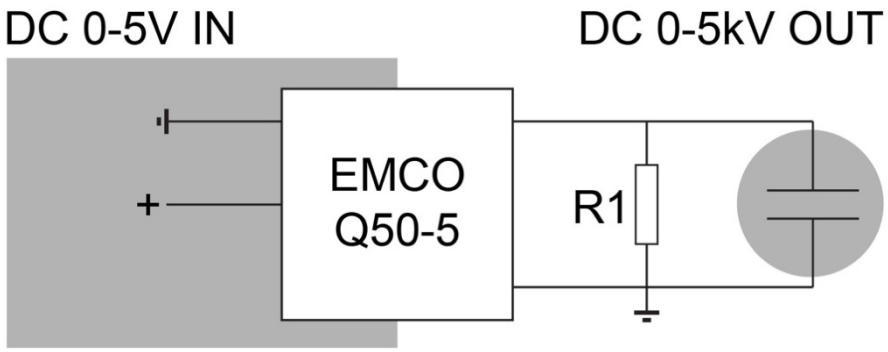

Figure 5-5 Schematic of EMCO Q50-5 with a high voltage load resistor in parallel to the HV output. The Capacitor with the grey circle resents the DEA device, the grey square represents the low voltage input of the circuitry.

The resistor used in this circuit is the HB series high voltage resistor by TE Connectivity Ltd (Switzerland) and has a value of 50MΩ. This value was selected in order to allow the EMCO to operate in the 'Loaded' condition that caters for linear voltage conversion (1:1000), as shown in figure (5-4). In order to allow the EMCO to operate in the "loaded" condition, the datasheet stipulates that a current draw of 0.1mA is required. Therefore, the resistance was calculated with the following equation:

$$R = \frac{Vmax}{Imax} = \frac{5000}{0.1\ 10^{-3}}\ V^2 = 50\text{M}\boldsymbol{\Omega} \tag{5.1}$$

To measure the linearity of the output of the circuit illustrated in figure (5-5), a desktop voltage supply was used to control the voltage across the low voltage inputs of the EMCO. The voltage was measured across the load resistor (R1 in figure 5-5), using a High Voltage probe (Testec TT-HVP40, Germany) at varying input voltages of up to 5V. Load resistors of values 0, 20, 50, 100, 150 and 200 MΩ were tested to access the shift in output voltage. The load resistors used were the HB series high voltage resistor by TE Connectivity Ltd (Switzerland). After 5 successive runs of the test, each result for each resistor at each different voltage level was accurate to within +-0.05kV, as measured with the high voltage probe and multi-meter; therefore, error bounds left out for display clarity.

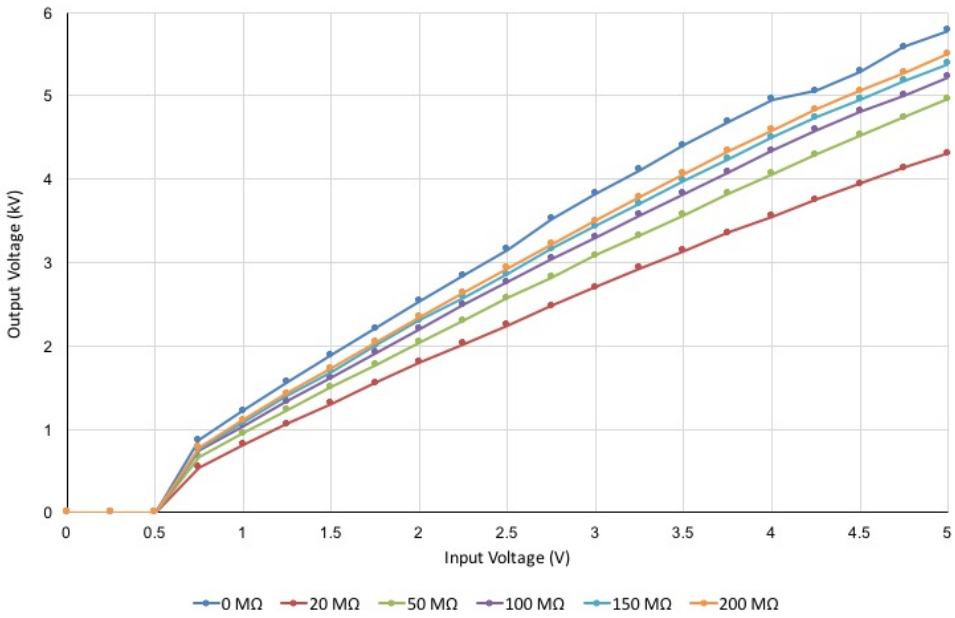

Figure 5-6 Results demonstrating the shift in high voltage output of the EMCO low-to-high voltage DC converter, with varying load resistor values.

One to one thousand ratio of input to output conversion is observed when a load resistor of 50MΩ is used. As expected, an activation input threshold of 0.7kV is required before a linear relationship is observed.

5.2 External micro-controller

In this work, the Arduino UNO and the Arduino 5V Micro (Arduino, Italy) provide the link between controlling software interface and the high voltage circuitry. These systems are capable of generating 0-5V, up to 400mA, pulse width modulated (PWM) signals over nine individually controlled channels. The devices are controlled over a wired USB interface and can be programmed using the C programming language.

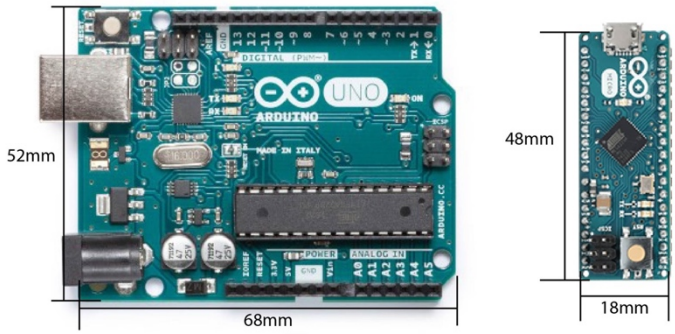

Figure 5-7 Left Arduino Uno, Right Arduino micro

The issues concerning the use of this system to drive the high voltage circuitry outlined in the previous section are firstly, the Arduinos used are only capable of generating Pulse Width Modulated (PWM) output signals which are erratically converted by the Emco low-to-high voltage converters. Secondly, the maximum current output is only 200 mA at 5V, suitable for driving only one Emco Q50-5.

5.2.1 Arduino analogue write, PWM signals and smoothing

The Arduino uses the following C code statement to write a PWM voltage to a specific output pin:

"AnalogueWrite(PWM Pin(int 0-8), PWM value(int 0-255);"

PWM stands for Pulse Width Modulation. As the ATmega32U4 microchip (Microchip, USA)("ATmega328 - Microcontrollers and Processors," 2018) used by the Arduino Micro("Arduino Micro," 2018) and the ATmega328P (Microchip, USA)("ATmega328P - 8-bit AVR Microcontrollers - Microcontrollers and Processors," 2018) used by the Arduino Uno("Arduino - ArduinoBoardUno," 2018), can only produce binary voltage signals, the Arduino employs a trick called PWM to create pseudo analogue signals by using a high frequency binary digital switching technique. In effect, a square wave between 0 and 5V is created with a duty cycle of 490Hz. To create a PWM voltage of 3V, the voltage output of the PWM pin is high for $3/5^{th}$ of that duty cycle. Each duty cycle lasts ~2ms, so the PWM pin would be high for 1.2ms, and off for 0.8ms. The ATmega chips used receives an 8bit value (an integer between 0-255), which then controls the PWM output of the PWM pins. A PWM value of 255 would represent 5V, 127 = 2.5V, 0 = 0V etc.

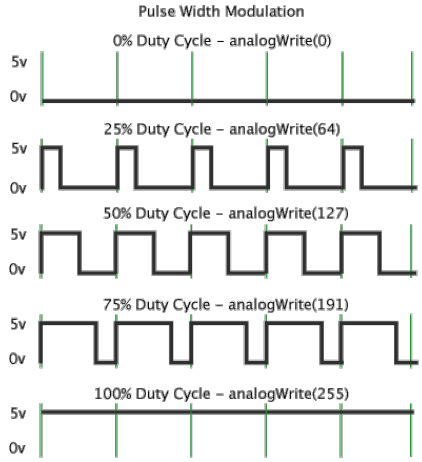

Figure 5-8 PWM diagram, green lines represents 500Hz (2ms) duty cycle. From top to bottom, PWM representative voltages of 0V, 1.25V, 2.5V, 3.75V, 5V.

As the Emco requires a smoothed analogue signal, probably due to the limitations of the high-frequency inverter circuitry used by the EMCO device, the 490Hz PWM output signal of the Arduino is smoothed. To these means, a low pass filter circuit consisting of 150Ω resistor in conjunction with a 4.7μF capacitor is used. These values are selected as a trade-off between response time and reduction of ripple which affected the linearity of the high voltage output from the Emco. Further investigation is to be conducted in order to optimise response speed and linearity of the system.

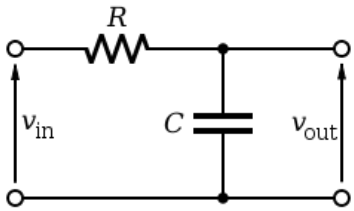

Figure 5-9 Low pass filter schematic, Vin is PWM signal, Vout is the smoothed analogue signal.

The second issue affecting the direct usage of the Arduino micro-controller is the low maximal current draw of 200mA. To meet the current draw requirements of the EMCO Q50-5, an operational amplifier (buffer), in this case, the TCA0372 from Motorola (USA), which has a maximal current draw of 1A is used.

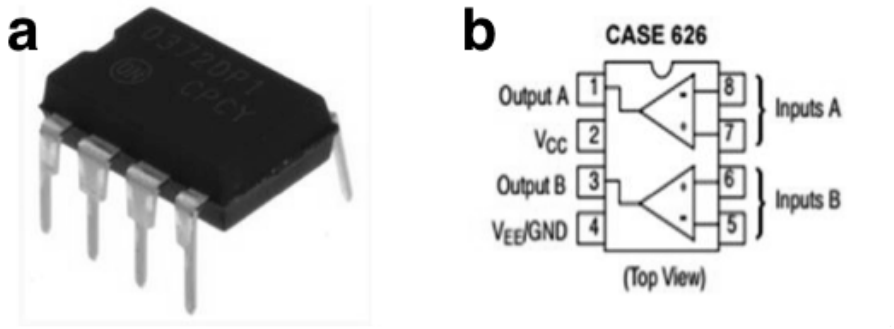

Figure 5-10 A is the TCA0372 operational amplifier, B highlights the pin connections.

This means an alternative 5V power source is required to drive the buffer. As the buffer requires a maximal current draw of up to 1A, two USB 2.0, which each has a maximal current draw of 500mA, can be used. In test setup proposed, a standard UK 230V mains to 5V, 1A DC output transformer is used to supply the power required to the operational amplifier. One advantage of this particular operational amplifier is that it is capable of operational amplification of two separate signals, which means one component can be used to supply the driving signal required for two of the high voltage circuits outlined in the previous section.

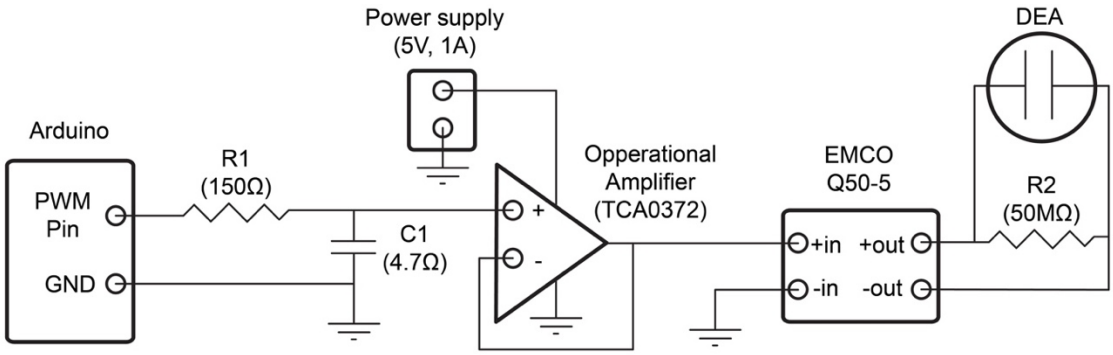

Figure 5-11 Schematic of a single channel DEA high voltage control circuit using an Arduino as the signal generator.

5.3 Multi-channel design

For the purpose of this work, multiple high voltage channels are required to controlled simultaneously; for the purpose of controlling the force rendered by multiple DEA tactile displays. To these means there are two approaches considered in this work; one, use more PWM signal output pins of the Arduino and use these signals to control multiple high voltage circuits listed above; or two, have a single high voltage source which is then multiplexed to control multiple DEAs through an array of rapidly changing transistor gates. In this work, the former is chosen due to implementation

simplicity. The pros and cons of both options will be discussed in the last part of this chapter.

5.3.1 Multi-channel DEA circuitry design scope

The basic requirements of the electronic controlling circuitry are as follows:

1. A robust and clear on and off switch.
2. All the electronics and connections contained within an isolating protective housing.
3. Provide stable voltages across each of the DEAs within the system.
4. Be able to control at least 4 separate DEAs.
5. Be as compact as possible.

The first priority is the safety of the user. Although the power requirements of the system are very low, <0.7W per Emco used; the high voltages involved can spark and cause small electric shocks if not contained. That's why the first two requirements concern safety features. It is important to know the power state of the system, therefore a LED indicating the on and off state is critical, as well as an emergency power cut-off switch.

Functional requirements 3 and 4 concern the ability of the system to control the voltage across multiple DEAs simultaneously. In this approach, the control of four different channels was selected as this would enable the rendering of two hand pinch gestures, where soft tactile forces can be rendered to the thumb and index fingers on two hands simultaneously. This is similar to the gestures used to control the Da Vinci telerobotic surgical system (USA) ("da Vinci Surgery - Minimally Invasive Robotic Surgery with the da Vinci Surgical System," 2018). Another advantage is that the TCA0372 (Motorola, USA) operational amplifier is dual-channel, therefore only two operational amplifiers are required in the circuitry. A system that can control ten different DEAs, one for each finger, would be preferential. But a limiting factor is the cost of each of the EMCO Q50-5, as each unit costs £300. Another limiting factor is the size of each of the EMCO components, which would conflict with point 5, being as compact possible.

5.3.2 Proposed multi-channel DEA circuitry design

Below, a schematic of the proposed four channel system is presented. The main additions within the system first proposed in figure (5-11), other than four times the high voltage control circuitry, is the addition of a kill switch and power indication LED.

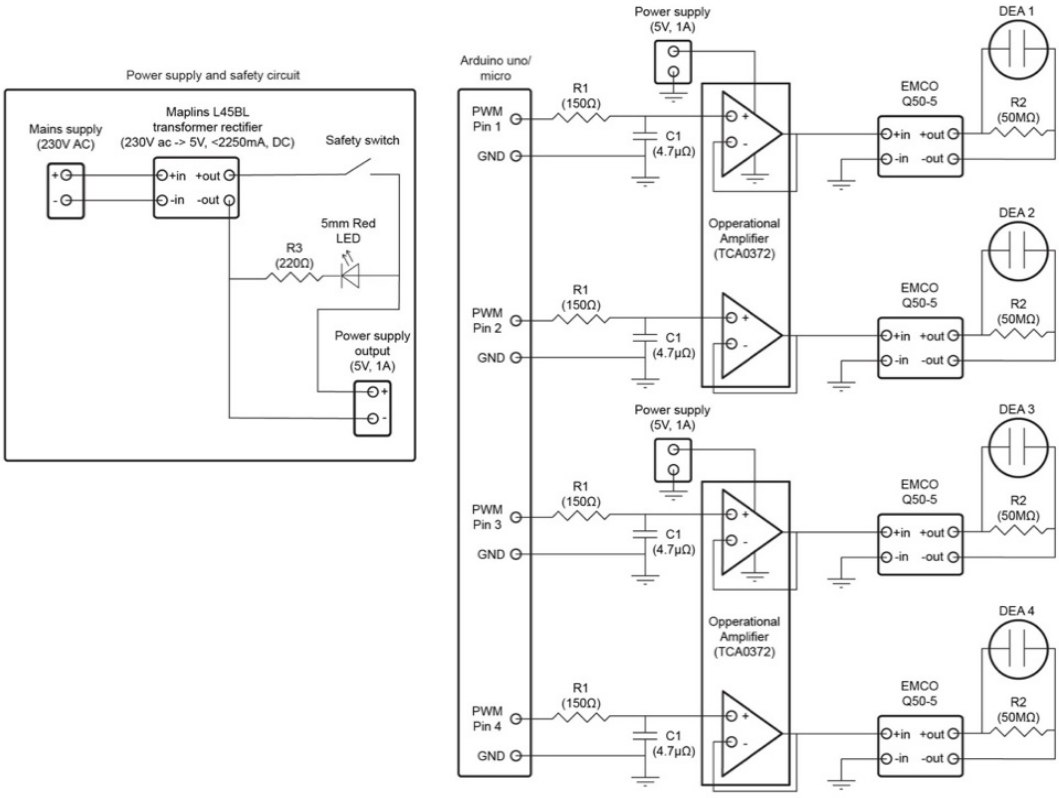

Figure 5-12 Schematic illustration of a four-channel high voltage system to control four separate DEA devices.

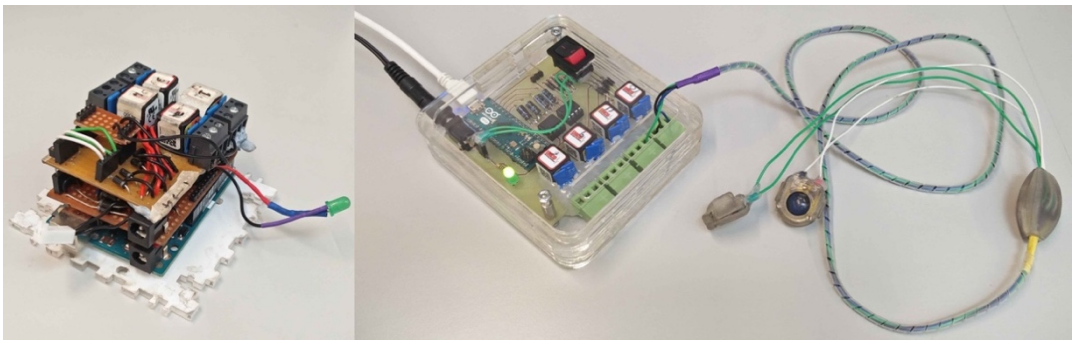

Figure 5-13 Left is prototype version 1 using stripboard, right is a PCB version in custom laser cut casing.

5.4 Arduino control interface protocol

The Arduino external microcontroller in this work is effectively a slave device to the controlling host computer. This is achieved using the Firmata protocol ("firmata/arduino," 2018).

5.4.1 Firmata microcontroller protocol

The Firmata protocol enables host computers to use external microcontrollers as slave devices. In essence, it allows software running on computing devices (laptops, phones, tablets, etc.) to control the functions of an external microcontroller. Firmata uses the midi message format ("Summary of MIDI Messages," 2018) which is composed of command bytes of 8 bits, and data bytes of 7 bits (*Documentation of the Firmata protocol*, 2018). The protocol has been widely adopted by the Arduino community as there are many software libraries developed for a variety of languages, enabling simple and fast slave control of the microcontroller without the need to write custom C code.

5.4.2 Pseudo code for host computer microcontroller communication

Below is the pseudo code to be executed by the host computer:

1) Discover and confirm the serial connection to the external microcontroller (Arduino) on a defined port.
2) Generate float value between 0 and 1 corresponding to the actuation value to be rendered by DEA (1 being full actuation, 0 being minimum actuation).
3) Map float value onto 8 Bit value range (0 to 255), to correspond to Arduino analogue write 8 bit PWM value range (255 PWM pin value = 5V output, 0 PWM pin value = 0V).
4) Call "Firmatata.analogueWrite (Defined PWM output Pin, 8 Bit value)" to send argument over a serial connection to the external microcontroller.

5.4.3 Diagram for host computer microcontroller communication

Below shows a pseudo programme flow of how the host computer communicates using Firmata(*Documentation of the Firmata protocol*, 2018), in this case, to control the values to the four outputs of the controlling circuitry. The outputs in this example relate to DEA actuators placed on the right thumb and index and the left thumb and index fingers.

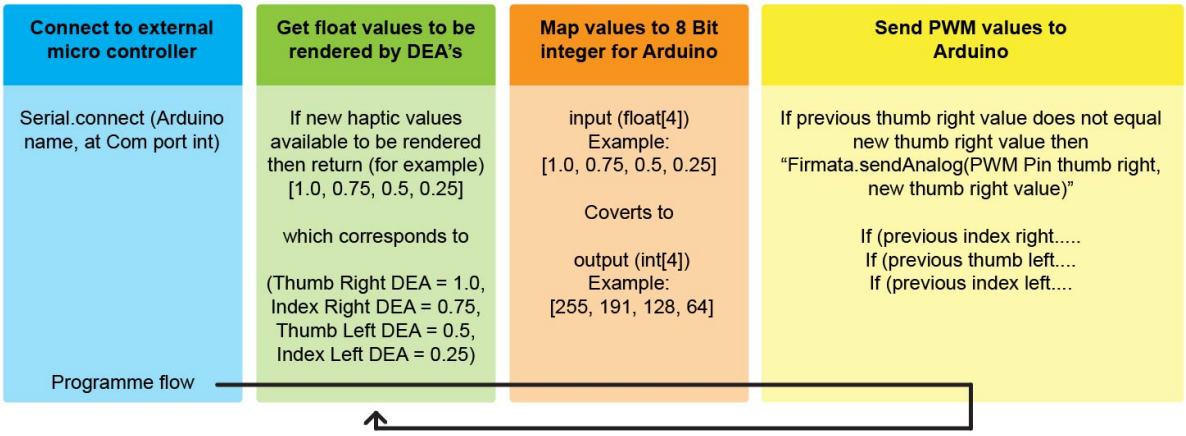

Figure 5-14 Programme flow of communication between host computer and microcontroller using the Firmata protocol.

5.5 Testing of multichannel control system

To accurately control the voltage across a DEA with the proposed system, the relationship between the 8 bit PWM value sent from the host computer to the output voltage of the circuitry needs to be accessed. To do this the following tests are proposed: firstly, measure the voltage output at different PWM increments, and secondly, examine the frequency response of the system.

5.5.1 8 bit PWM control value to output voltage

To verify the voltage output from the multi-channel control system based upon the PWM value sent from the host computer, the following test will be performed. For the 8 bit PWM values capable of being sent from the host computer to the Arduino Micro microcontroller (an integer between 0-255), the output voltage will be measured using a high voltage probe (Testec TT-HVP40, Germany) and a multi-meter (Rapid 318D, UK). Refer to Figure 5-15 for the schematic.

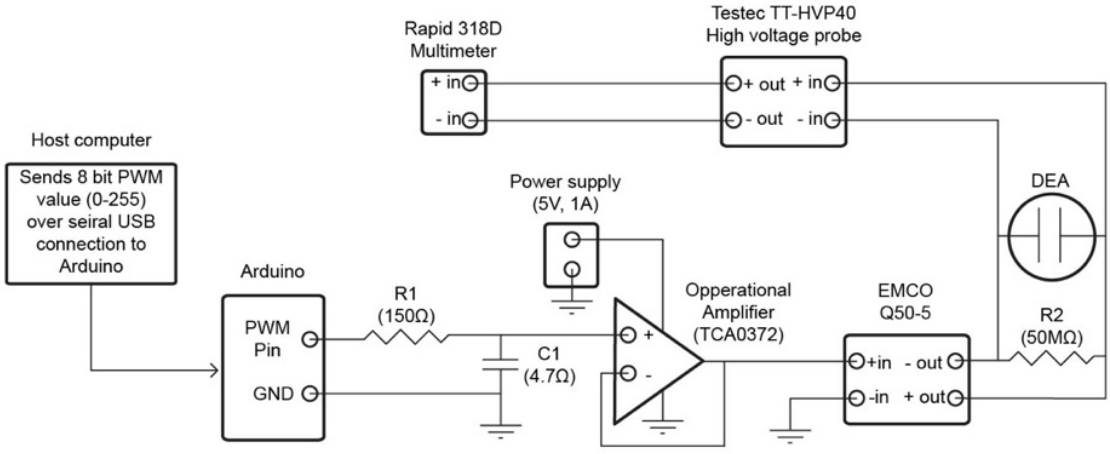

Figure 5-15 Schematic illustration of the experimental setup to examine the relationship between Arduino PWM of high voltage output circuitry.

Each test was repeated 5 times. Tests were repeated on different channels of the system proposed, but little to no variance is observed. Therefore, for simplification of presentation, results pertain to a single channel of the four-channel system. Results are plotted in Figure 5-16.

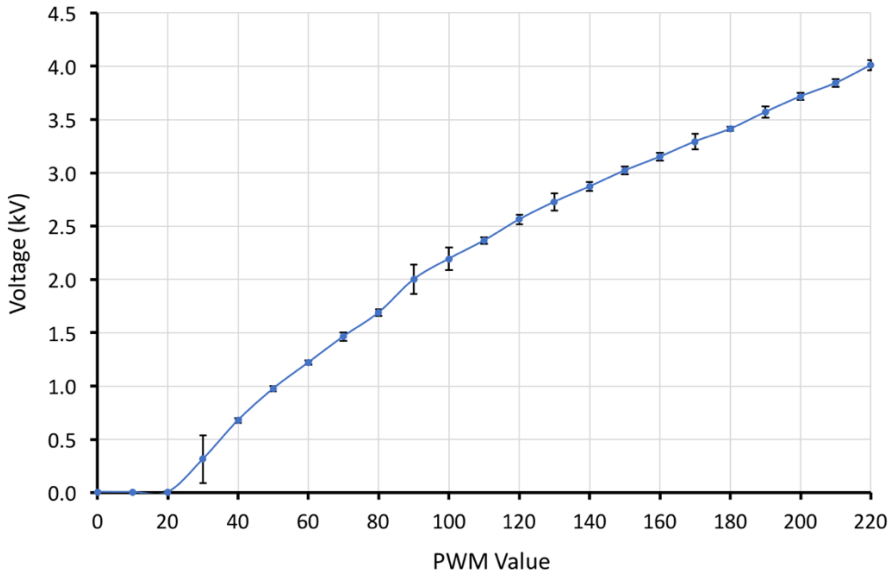

Figure 5-16 Voltage output generated from circuit outlined in figure (5-15). For different PWM control values.

As expected, the Emco low-to-high voltage converter starts outputting the HV signal after an actuation threshold of around 20PWM. But as seen in Figure 5-16, linear control does not occur until a PWM value of 40. Considering a PWM value of 40, corresponds to a smoothed DC voltage of ~0.7V; this is consistent with values stated in the datasheet of the Emco unit. To link the PWM control value to voltage output, the following plot is presented (Figure 5-17).

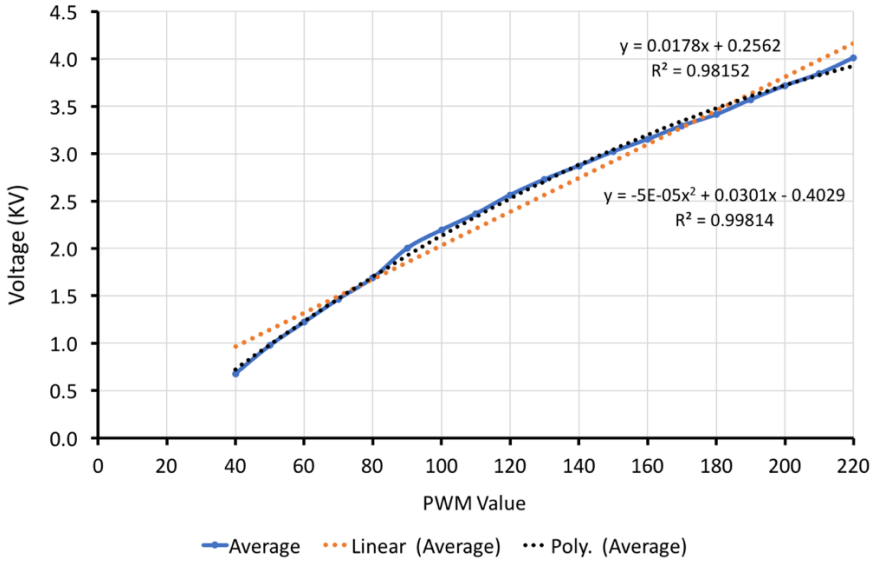

Figure 5-17 Plot showing the recorded voltage output based on PWM value (blue), orange dotted band shows linear fitting line, black dotted line shows second order polynomial fitting line.

The system can be modelled as a linear function with an R squared value of 0.982 or a second-order polynomial with an R squared value of 0.998. Considering the minor improvement of using a second-order polynomial expression to link PWM value, the linear system is adopted in the control of the voltage.

5.5.2 Frequency response

Frequency response is a way to measure the dynamic responses of a system based upon an inputted signal. In this case, a square wave of varying frequencies generated by the controlling host computer is sent to the Arduino microcontroller. A square wave is used to maximise response time and limit sin wave resolution issues at higher frequencies. The corresponding high voltage output signal is then measured. The square wave alternates between states of 4kV and 0V. To do this, a high voltage probe connected to an analogue input pin of the Arduino (A0), and another analogue read pin (A1) will be used to measure the outputted voltage from the PWM pin. This will enable the original PWM signal outputted from the Arduino to be compared to the high voltage signal within the same programme execution cycle of the microcontroller. The schematic of the circuit is illustrated in figure 5-18, on the following page.

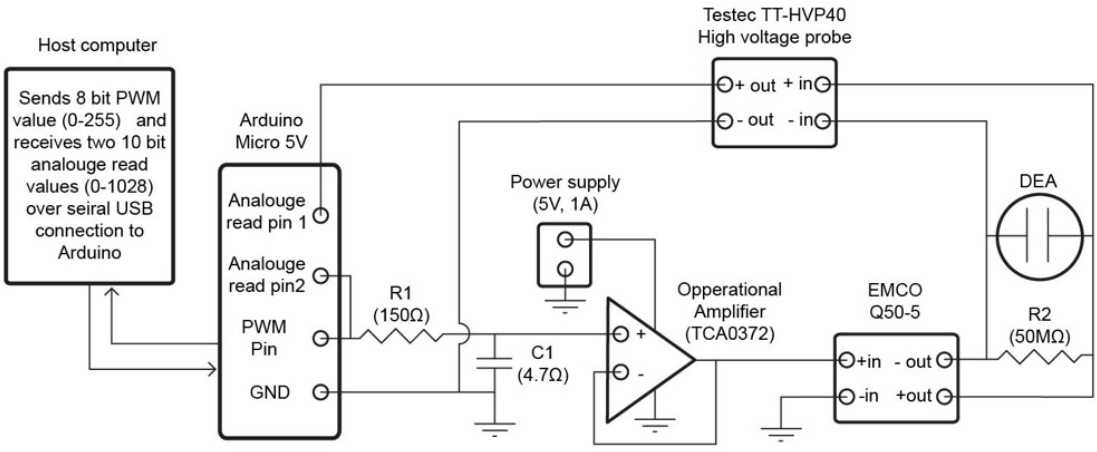

Figure 5-18 Schematic illustration of the experimental setup to examine the relationship between Arduino PWM of high voltage output circuitry for varying control frequencies.

Figure 5-19 illustrates the voltage delta drop due to a square wave signal at varying voltages. Tests were repeated 5 times for each frequency between 0.1 and 5Hz measured at 0.1Hz increments. The tests were performed on the circuit outlined in figure (5-16). The capacitance of the DEA in this system was measured to be 365pF un-actuated, which represents a triple layer HC-DEA.

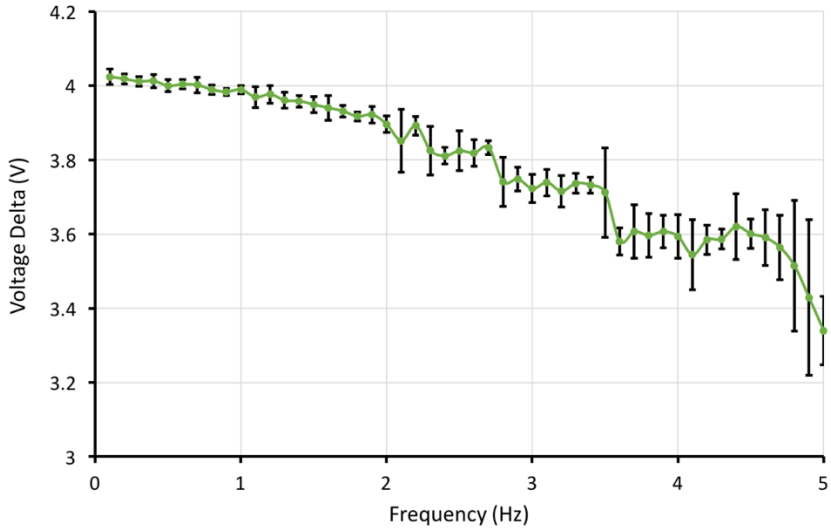

Figure 5-19 Average voltage delta between 0-4kV square wave actuation at varying frequencies between 0.1 and 5Hz at 0.1 Hz increments. Error bars represent 2 standard deviations from the mean, 95% confidence level.

As can be seen in figure (5-19), the voltage delta drop is constant until 2Hz, then larger deviations and erratic behaviour is observed. This could be due to the discharge time of the DEA actuator.

5.5.3 Discharge time measurement of DEA actuator

The voltage discharge of the system with and without the DEA actuator was measured. This was achieved using the same setup as previously used in the frequency response test, see Figure 5-19. The difference is that in this test, the voltage drop was measured from a state of 4kV actuation, to 0V, sampled every 40ms.

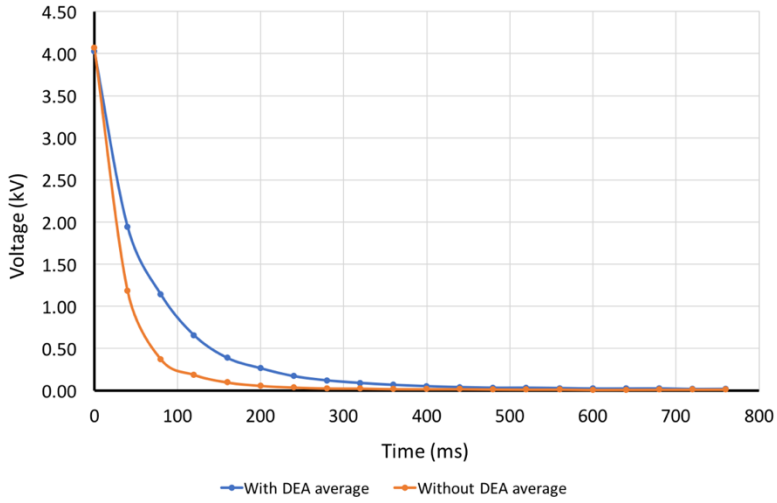

Figure 5-20 Voltage over time due to a switch from 4 to 0kV. Blue line represents the voltage drop with the DEA actuator as shown in the schematic in fig (5-16). Orange line represents without DEA in the system.

As expected, the discharge time of the circuit is slower due to the addition of the DEA. Considering the load resistor has a value of 50MΩ and the DEAs capacitance at rest was measured at 365pF, the discharge time constant is 0.01825s (time constant = capacitance x resistance), therefore at five-time constants representing full discharge at ~0.1s, is consistent with the data collected.

5.6 Discussion

A four-channel high voltage controller suitable for controlling four DEAs' simultaneously is proposed. The cost of the device is around £1230, with £1200 being spent on four EMCO Q50-5 low-to-high voltage converters. From testing the system, it has demonstrated that the system is robust, consistent and easily integrated with a controlling host computer. The power consumption of the system was measured at 1.15A at 5V equating to 5.75W, when all four actors are driven by 4kV. To further the progression of this system, especially towards making a consumer-ready multichannel DEA control system, there is still work to be done in the following areas:

1. Reducing the cost amount of the low-to-high voltage converters through either finding an alternative method of high voltage generation/ reducing voltages required through the actuator material choice, construction and multiplexing of a single high voltage source.
2. Shrinking of the circuitry by creating a custom PCB that has its own application-specific microcontroller.
3. Adding a wireless communication module such as Bluetooth or Wi-Fi with a battery power supply to make an untethered wearable device.
4. Self-monitoring control loop and breakdown detection system.
5. Reducing the cost and size of the system through multiplexing a single high voltage source.

As stated, the most expensive part of the proposed system is the EMCO Q50-5, of which there are four in our current design. In order to bring the cost and also the size of the system down, less of these components would be desirable. One way to do this would be to multiplex a single high voltage source, perhaps through a rapidly changing transistor or MOSFET gates. A configuration below is proposed:

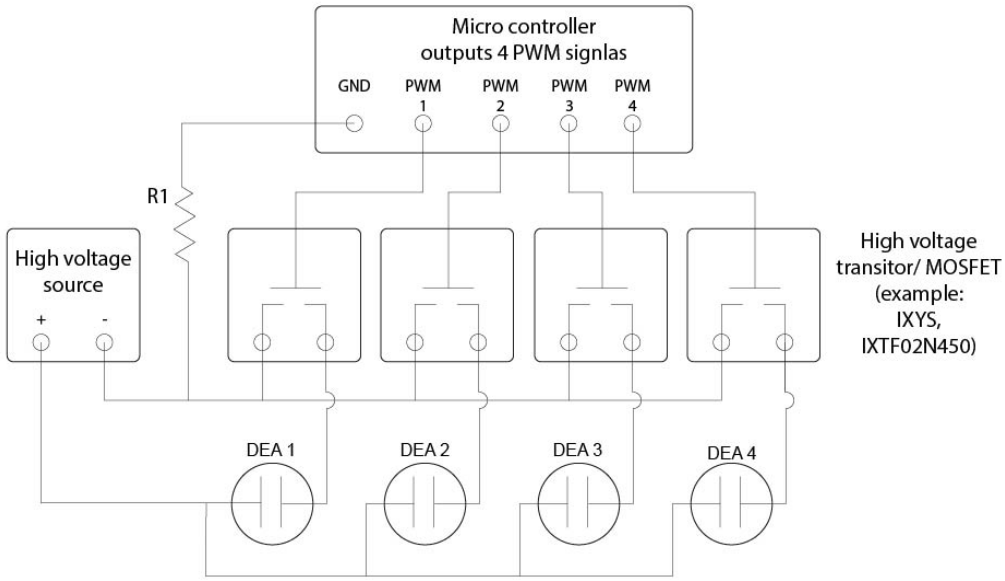

Figure 5-21 Shows how a potential multi-channel high voltage system could be created using a single high voltage source and multiple transistor gates.

If the transistor proposed in the diagram above was to be used (IXTF02N450, IXYS, USA), it is possible to drive the gates using an unmodified 5v 490 Hz PWM signal produced from an Arduino Micro microcontroller as the gate to source voltage is 4V at 200mA ("IXTF02N450 IXYS | Mouser," 2018). The cost of each of the transistors is currently (in 2018) around £22, therefore the cost of the entire system could be produced for around £400. But the limitations of such a system would involve either PWM signal driving the DEA, which might cause unwanted vibrations. Another option could be to use an alternative manufacturer of the low-to-high voltage converters, for example, there are few manufacturers of these devices for prices as little as £10 but these are yet to be tested in lab conditions, and the size of these devices are significantly bigger (50x20x20mm) (Banggood.com, 2018).

Adding a wireless serial communication module, such as a low power Bluetooth or Wi-Fi module, and then powering the system with a battery pack would enable an untethered device, and therefore enable larger scale interactions, rather than just desktop based ones as with the current system. One of the reasons for not designing this from the start is that the hand tracking system has to be tethered to a desktop or laptop computer via a USB 3.0 connection and only operates at the desktop scale. A wearable high voltage system has been demonstrated by Frediani et al (2014b) for a single DEA tactile device but has yet to be incorporated into a 3D tracking system for larger area interaction.

Ghilardi et al (2017) have proposed a simple breakdown detection system that makes use of a voltage divider circuit and an analogue read pin of an external microcontroller to compare the low voltage output logic of the microcontroller to the high voltage output of the high voltage circuitry. With this system, it is possible to detect abnormal behaviour such as a high voltage system failure, and depending on the material choice of the DEA, electrical breakdown. This is due to excessive current draw that typically happens when the isolating material of the dielectric breaks down and forms conducting channels between the opposing sides of the previously capacitive system. The material choice is important here, as the speed at which this breakdown occurs varies depending on material choice, and the detection system has to be sampling at a frequency faster than that or the duration of electrical conductance during breakdown.

6 Electromechanical characterisation HC-DEA

The aim of this chapter is to explore how the different parameters such as prestretch of the VHB elastomeric film, diameter of the Hydrostatically Coupled – Dielectric Elastomer Actuator (HC-DEA) bubble and number of layers used in the construction of the HC-DEA effect the mechanical performance of the actuator when driven with the electronic control unit proposed in the previous chapter. By mechanical performance, the uniaxial force output and vertical displacement of the actuator in response to an applied electrical signal will be accessed. The ultimate aim of this chapter is to determine a configuration of HC-DEA that improves upon Frediani et al (2014b) initial approach by increasing force output, and minimising the lateral diameter of the actuator as to fit within the lateral diameter of the average fingertip (sub 20mm). What is beyond the scope of this work is a full electromechanical characterisation of the HC-DEA design proposed. It was found that due to the viscoelastic properties of the VHB film used in this work, there is difficulty in determining the exact behaviour of the actuators at any given time.

The structure of this chapter is as follows: Firstly, the methods to determine uniaxial force output (6.1) and uniaxial displacement (6.2) will be described. Then an investigation into the effects of prestretch on the electromechanical performance will be investigated (6.3). Then the lateral diameter of the HC-DEA bubble will be varied as to see how this influence overall uniaxial force output (6.4). Lastly, a multilayer construction for the active membrane of HC-DEA will be evaluated (6.5). This chapter will conclude with general methodologies in order to the improve aforementioned performance characteristics, but will also discuss potential methodologies to construct a more robust and longer lasting actuator.

6.1 Uniaxial force performance methodology

In this work, the metrics of uniaxial force and displacement are used to understand the performance of the different HC-DEA configurations tested. In this subchapter (6.1), the methods pertaining to obtaining these metrics are outlined.

The tactile display system proposed in this work has been designed to be mounted directly onto the fingertip. In effect, the device is capable of applying a uniaxial quasi-static force to the tissue pulp of the fingertip. As the outer-casing of the device is attached to the finger, as illustrated below, the movement of the actuator is effectively blocked by the tissue of the finger-tip, and therefore a static blocking pressure occurs between the fingertip and bubble. This is due to the bubble being unable to move into its relaxed unblocked state. It can be said that this is a quasi-static blocking force, as the bubble can dynamically move up and down in a single axis due to the expanding and contracting membrane of the active region of the HC-DEA bubble.

What is to be accessed in these loadcell tests is the uniaxial force that different configurations of HC-DEA will deliver in the aforementioned conditions. The fabrication technique of each of these specimens is in line with the finding of chapter 4. The ultimate aim is to maximise the quasi-static force output of the actuators whilst still maintaining the wear-ability criterion, i.e. fit within a lateral width of <20mm.

6.1.1 Uniaxial loadcell test equipment setup

To determine the static force output as a function of the applied voltage, tests were performed with a dynamometer (3300 single column, Instron, USA), equipped with a 10N load cell (2519-10N, Instron, USA), in conjunction with a circular 12mm diameter flat faced indenter. It was decided to use a flat circular indenter as to align with previous methodologies employed by our group (Frediani et al., 2016), in order to gain a comparative metric. Although this flat indenter does not accurately simulate the forces applied to the finger pulp, due to geometric properties and material compliance of the finger-tip, it is assumed that the control voltages to induce these forces on a flat indenter are comparable. Again, the primary function of these tests is to have a metric in order to access the force output of the HC-DEA, as it is believed a higher force output will enable the tactile display system to render a wider range of pressure sensations perceivable by the user.

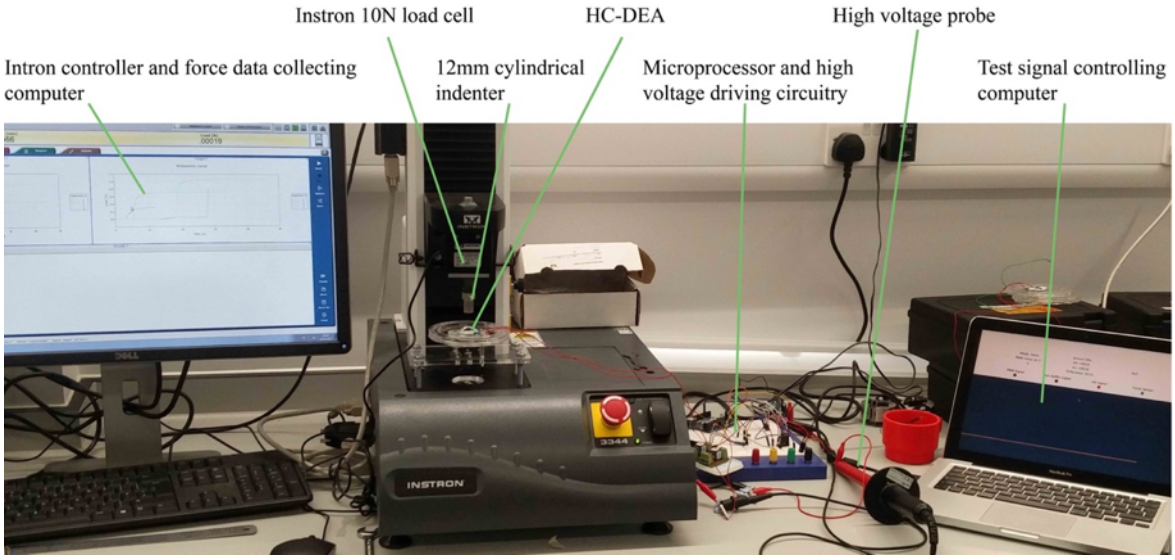

Figure 6-1 Labelled uniaxial loadcell test set-up consisting (From left to right) Loadcell data capture computer, uniaxial loadcell machine with HC-DEA bubble specimen, controlling electronics (as concluded in chapter 5), High-Voltage probe, HC-DEA test signal controlling computer.

The control electronics described in the previous chapter (5) were used to drive the actuators. A test signal controlling computer runs a custom programme built with the Java 8.0 programming language, and as discussed in the previous section, sends an 8bit PWM value over a wired USB connection to the controlling electronics, which then drives the actuators with a 0.7-4kV DC driving signal.

6.1.2 Uniaxial HC-DEA voltage induced force testing method with a ramping signal

At the start of each test, the actuator was deformed through the application of 4kV, which was controlled by the electronics described in the previous section. The applied voltage causes the actuator's passive membrane to move down to an actuated position. The indenter was then lowered onto the deformed passive membrane until a contact force was established. The latter was defined as the situation corresponding to a force of 0.05N, a value chosen due to the sensitivity of the load cell (2519-10N, Instron, USA). As described in the previous section, the controlling host computer communicates an 8bit PWM value, which is then converted to the DEA driving voltage as stated in 5.1.2 figure 46. In this experimental setup, a value of 200 was used to set the voltage across the actuator to 4kV at the start of each test. The controlling computer then sends a ramping decrement PWM value (199, 198, 197, etc.) every 40ms (25Hz), until a PWM signal of 36 is reached. Linear voltage control which corresponds to the minimum linear activation threshold of the EMCO device

used is 0.7V, which corresponds to a PWM value of 36. Each PWM voltage step corresponds to around ~20V voltage steps. Force data is collected at a rate of 100Hz which equates to 4 samples per PWM / voltage step. The figure 61 highlights how the flat indenter is lowered onto the passive membrane of the HC-DEA, and figure 62 shows a ramping voltage signal applied across the actuator during the test.

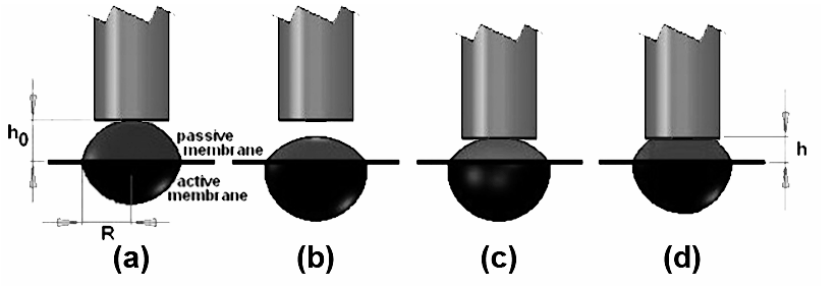

Figure 6-2 Uniaxial loadcell testing of HC-DEA, A) Actuator at rest 0V, B) Actuator is driven by 4kV, C) Loadcell indenter lowered on to the top membrane until a 0.05N force recorded, D) Voltage across actuator decreased to 0.7kV.

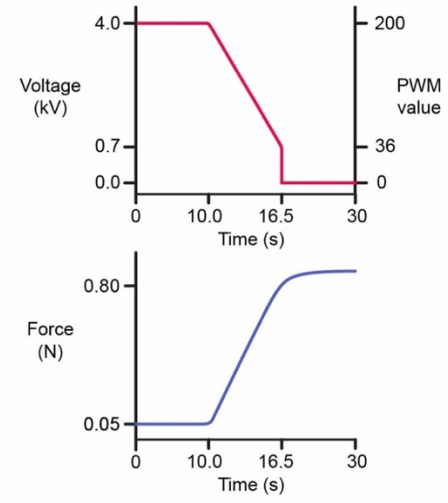

Figure 6-3 Top graph demonstrates the electrical signal (voltage) across the actuator during the testing and an expected resultant change in the uniaxial force as applied to the load-cell.

6.1.3 Uniaxial HC-DEA maximum rate of static force application test (Actuator relaxation test)

An important parameter to understand in the application of force in which can be rendered by the HC-DEA is the maximum rate at which the actuator can deliver its force from a state full actuation (4kV) to the least actuation state (0V). An example of how we can use the data is to understand the maximum rate at which a force can be applied to a user's fingertip. For example, as a person palpates a soft tissue, the rate at which force is applied to the finger through the active object palpation, is linked to elastic properties of the soft object. The fastest rate at which the force can be applied

to the user's finger through the actuator, which therefore dictates the type of tactile interactions and materials capable of being rendered with the proposed system.

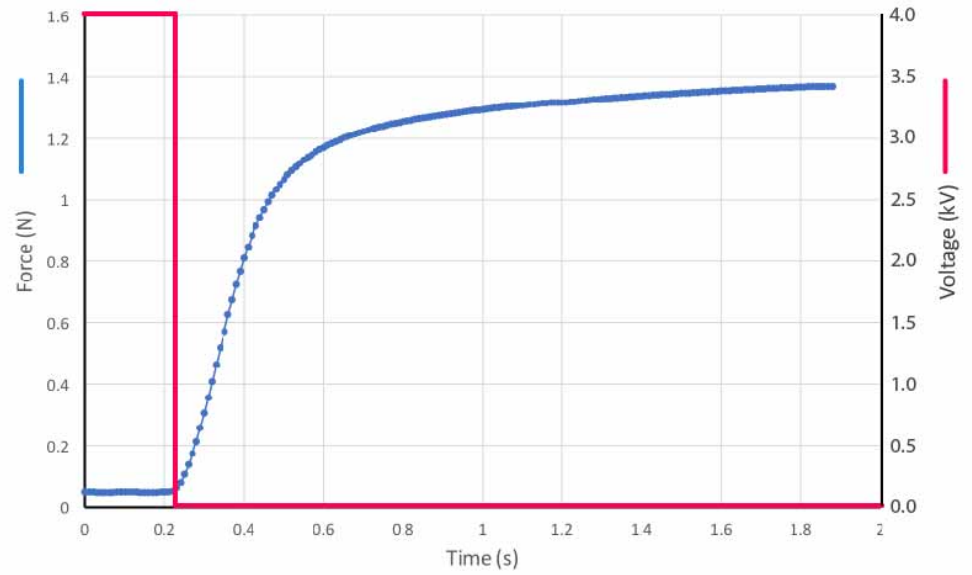

Figure 6-4 Example of the maximum rate of static force application test. During the test, the actuator is fully actuated at 4kV then dropped to 0kV (redline), the force data is then collected over a period of 10 seconds (blue line).

To conduct these tests, the actuator will be placed in the loadcell machine and actuated through the application of 4kV. The end effector is then programmatically lowered until the offset force of 0.05N is reached. The voltage is then dropped to 0V by sending a PWM signal value of 0 to the controlling electronics. The resulting force data from the load cell will then be collected for 10 seconds after this voltage drop at a rate 100Hz.

6.2 Laser measurement uniaxial-displacement testing methodology

The uniaxial displacement of the bubble was measured using a laser measurement device (optoNCDT ILD 1402-5, Micro-epsilon, UK). It is capable of measuring 0-5mm displacements with 14bit resolution (~0.003mm). To interface with this device, it was connected to a host computer via a USB connection. This host computer also controls the electronic control system described in chapter 5 and was sampled the measurement device at a rate of 25Hz. It was found that using the measurement device on clear VHB produced strange inconsistent results, which we believe is due to the reflectance properties of the VHB HC-DEA bubble. Therefore, a small spot (~2mm) of the silicone and carbon black compliant electrode mixture was applied to the top passive membrane using a brush. It is not believed this painted spot significantly affects the actuation performance of the bubble.

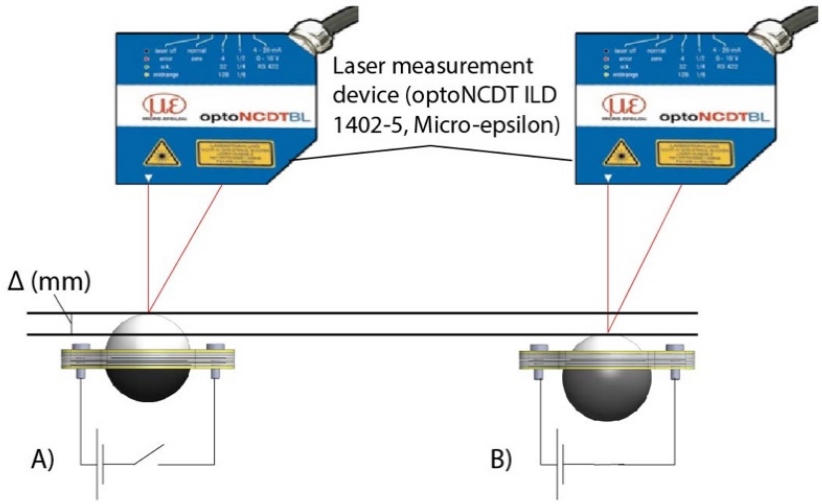

Figure 6-5 Uniaxial free-stroke displacement test setup. A) demonstrates the actuator at rest, B) demonstrates the actuator when a voltage is applied.

6.2.1 Free-stroke voltage induced displacement

To investigate how far the HC-DEA bubble actuates when there is no finger present, a free-stoke voltage induced displacement test was conducted. In this test, the voltage induced displacement was measured by increasing the voltage across the actuator from 0 to 4kV. As mentioned previously, the low-to-high voltage DC converter is only capable of producing a linear output after a 0.7V activation input is reached. Therefore, the linear control range of the electronics and signal to the actuator is between 0.7 to 4kV. But a 0V output can be achieved with an input supply voltage of

under 0.7V. As the control electronics converts an 8bit PWM value (0-255) to a corresponding 0-5V signal applied across the low-to-high voltage converter; incrementing PWM values starting from 0 (0kV) and ending at 200 (~4kV), corresponding to ~20V steps, where sent at a rate of 25Hz. In effect, an increasing voltage applied across the actuator that starts at 0kV and ends at 4kV overs 8s.

6.2.2 Free-stroke dynamic response

To access the frequency response of the system proposed, electrically induced displacement was tested in the range 0.1-3 Hz at 0.1 Hz increments for every 5 oscillations completed at the frequency. For this test, we used a square wave driving voltage which varied between 0 and 3.5 kV for five cycles at each frequency. A square wave was selected as the controlling host computer is limited to a <60Hz frame refresh rate, so rather than sending an 8bit integer value representing a sinusoidal signal 60 times a second, a simpler binary signal could be sent at the required time frames. Another reason for using a square wave is that we can only generate sinusoidal values between 0.7 - 4.0kV due to the activation voltage required for the EMCO low-to-high voltage converters. But alternatively, 0V output can be achieved by through 0V to the input. The difference between maximum displacement and minimum displacement were averaged for the five cycles to produce an average displacement value for that frequency. It was decided to run the tests at a reduced voltage of 3.5kV instead of 4kV (maximum voltage for the voltage induced displacement tests) as we found the actuators could sometimes fail at a frequency below a maximum frequency of 3Hz in preliminary tests. This could be due to inconsistencies during the fabrication of the actuators or potentially highlights limitations of this particular design.

6.3 Initial prestretch of membranes before formation into HC-DEA bubble

It is a widely known and excepted that the pre-strain of the dielectric materials effects the electromechanical actuation properties of DEAs, this is discussed in chapter 3. For the material used in this work (VHB, 3M, USA), a final prestretch of 400% is desirable for optimal performance, as reported by Koh et al (Koh et al., 2011a). But with the HC-DEA configuration, there is effectively three stretching periods; one where the material is first radially stretched in the pre-stretching process illustrated in the following figure (6-1); secondly, when the membranes are formed into a spherical shape due to the addition of a coupling gel; and lastly when the finger is brought in contact with the passive membrane during use.

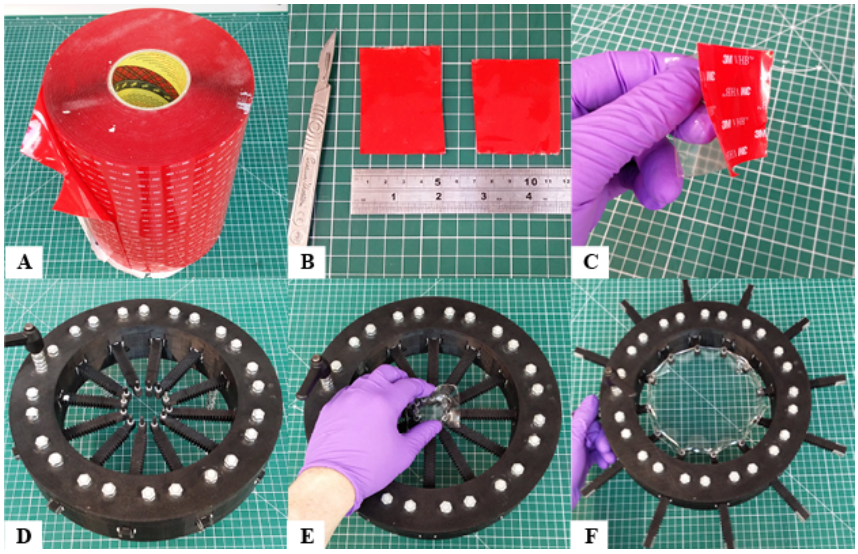

Figure 6-6 Radial stretching steps of VHB film. A) Roll of VHB (VHB 4910, 3M, USA), B) Cut into 50x50mm squares, C) Backing layer removed, D/E) placed in a biaxial pre-stretching device, F) Stretched by a predetermined amount. In these steps, the material is getting stretched by a factor of four.

Given a constant volume of coupling gel of 8ml for a 12.5mm diameter single layer HC-DEA bubble, radial prestretch in the illustrated above process will be conducted at 1x, 2x, 3x and 4x to see how this affects voltage induced force output and displacement characteristics.

6.3.1 Results of prestretch investigation

To access how the initial prestretch of the 1mm thick VHB film effects the performance of the HC-DEA design proposed, maximum displacement and force tests were conducted. Here, a 4kV voltage is applied and then switched to 0V and the data is recorded for the subsequent 10s. Below, the results of the maximum displacement test are presented.

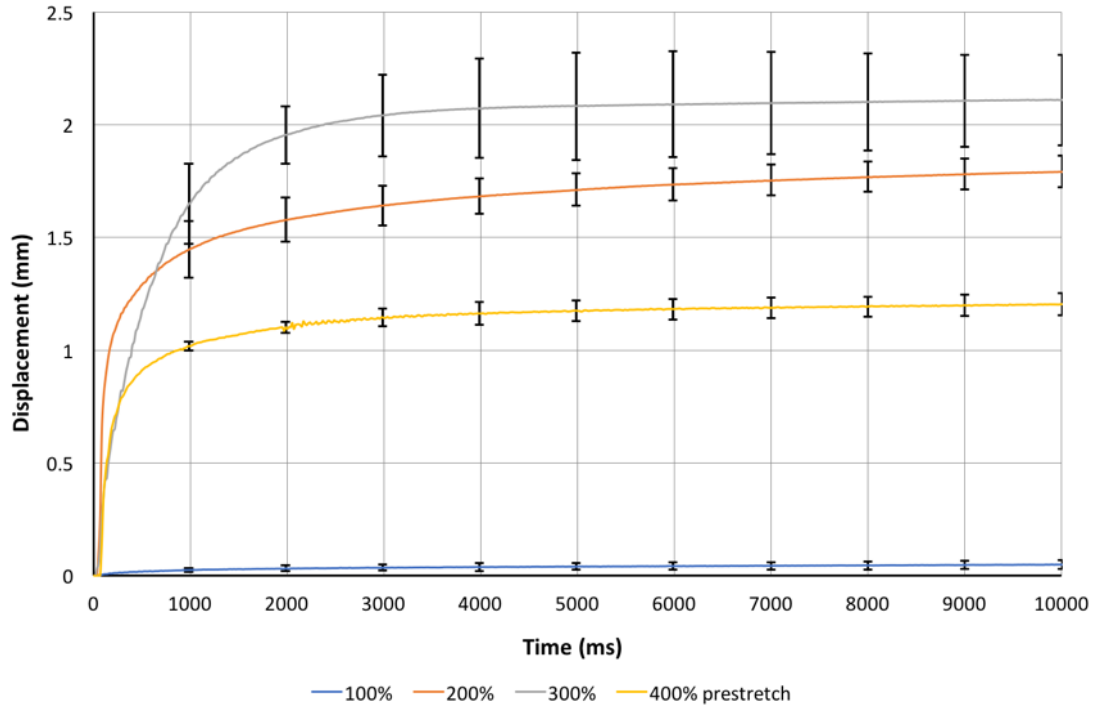

Figure 6-7 Average maximal displacement due to the application of a 4kV signal held for 20 seconds then relaxed to 0V for 20 seconds for initial prestretch of 100, 200, 300 and 400%. For each prestretch amount 5 samples were tested, except for 400% which only represents one sample tested 3 times, as the 400% samples were found to be unstable. Error bars represent 2 standard deviations from the mean (95% confidence level).

An initial prestretch of 300% provided the largest maximal displacement. The average maximal displacement for the 300% prestretch actuators was around 2.2mm. It is also apparent that there is a larger variance between the 300% stretch samples tested as compared to the other prestretch amounts. This could possibly be due to stretching errors using the bi-axial stretching device, described in 6.1.2. These errors could be exacerbated around the optimum prestretch value, as compared to other prestretch levels. The 200% prestretch VHB has an average maximal displacement lower than that of the 300%, at around 1.8mm as compared to 2.2mm, but there appears to be a higher consistency between the performance of the 5 actuators tested at this prestretch level. Considering that the difference in displacement performance between the 200%

and 300% prestretch actuators is ~0.4mm, it may be beneficial to opt for the 200% actuator due a more consistent performance and a potentially more robust choice due to the reduction in stress across the membrane which could reduce the viscoelastic performance drop off inherent with VHB. To further explore this potential, the electromechanical force performance of 200 and 300% stretched actuators will be further investigated. Another thing to note from the results presented in figure 70, is that 300% stretched actuators seem to move at a slower rate than that of the other stretches. To produce the initial 1mm of displacement, from full actuation (4kV) to zero (0kV) takes 380ms for 300% and 170ms for 200%.

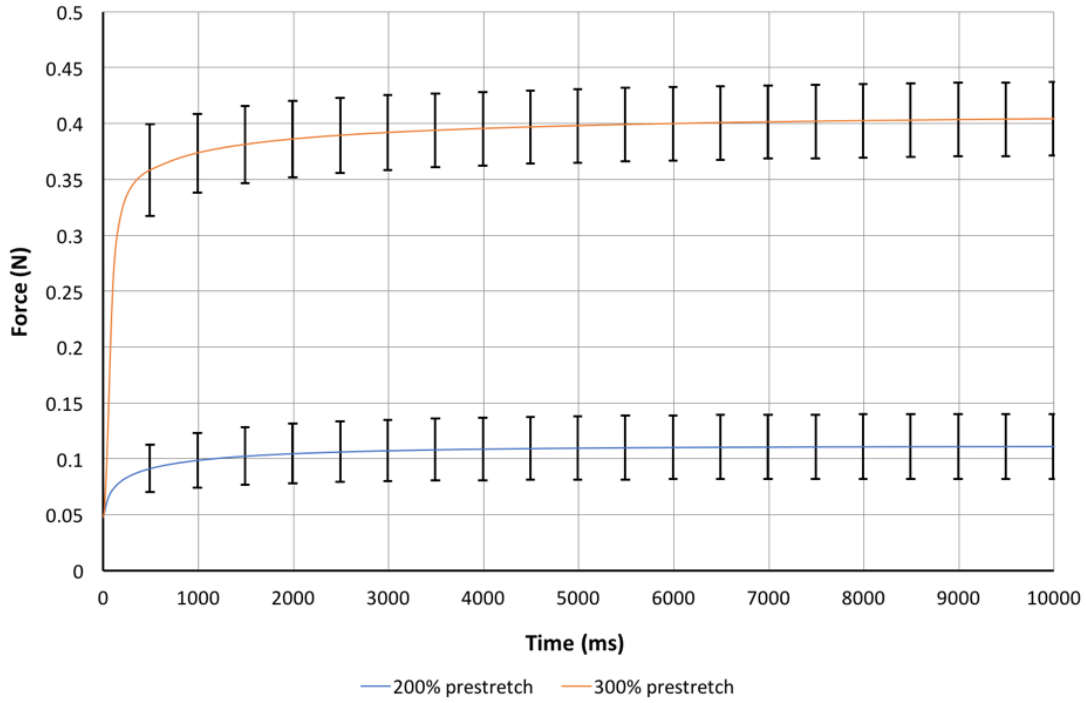

Figure 6-8 Force delivered from actuators from the state of full actuation (4kV) to zero actuation (0V). For each prestretch amount 5 samples were tested. Error bars represent 2 standard deviations from the mean (95% confidence level).

It was found that 100% prestretch actuators did not provide enough force output that could be detectable in the test setup used. It was also found that 400% actuators were too temperamental and would typically fail before the measurements could be taken in this test, so data was not able to be collected. Comparing the 300% and 200%, it is apparent that there is a significant force output performance increase between the 200% and the 300% prestretch actuators. The 300% seems to outperform 200% actuators by almost a factor of 4. When touching the 200% actuators with the finger, non-actuated (0V), it noticeable that actuator feels a lot less taut compared to the

300% stretch. 400% actuators feel the tautest but are prone to mechanical and electrical breakdown. Moving forward, it appears from these tests that 300% seems adequate for the actuator design proposed.

6.4 Investigation of lateral diameter of HC-DEA on uniaxial force output

To see how the lateral diameter of the HC-DEA bubble affects the force output of the system; 10, 12.5 and 15mm diameter HC-DEAs (see fig below) were investigated. Frediani et al (2014b) initially proposed a HC-DEA tactile display, a bubble of effectively 21mm in diameter was created. The size of this bubble is too large as to be placed on multiple fingertips of the hand simultaneously, and therefore is unsuitable for a multi-finger tactile display system. To change the lateral dimensions of the HC-DEA bubble the internal diameter of the laser cut internal support frame needs to be altered. See next figure (6-1).

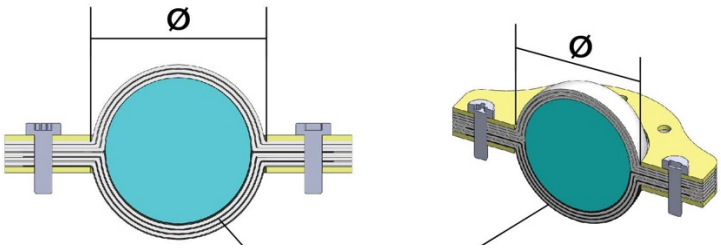

Figure 6-9 A sliced front and isometric view illustration of a triple layer HC-DEA, with the frame diameter/ HC-DEA bubble diameter labelled.

Changing the internal diameter of the support frame will also affect two other aspects of the HC-DEA. These are the overlapping electrode area on the active membrane and the volume of coupling gel within the bubble. Changing the overlapping electrode area is relatively trivial, as the laser cut stencil used to apply the electrodes is easily changed to the diameters tested. The volume of gel, on the other hand, has to be calculated to provide the same stretching of the membrane across the comparative samples, as varying prestretch amounts of the material will affect actuator performance, as discussed by Koh et al (2011b). The diameters of bubbles to be tested in this work are 10, 12.5 and 15mm. To produce a 12.5mm diameter bubble with a single layer membrane, 0.8ml of coupling gel was used. 0.8ml was rather arbitrarily selected as this enabled the most amount of gel to be inserted in the bubble without over-stretching either the active or the passive membranes in the vacuum cavity process. In order to get higher gel volumes into the bubble, one of the membranes, either the active or the passive, would have to be over-stressed, causing one side of the bubble to be larger in area than the other when the bubble is formed by both the

passive and active membranes being in the relaxed elastic state. If we make the assumption that the bubble is two spherical caps, the following calculation was used to ensure each different diameter bubble has comparable stretches:

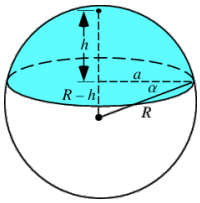

$$Vcap = \left(\frac{1}{6}\right)\pi h(3a^2 + h^2)$$

The previous equation gives the volume of a spherical cap. Considering our HC-DEA is formed of two spherical caps, Vcap is multiplied by 2 to get the total coupling gel volume Vgel. Considering this formula and that a 12.5mm diameter bubble has a vertical height diameter of ~10mm and contains 0.8ml of coupling gel, the following values are obtained for 10mm and 15mm diameter bubbles:

Table 6-1 Table of gel volumes HC-DEAs at 10, 12.5 and 15mm in diameter.

Ø (mm)	A (mm)	h (mm)	Vcap (ml)	Vgel (ml)
10.0	0.500	0.4	0.191	0.382
12.5	0.625	0.5	0.375	0.750
15.0	0.750	0.6	0.643	1.286

Considering the accuracy of injecting the gel into the cavity formed by the vacuum in the manufacturing process, +-0.05ml being the minimum increment of the syringes used, 0.4, 0.8 and 1.3ml of coupling gel will be used for bubbles of 10, 12.5 and 15mm respectively.

6.4.1 Results pertaining to change in lateral diameter on force output

To investigate how the lateral diameter of the HC-DEA affects the uniaxial force performance, the tests described in section 6.2.3 with the HC-DEAs are described in 6.1.1. A 4kV voltage was applied across the actuators relating to 10, 12.5 and 15mm in lateral bubble diameters with corresponding gel volumes of 0.4, 0.8 and 1.2ml accordingly. A load cell was then placed upon the deformed passive surface of the actuator, once a contact force of 0.05N was recorded by the load cell, the voltage was switched to 0V and force values were recorded at a rate of 100Hz. It was decided to only present the force data pertaining to the first 1000ms as ~95% of the full force was typically applied in this time period. 300% prestretch was applied to membranes before forming into bubble configuration. The data pertains to 5 samples at each diameter size.

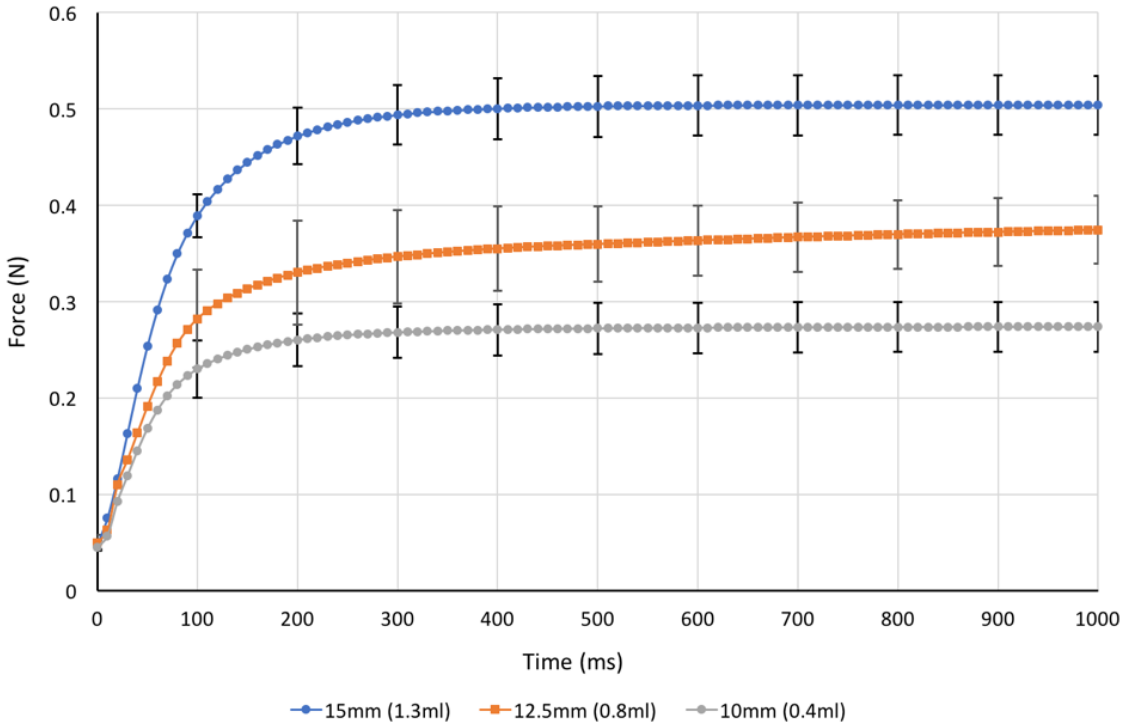

Figure 6-10 Force delivered by actuators over a period of 1000ms from a switch in state of full actuation (4kV) to zero actuation (0V), for different lateral diameter HC-DEA bubbles filled with proportional coupling gel as described in 6.1.1. For each diameter, 5 samples were tested. Error bars represent 2 standard deviations from the mean (95% confidence level).

There appears to be a clear performance increase with the larger diameter HC-DEA bubbles fabricated for this test, with 15mm in diameter bubbles reaching 0.5N within 300ms. A potentially surprising finding in this test is the rate at which the 15mm diameter HC-DEA applies its force, as the actuator has to move a larger volume of

coupling gel. Although not seen at this scale, this could be a potential issue at larger diameter HC-DEAs. Below is a graph showing the force delta (F(n+1)-F(n)) for the tests performed, and showing the rate of change of force applied over the first 400ms.

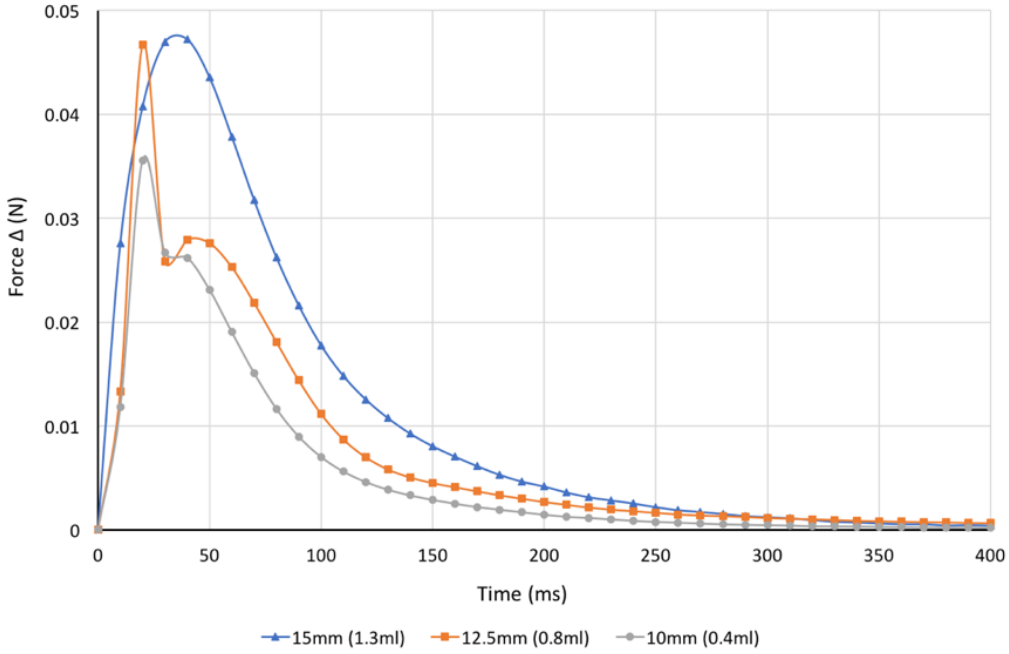

Figure 6-11 Average change of force between samples collected by load cell at the different diameter actuators tested over the first 400ms. For each diameter, five specimens were tested.

The peak rate of force application appears to happen within the first ~25ms for 12.5 and 10mm actuators, whereas this is shifted to ~40ms for the larger 15mm diameter bubble. Potentially due to the increased mass of coupling gel. An interesting feature is the double peak in the small diameter actuators. A potential cause for this is that the same cylindrical 12mm in diameter loadcell indenter was used for all the tests performed, and the interaction of the passive membranes for differently sized actuators could potentially give varying rate of force application profiles. One way to test this would be to use load cell indenter parameters that are proportional to the actuator diameter being tested.

To test how the force is applied to the loadcell due to a linear ramping signal, the test described in 6.2.2 is performed on the differently sized actuators. Below are the results from 5 samples for each of the different diameters, again with the initial prestretch of 300%.

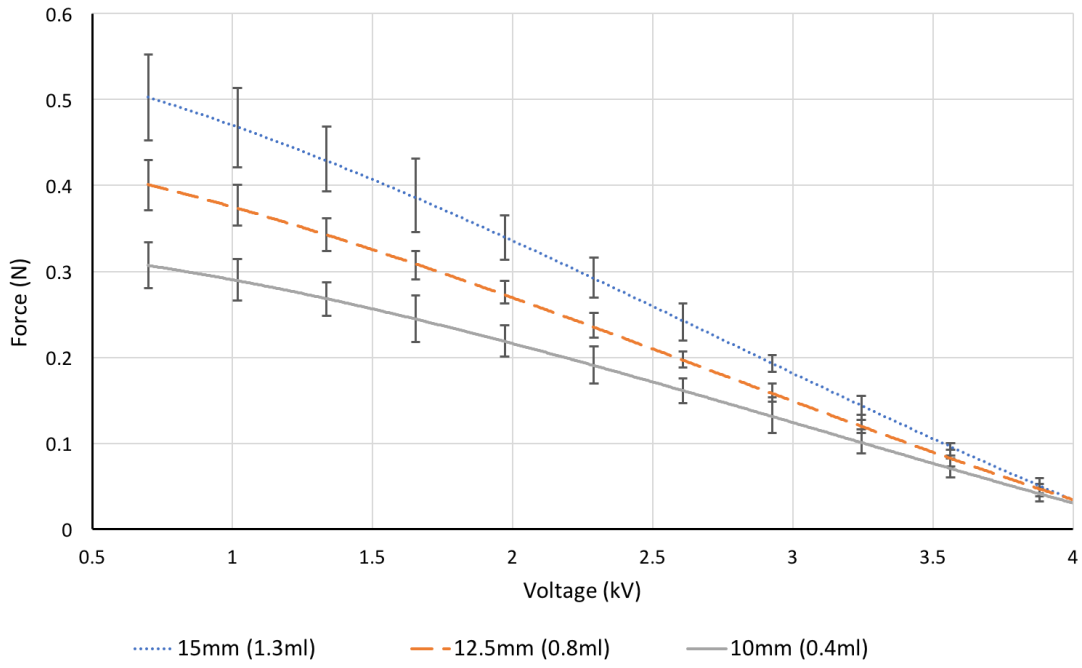

Figure 6-12 Results of the voltage induced force test outlined in 6.2.2 for different diameter actuators. 5 samples were tested at each diameter and a fitting line drawn. Error bars represent 2 standard deviations from the mean (95% confidence level).

In the above figure (6-17), the performance increase of the larger diameter actuators can be seen. As expected there is a slight curve to voltage induced force, as identified by Fedianni et al (2014b). As described in 6.2.2, the voltage was decreased linearly from 4kV to 0.7kV (linear operating range of circuitry) over a period of 6.5 seconds.

Considering that this actuator is to be placed within the width of the fingertip (<20mm), we opt to compromise between the force output and lateral diameter by using the 12.5mm as the diameter actuator. An important factor to consider is the size of the supporting frame and the plastic enclosure of the actuator, as this currently requires a further lateral width across the fingertip. Therefore, to increase the force performance of the actuator, the multi-layer approach described in chapter 4 will be tested using 300% pre-stretched membranes with a diameter of 12.5mm.

6.5 Effects of a multi-layer construction of the Hydrostatically Coupled – Dielectric Elastomer Actuator bubble

The last parameter to be tested within these electromechanical tests concerns the number of layers used in the construction of the active and passive membranes of the HC-DEA bubble. As mentioned previously, one of the limitations of Frediani et al (2014b) initial HC-DEA device was a low force output, which was indicated as a possible reason for low psychophysical perceptual threshold performance. To try to increase the force output without increasing the driving voltage, the number of layers used in the construction of the active and passive membranes will be experimented with. To do this we will use the process developed in chapter 4. A recap of this is illustrated as follows:

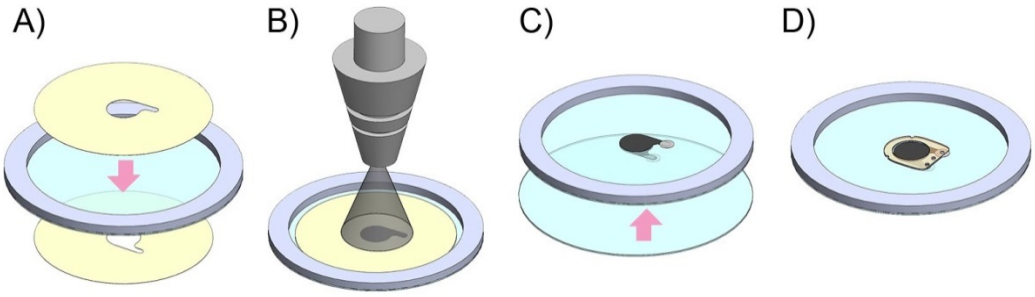

Figure 6-13 Fabrication of the active membrane. A) Addition of laser cut stencils to membrane material. B) Spraying of the compliant electrode. C) Addition of another pre-strained membrane. D) Support frame added to one side. Steps A to C is repeated depending on the number of layers required for the membrane.

Firstly, a 1mm thick VHB film (VHB 4910, 3M, USA) which had been pre-strained in the process described previously, is applied to a laser cut 3mm thick acrylic ring. The aforementioned stencils are applied to either side of the film (A). The compliant electrode mixture is then sprayed on to either side and cured at room temperature for 10mins (B). Once the stencils are removed, aluminium foil cut into 4mm circles is then placed at the end of the electrical connection tabs of the compliant electrodes. The aluminium improves the connection reliability of the electrical contacts which is discussed later on. Pre-strained layers are added carefully as to avoid trapping air between the layers (C). The passive membrane is formed in a similar fashion, except compliant electrodes and aluminium are not applied. Support frames are then attached to one side of the now formed active or passive multilayer membranes (D).

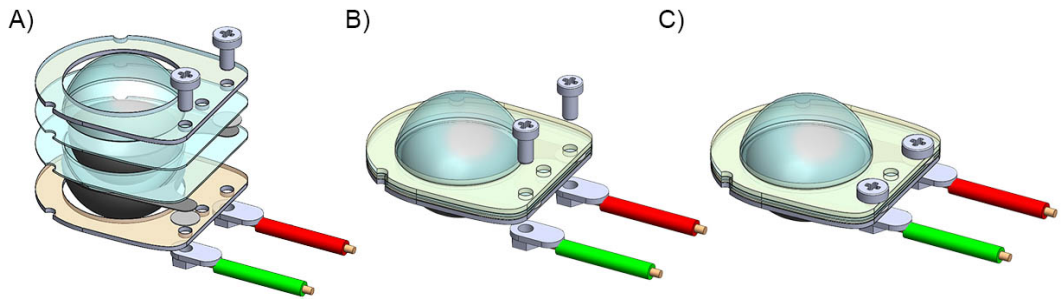

Figure 6-14 Schematic illustration of the attachment of the high voltage transmission cables. A) shows an exploded view of the different layers of the HC-DEA which have to connected to the wires. The two middle layers (of four shown) represent the multilayer passive (top), multilayer active membranes (bottom) B) shows the bolts that penetrate the different layers of the HC-DE. C) Final attached configuration.

6.5.1 Multi-layered HC-DEA results

The mechanical performance results of the multi-layered actuators developed in chapter 4 are presented here. In essence, each additional layer increases the stiffness of the system similar to how using multiple elastic bands increases the stiffness and force output of a slingshot. Firstly, the relaxation test described in 6.2.3 was performed on 5 samples of each of the layer variations described in 6.1.3.

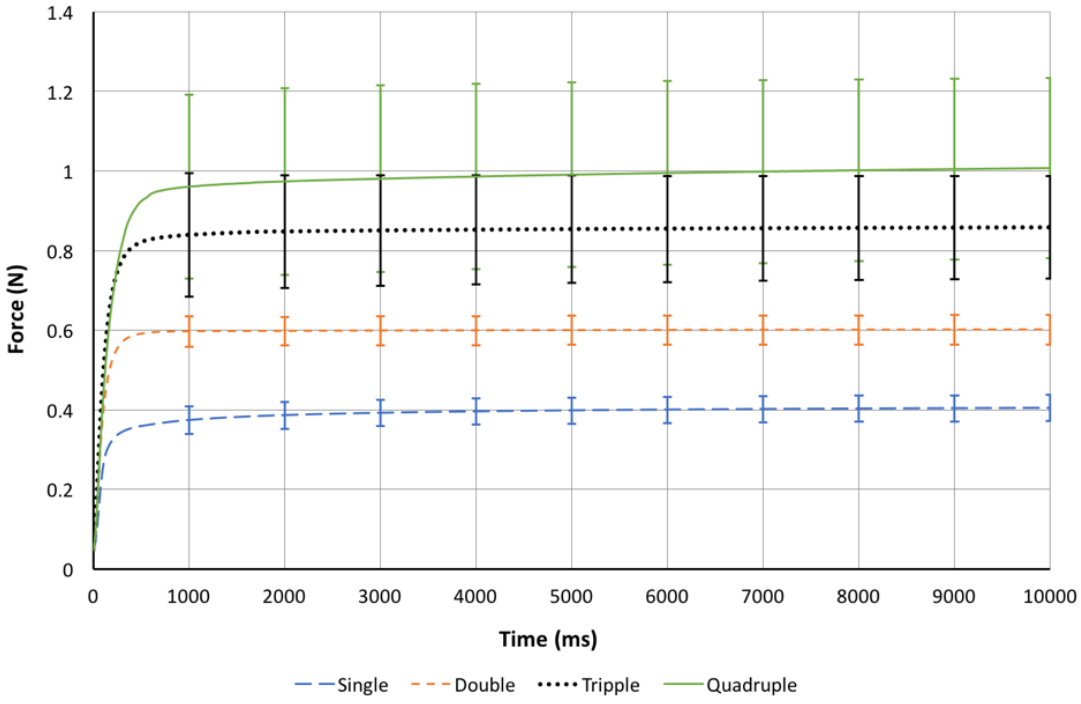

Figure 6-15 Graph showing the relaxation test performance of the actuators described 6.1.3 over a 10 second period. Error bars represent 2 standard deviations from the mean (95% confidence level).

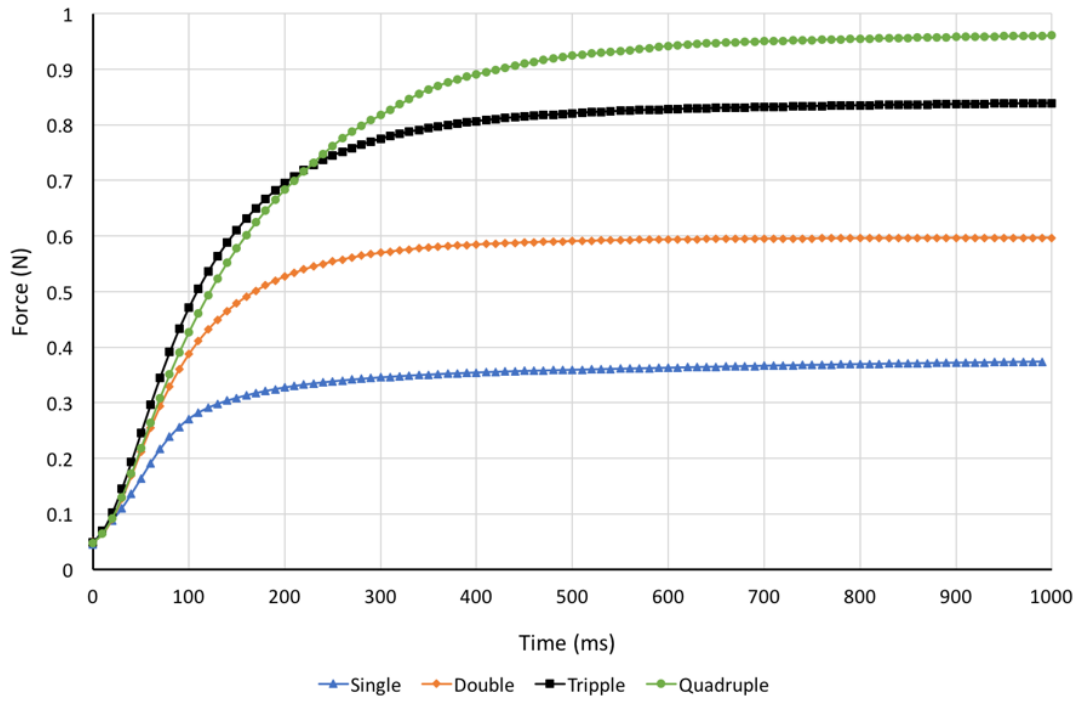

Figure 6-16 Graph showing the relaxation test performance of the actuators described 6.1.3 over a 1 second period.

The above figures show the relaxation of the differently layered HC-DEAs from a state of full actuation (4kV) to zero actuation (0V). It is clear that the multilayer approach significantly improves the uniaxial force output of the actuators. What is also apparent is that there is more variation between the samples tested with a higher number of layers. This could be due to not only the larger force ranges in which they operate, but also due to manufacturing inconsistencies in the prestretch phase, which are compounded with each additional layer. It was also found that quadruple layer actuators appeared to be the manufacturing limit with design and material used in this in this work. Higher layer numbers would often fail due to rupturing of the interface between the active and passive membranes, as there is more stress upon this bond. A potential way to negate this could be to increase vertical clamping pressure of the rigid upper and lower support frames in the fabrication phase or to increase the bonding surface area of where the active and passive layers adhere. An issue with the latter is that this would increase the lateral diameter of the device, and therefore would not be suitable for a multi-finger wearable solution. It was also found that for higher layer numbers, triple and above, it would be more likely to work very poorly or not work at all. It is believed this could be due to electrical contact issues between the penetrating electrode bolt and the compliant electrode material used.

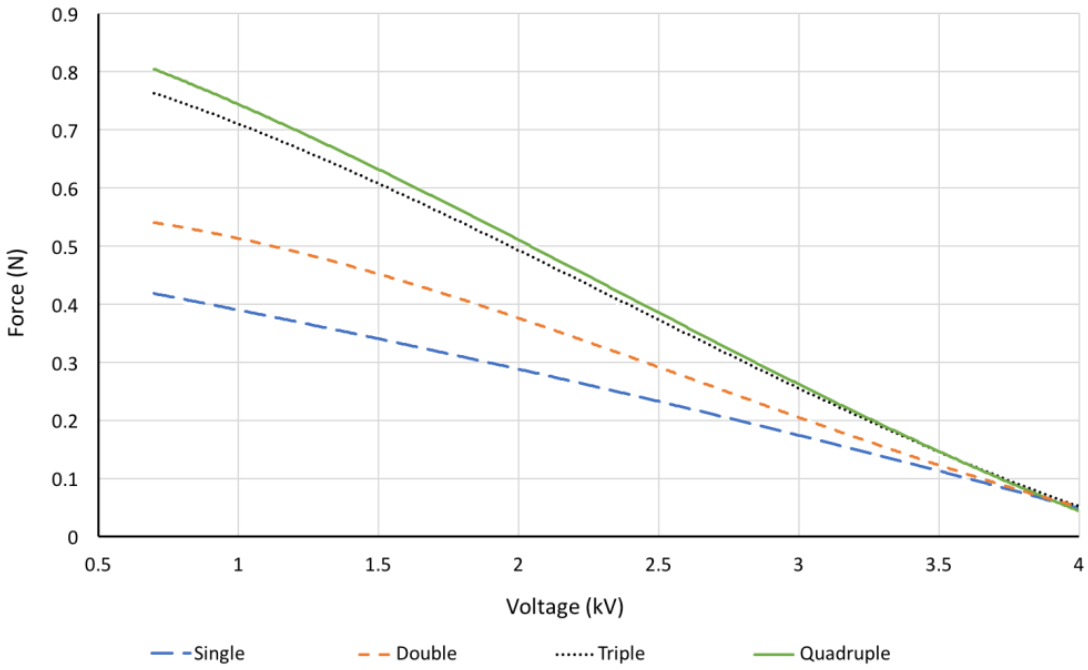

Figure 6-17 Results of the voltage induced force test outlined in 6.2.2 for different layered actuators. 5 samples for each of the different layer numbers were tested and a fitting line drawn.

The above figure shows the voltage induced force for a ramping signal as described in 6.2.2 for the differently layered actuators. One of the most interesting aspects of this test is the poor average performance of the quadruple layer actuators. A possible reason for this could be due to the larger capacitive surface area of the quadruple layer configuration increasing the time it takes to electrically discharge through the load resistor. A possible way to test this could be to short both sides of the actuator at the same time as switching off the voltage supply, and seeing how this affects the force relaxation profile, as shown in figure (6-19). Another issue is again the spread in performance across the higher layered actuators, with triple and quadruple typically performing around +-12.5% around the mean, and single and double this being ~+-2.5% and 5% respectively. Again, this is believed to be due manufacturing inconsistencies which are compounded with higher layer numbers.

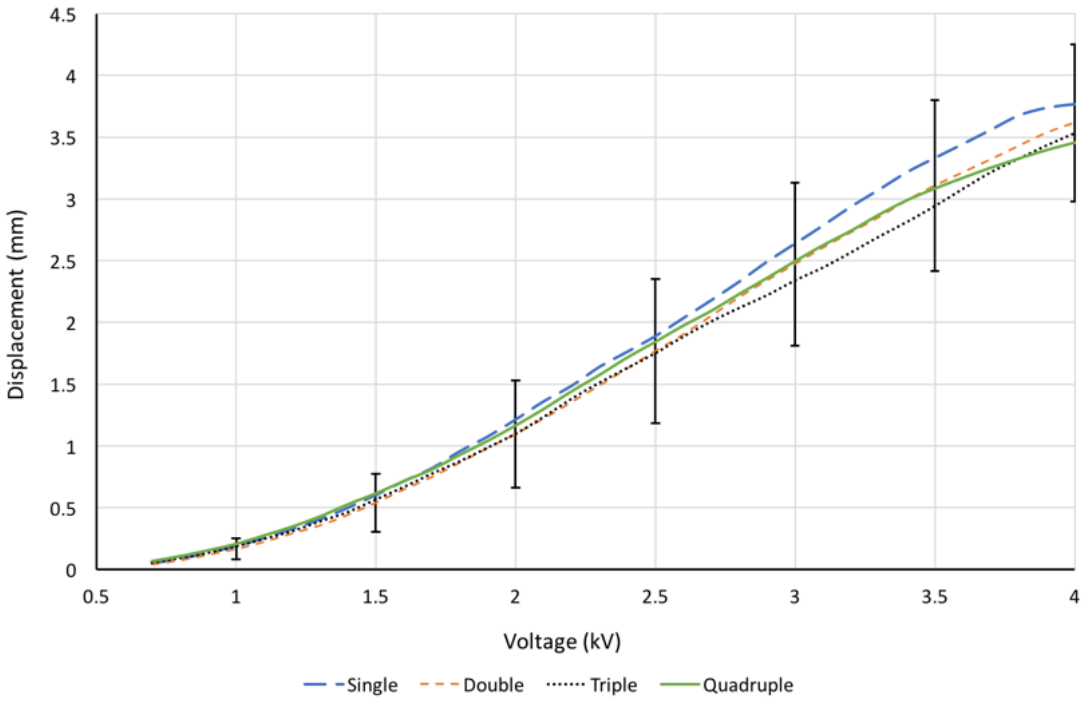

Figure 6-18 Results of voltage induced displacement test outlined in 6.3.1 for different diameter actuators. 5 samples for each of the different layer numbers were tested and a line that represents the average of the five samples is drawn above. Error bars represent 2 standard deviations from the mean (95% confidence level) for all the samples tested.

The above figure (6-21) shows the displacement performance across the four differently layered actuators described in 6.1.3. It appears that the displacement performance of the actuators is not significantly affected by the addition of more layers in this test. The error bars in the above diagram represent two standard deviations from the mean performance of all the samples tested. As expected there is a slight increase in the spread of triple and quadruple layer actuators, but not as significantly as seen in the force induced voltage tests. To test if the addition of more layers to the actuator changes their frequency response performance, the test described in 6.3.2 was performed.

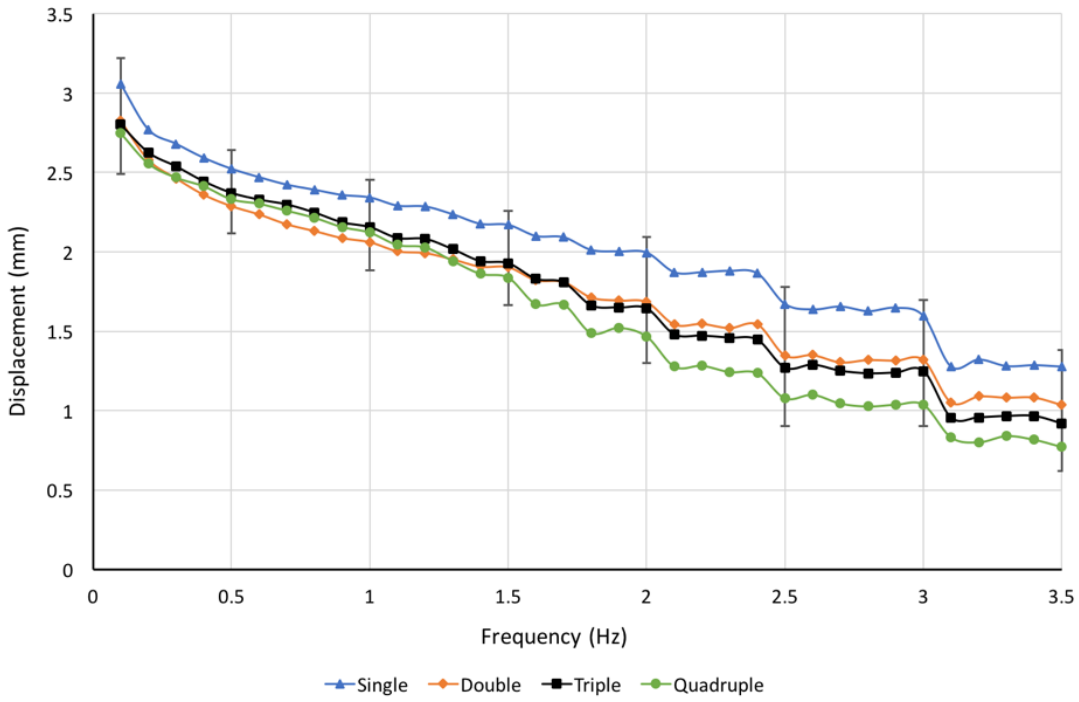

Figure 6-19 Results of the voltage induced displacement test outlined in 6.3.2 for different diameter actuators. 5 samples for each of the different layer numbers were tested. The line that represents the average of the five samples in drawn above. Error bars represent 2 standard deviations from the mean (95% confidence level) for all the samples tested.

Given the circuitry and control system described in chapter 5, the addition of more layers does not appear to significantly affect the frequency response of the actuators. An interesting feature to notice in the above figure (79), is that there seems to be a plateau in the frequency response at 2.1, 2.5 and 3.1 Hz. Further tests need to be conducted to see if this issue with the high voltage controlling electronics system described in chapter 5, or perhaps a feature of the actuator itself.

6.6 Conclusions and discussion of the electromechanical characterisation tests

In the tests conducted, it was found that the larger uniaxial forces can be generated with larger diameter HC-DEAs. It has also been found that applying more layers to HC-DEA membranes as shown in 4.4.1, will increase the overall uniaxial force performance without increasing the driving voltages required. As concluded at the end the chapter 6.4.2, 12.5mm HC-DEA appears to be an optimal compromise between force generation and minimal lateral width. It was discovered that quadruple layer actuators provided the highest force output but that these would be more prone to failure due to a peeling and rupturing between the passive and active membrane interface. A possible way to overcome this limitation, is to develop a method that improves the adhesion between these two membranes, possibly by using a bonding agent or double-sided tape; Another method would be to apply an external clamping pressure to these membranes through the laser cut support frames in between the phase when the HC-DEAs are formed in the vacuum cavity process described in 4.4.2, and when the actuator is clamped together within outer protective casing developed in chapter 4.

The design opted for use within the psychophysical performance tests is the 12.5mm, 300% prestretch, triple layer HC-DEA, due to its good uniaxial force performance range of ~0.8N (+-0.1N). It was found that within the voltage induced force tests that we could achieve an almost linear relationship between control voltage and force output between 0.7 to 4kV. To mitigate the viscoelastic performance drop-off effects of the VHB film, tests were performed the day after actuator fabrication.

7 Psychophysical testing

In this chapter, the ability of the system to render distinguishable soft tactile forces will be assessed. It is important to note that the limits of human perception for tactile interactions are not being accessed, but instead, the aim is to see how the system proposed performs within standardised perceptual threshold tests. To do this, four psychophysical tests are proposed.

7.1 Psychophysical testing methodology

The primary psychophysical testing metric in this work is JND, which is then used to calculate Webbers fraction, also known as the K value. The K value relates to the proportional change of intensity of a stimulus that needs to occur, in order for a difference to be perceived. This has been selected as it is a common psychophysical performance metric used to evaluate haptic devices (Faimagne, 1986; Fan et al., 2009; Jones, 2000; Jones and Lederman, 2006). JND is discussed in more detail in section (2.1.4).

In this work, the ability of a user to differentiate between electronically controlled uniaxial soft forces applied to their fingertips generated from the device developed in this work will be examined. For this, two types of touching tests have been designed; one where force is rendered to a single fingertip (7.1.4), the other where force is rendered to multiple fingertips (7.1.5). In these tests, the soft force stimuli rendered are not proportional to object penetration, as with the 'dynamic tests', instead they are applied in a single step, as is comparable to the maximum rate of static force application test described in 6.2.3.

Whereas for the 'dynamic' tests, the user has to perform an active motion upon a virtual soft object to deduce its tactile properties. To these means, the low-cost optical tracking system known as the Leap Motions will be used. Two dynamic tests have been designed. In the first test, the tactile display is placed on the thumb and the index finger in order to render a 'pinch gesture' upon a virtual soft ball object, which renders varying maximal soft forces to the user's fingertip (7.1.6). The second dynamic test involves the ability of the user to distinguish how far an object has to be pushed in order for a fixed maximal force to be rendered. Thus, identifying a softer or harder virtual object (7.1.7).

In all of these psychophysical tests, the triple layer, 12.55mm actuator is used. This configuration is used as it generated significant forces (up to ~0.7N) in a compact form factor, without being prone to rupturing as found with the manufacture of quadruple layer HC-DEAs. The multichannel high voltage control unit developed in chapter 5 was used for all the tests conducted. The actuators were constructed the day before the user tests were performed, as to be comparable to the timeframe between construction and testing within the mechanical performance tests in section 6. To link voltage control to force output, it is assumed the actuator performs as concluded in mechanical characterisation section, chapter 6 for this configuration.

15 volunteer participants were enlisted, 9 males and 6 females, with an age range of 22 to 36. None reported any conditions that would affect their ability to perform the tests. Each participant had to read and sign an information sheet outlining tests they had to undertake, and which were approved by the ethical approval board of Queen Mary University of London (See appendix).

7.1.1 General Just Noticeable Difference test methodology used in this work

For all of the JND tests conducted, the user is presented with two virtual objects to compare. One reference object that has fixed tactile properties, and one comparator object, which has changeable tactile properties.

The focus of these tests is to determine the just noticeable difference threshold: the amount that the comparator object has to change from the reference object, in order for a difference to be perceived between them. The tactile properties of the virtual objects can change by either adjusting the maximum force rendered to the user's fingertip or by changing the amount of distance the user has penetrate or squeeze the object. In this work, the 'method of limits' is used to find the JND threshold which is described as follows.

At the start of the experiment, two virtual objects with the same tactile stimuli properties are presented to the user: One which is the reference object, and the other which is a changing object. These two objects exist in a space directly in front of the user and are presented on the left and right side of the user. The relative positions of these objects are displayed graphically on a monitor placed in front of the user, along with the relative positions of their finger or fingertips within this virtual space. The two objects are graphically identical, and the participant is not made aware which is

the reference object (the one with fixed tactile properties) and which is the competitor object (the one with changeable tactile properties), but the user is made aware at the start of the experiment that objects have identical tactile properties. The user is then asked to familiarize themselves with the identical tactile properties of the two objects. The comparator object is then lowered in intensity by a predetermined incremental step. Intensity, in this work, either relates to the maximum force a virtual object delivers once touched, or the distance the user has to penetrate or squeeze the object. The participant is then asked to compare the two objects to identify if they perceive a difference. The user is allowed to compare the two objects presented as many times as they wish at each incremental level. This process is then repeated until the user can correctly perceive a noticeable difference between the two objects presented and identify which is the reference and which is the comparator. The difference between the tactile properties of the two objects at that point represents the Just Noticeable Difference (JND) for that particular reference level. In this work, five different reference levels are selected for each of the tests. These reference levels correspond to five equally spaced force values, or five equally spaced object penetration distances as outlined in subsequent sections. These five results are then plotted on a graph of JND against original reference level. Using the least square method, a linear fitting line is drawn through the 5 points of the graph. The slope of this linear fitting line represents the K value or the Webbers fraction for that test.

7.1.2 Psychophysical testing programme environment

In this work, a custom testing programme was developed for the psychophysical experiments. The general purpose of this software for each of the tests is as follows:

1. Present two comparable stimuli to the user.
2. Allow the experimenter to change the intensities of the stimuli presented.
3. Record the intensities of the two stimuli when a difference is perceived by the user.
4. Test for a different stimuli intensity reference level.

The first goal is achieved based upon the basic haptic rendering model outlined by (Salisbury et al., 2004). Inputs to the system, position of the user's fingertips, are provided through the Leap motion tracking system. For the programme to interface with the optical tracking hardware, the Leap motion SDK version 2.3.1 for Macintosh

64 bit is used. In this work, the Cartesian 3D coordinate positions of the index and thumb fingertips above the sensor are used. The tracking system provides data in millimetres at a maximum rate of ~60Hz. Once the position data is acquired, it is then compared to the positions of the objects within the virtual scene. If there is a contact between the virtual position of the user's hand and that of the virtual object, a corresponding value relating to the stimulus to be rendered for that object is sent to the tactile control unit as described in section (5.4.3); and a corresponding graphical output is rendered, this occurs at a rate of ~30Hz. The graphical output is generated using the Processing 3.0 Java library ("Processing.org," 2017). For the four interaction types tested in this work, there are four corresponding graphical user interfaces. These are described in methods relating to each test.

The second goal of the programme is to act as an interface for the experimenter to select the tests to be conducted, and to change the intensity of the comparator stimuli for each of the reference values for that test. To these means, the tester interface is rendered on a separate screen to that of the participant interface and controlled with a keyboard interface. In this experimenter interface, units of the intensity of the stimulus are given as a percentage of the maximum stimuli for that particular test. For example, in a force discrimination test, 100% will represent a maximal force, in this case with HC-DEA used, ~0.72N. This corresponds to the voltage across the actuator switching from a state of 4kV to 0.7kV, when one of the stimuli zones is touched. The experimenter can then lower the comparator stimulus zone intensity by steps of 1%, which equate to ~0.0072N steps or increments of ~33V.

The last objective of the programme is to record the JND for each of the reference values for each of the tests. This is done by generating a Comma Separated Value (CSV) file for the results of each of the participants. In this experiment, all data is kept in a pseudo-anonymous fashion as no personally identifiable tags other than the age, sex and dominant hand of the participant are kept.

7.1.3 Placing and fitting of the tactile display

As discussed in the final design presented in chapter 4, the device is fitted to the participant's fingertip using cast silicone straps. These straps vary in size to account for the different fingertip diameters of the participant's fingers. In this work, the tactile display is mounted as to stimulate the pulp of index and thumb fingertips. At

the start of the testing, the participant is asked which is their dominant hand. The device is then placed on this hand by the experimenter, as shown in figure 7-1. A strap to hold the cables out of the way of the optical tracking system is also used.

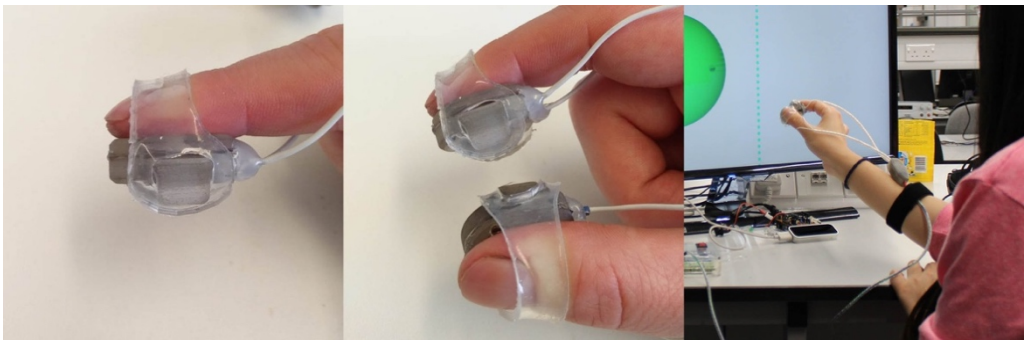

Figure 7-1 Left: tactile device placed on the index finger, Middle: Placed on Index and thumb, Right: With cable strap.

7.1.4 Just Noticeable Difference test methodology for single finger touch interaction

For this test, the users were presented with two stimuli zones which were navigable with the optical tracking system described (Leap Motion, 2018). There was also an accompanying 2D graphical output displayed on a monitor placed in front of the user, which shows where the participant's fingertip is in relation to virtual stimuli zones.

For this test, a uniaxial force is applied to the participant's index fingertip when their fingertip is within one of the stimuli zones, as illustrated by the grey cylinders in figure 80.

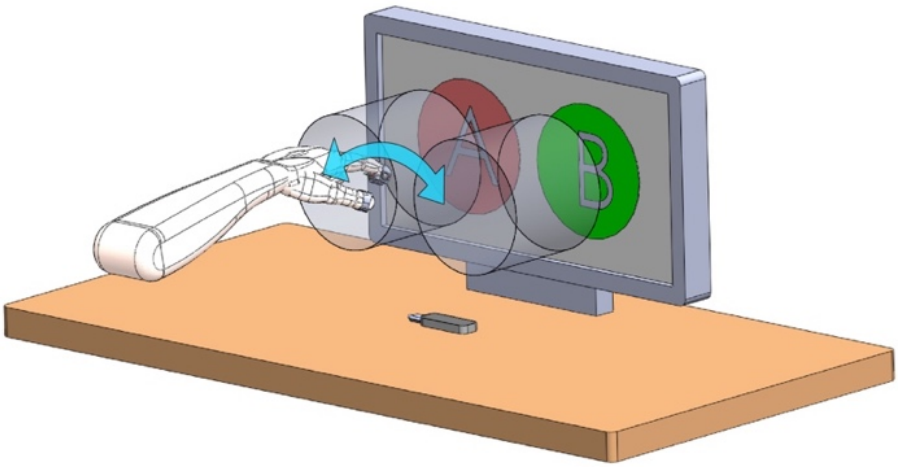

Figure 7-2 Rendering of non-dynamic touch interaction scene, displaying stimuli zones A and B. When a user's hand is within one of these stimuli zones displayed as the grey cylinders, a force corresponding to that object is rendered by the display to the fingertips. The blue arrow shows the movement of the user to compare the two zones.

The pseudo code for this interaction is as follows:

1. Is hand in the leap motion scene?
2. If yes, get index fingertip position from leap motion.
3. Check if fingertip position is within one of the two stimuli zones.
4. If yes, render force corresponding to that stimuli zone by dropping voltage from 4kV to the voltage of that stimuli zone, and update the graphical scene.
5. If no, no force applied to fingertip, 4kV applied across actuator.
6. Loop back to 1.

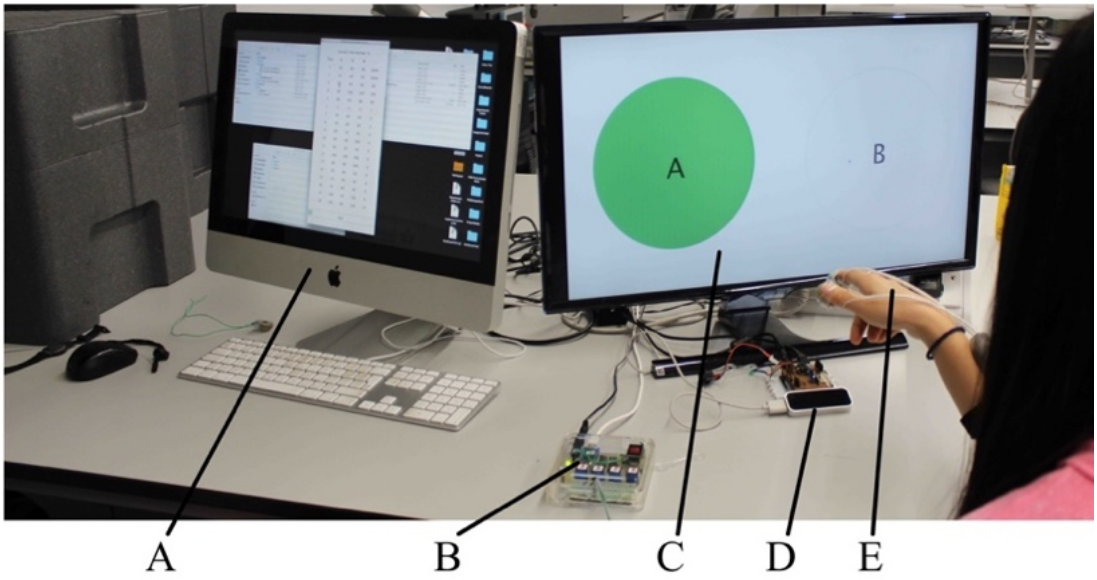

Figure 7-3 A) Control computer and experimenter interface; B) Multichannel HV system developed in chapter 5; C) Graphical interface for user; D) Leap motion optical hand tracking sensor; E) Wearable tactile display system developed in chapter 4. Image shows a participant touching a virtual object on the right side of the screen.

At the start of each of the tests, the user was asked to navigate between the two stimuli zones to familiarize themselves with the stimuli presented. In this case once the fingertip, displayed as a purple dot, was within one of the stimuli zones, displayed as a green circle, the voltage across the actuator would be switched from 4kV (V_0), to one of the five reference voltages ($V_{1\text{-}5}$), and the circle would change colour indicating a touch. The reference voltages correspond to five equally spaced forces ($F_{1\text{-}5}$) as determined below.

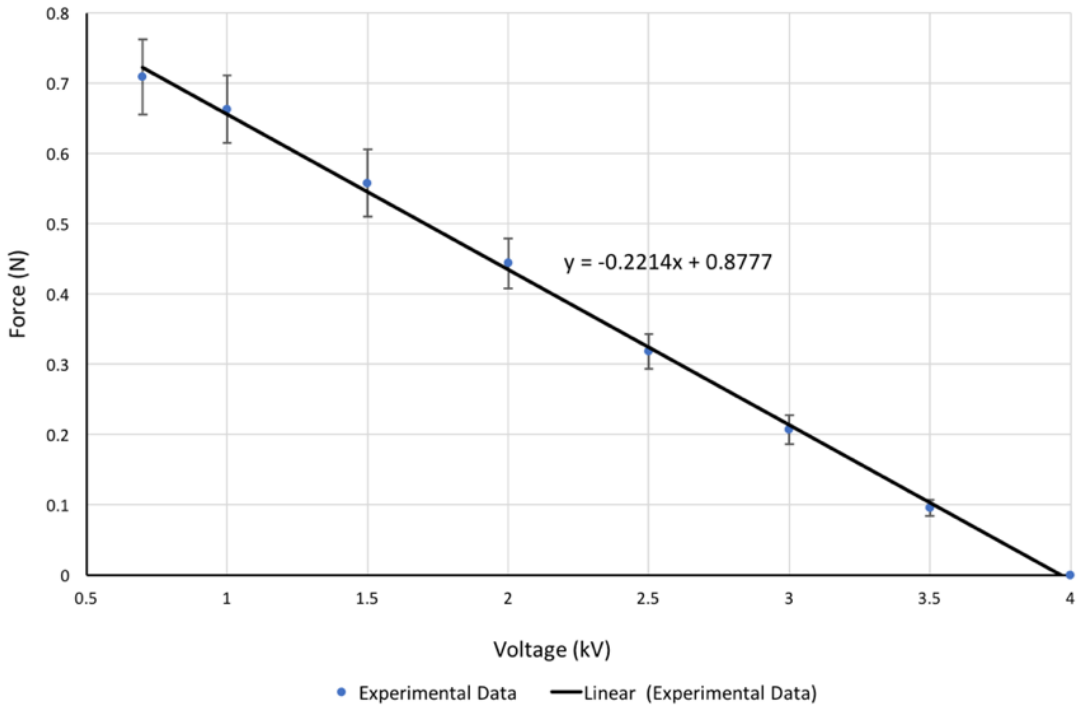

Figure 7-4 Linear fitting line applied to experimental data of triple-layer, 12.5mm HC-DEA actuator used in the psychophysical experiments. Error bars represent a 95% degree of confidence.

As found in the uniaxial voltage induced force tests described in 6.2.2. An almost linear relationship was discovered between voltage and force output between the voltages of 0.7 and 4 kV, as shown in the above figure (81). Offsetting the data to start at 0N at 4kV, and using the least squares method to calculate the gradient of the linear fitting line, the following equation was deduced:

$$F = -0.2214V + 0.8777 \quad (1)$$

Using the above equation, the five reference voltages ($V_{1\text{-}5}$) and corresponding forces ($F_{1\text{-}5}$) are outlined in table 1. The table also shows the digital 8 bit PWM value, the value sent from the control programme via a wired USB connection to the multi-channel high voltage control unit described in chapter 5.

Table 7-1 Table showing five equally spaced force values and the corresponding control voltages and digital PWM value.

Referenc e	Corr. force value (N)	Reference	Voltage (kV)	Digital 8 bit PWM Value	Stimulus intensity (%)
F0	0	V0	4.0	200	0
F1	0.15	V1	3.3	168	20
F2	0.29	V2	2.7	135	40
F3	0.43	V3	2.0	103	60
F4	0.58	V4	1.3	69	80
F5	0.72	V5	0.7	36	100

Once the user familiarized themselves with this reference force stimulus rendered in both the reference zone and comparator zone at the start of each test, the user was asked to navigate back and forth over the two zones presented. The experimenter then gradually decreased the force applied from the comparator zone, until the user indicated that they could feel a noticeable force difference between the two zones. Once the user could perceive a difference between the zones, by indicating to the experimenter that could perceive a difference, they were then asked which zone had the lower intensity. If the user stated the correct position of the comparator zone, the delta in intensity between the zones was recorded as the Just Noticeable Difference for that reference value. If not, another reference value was tested, and the previous test would be repeated until the correct position of the comparator zone was consistently identified, but in practice, this never occurred. The position of the comparator zone and the reference zone alternated in a random fashion between tests. The reference levels were also tested in a random order as it tended to keep the participant more focused on the task.

7.1.5 Just Noticeable Difference test methodology for multi-finger touch interaction

To demonstrate that forces can be applied simultaneously to multiple fingertips with the system proposed, a multi-finger JND test is performed. The test methodology is almost identical to that of the single-finger force discrimination test, but in this version, a force is applied simultaneously to the thumb and index finger upon a touch of a stimuli zone. To simplify the graphical interface and also the collision detection, a single marker representing the mid-point of the two fingertip positions is displayed.

7.1.6 Just Noticeable Difference test methodology for pinch interaction

For the third experiment, a pinching JND force discrimination task, a pinching motion using the thumb and index fingers was required in order to compare the force output between two virtual 3D soft balls. In each test, the user had to distinguish between two virtual ball objects, which were rendered depending on which side of the screen the participant was performing the pinch motion upon. As you can see in Fig. 84. the participant is performing a pinch motion on a virtual ball object on the left side of the screen. The participant then has to perform a pinch motion on the right side of the screen where the other comparison virtual ball object will be rendered. Similarly, to the touching tasks, the participant is asked to compare the two to see if they perceived that pinching one ball rendered a higher force during the pinch motion compared the other.

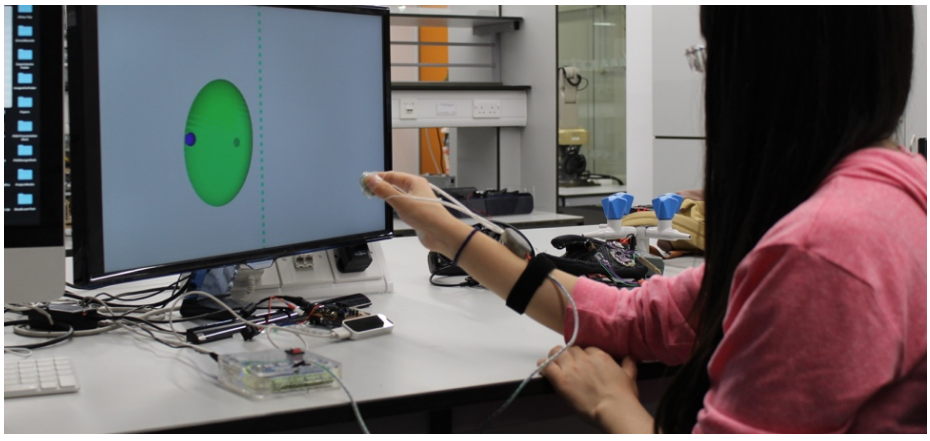

Figure 7-5 User performing the pinch gesture on the left side of the screen.

The pinch motion effectively allowed users to test the mechanical compliance of a 3D virtual ball. To make it easier for the users to pinch the virtual ball objects, the ball objects would track to the 3D coordinates of user's hand above the leap motion. This

allowed the participant to perform the pinch motion effectively anywhere on either the left or right side of the screen/ motion tracking area. In effect, it is similar to having a soft ball gripped between the thumb and index finger, and by moving the thumb and index finger closer and further apart, the compliance of that ball can be perceived, as force would be linearly ramped upon the fingers across this motion.

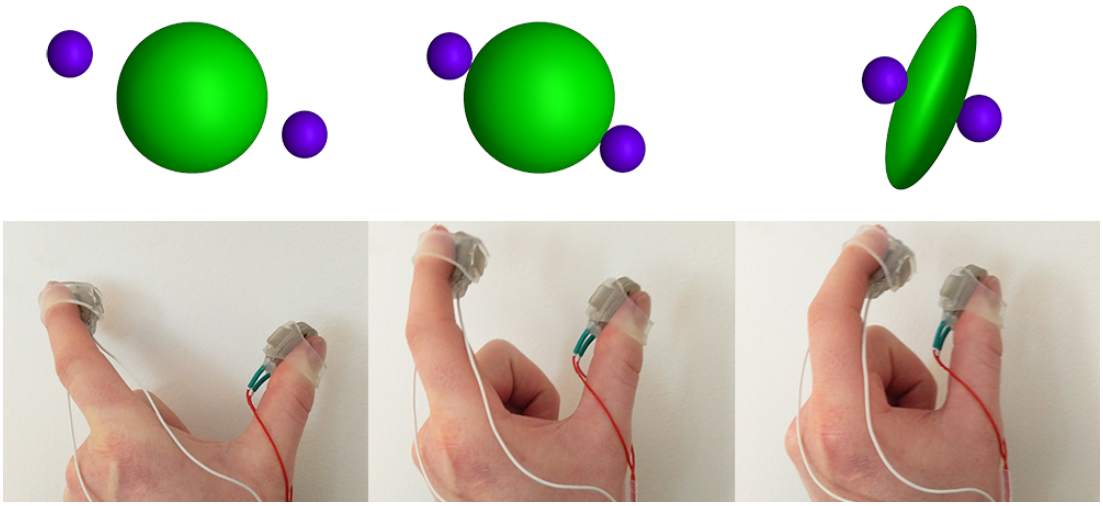

Figure 7-6 Figure showing the pinch motion of the user. Top: virtual graphical representation displayed to user, Bottom: real-life position of the user's hand. Far Left: fully open pinch position, Middle: ¾ pinch position where force starts to be applied to the user's fingertips, Right: Full force for that stimuli ball at ¼ pinch position.

The virtual ball was effectively 75mm in diameter. This meant that the participant starts to feel a linearly ramped force when their index and thumb fingers are 75mm apart, as recorded by the tracking system. Maximal force for the pinching of the ball would be applied when the fingers are <=25mm apart. Effectively this gave a pinch motion range of 50mm. These values were selected as it catered for a comfortable pinch range, whilst still be large enough to be adequately detected by the leap motion, which has a resolution of ~1mm.

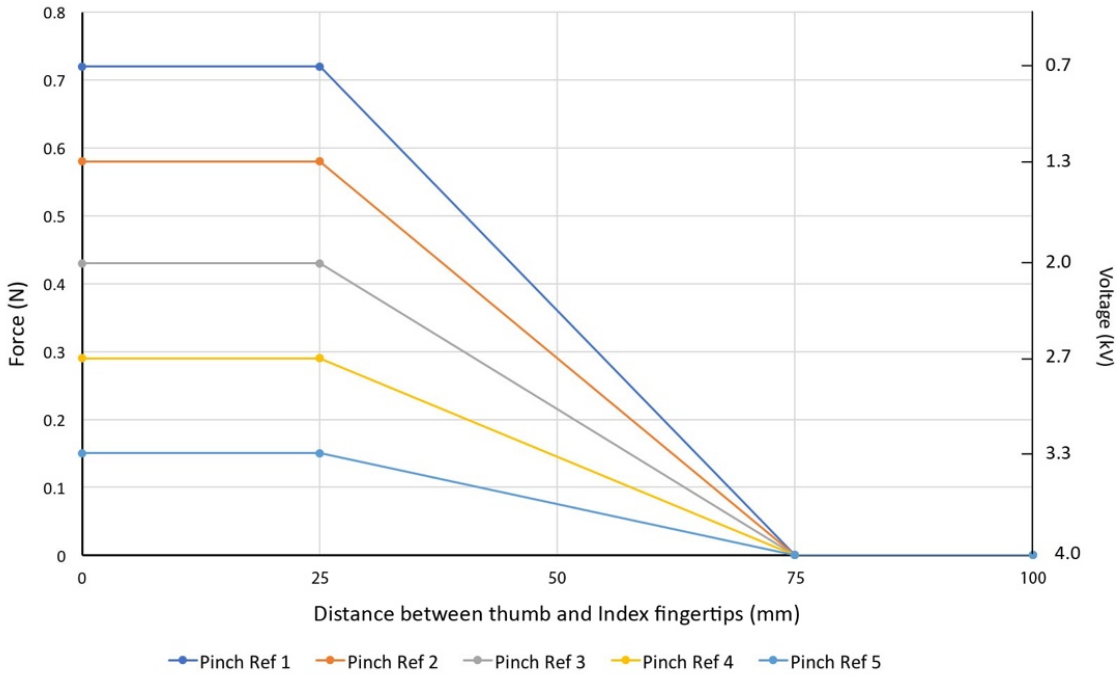

Figure 7-7 Graph showing how the force is applied over the five different reference values over the pinch motion assuming a linear relationship between voltage and force output over the 0.7V-4V range.

As with the previous JND tests, five reference force levels were tested. These correspond to five equally spaced forces, as shown in figure 7-7. At the start of each reference value test, both balls rendered the same maximal force when a pinch motion is applied. Then the experimenter would lower the force rendered for one of the virtual balls in a similar fashion to that of the single and multi-finger JND force discrimination tests.

7.1.7 Just Noticeable Difference test methodology for soft object palpation

For this test, the participant is presented with two virtual soft boxes. When the participant lowers their hand upon one of the boxes, a force based upon the vertical object penetration distance is applied to their index and thumb fingertips. In effect, the sensation is similar to palpating a soft deforming object lying on a table. In this test, instead of changing the maximal force applied when interacting with the virtual object, the distance in which the user has to palpate the object is changed. This is to simulate touching "softer" and "harder" static objects. In this test, softer boxes relate to a force being applied over a larger palpation distance; in which case, the user will have to move their hand further to perceive the same maximal force. Harder boxes apply the same maximal force, but over a shorter palpation distance.

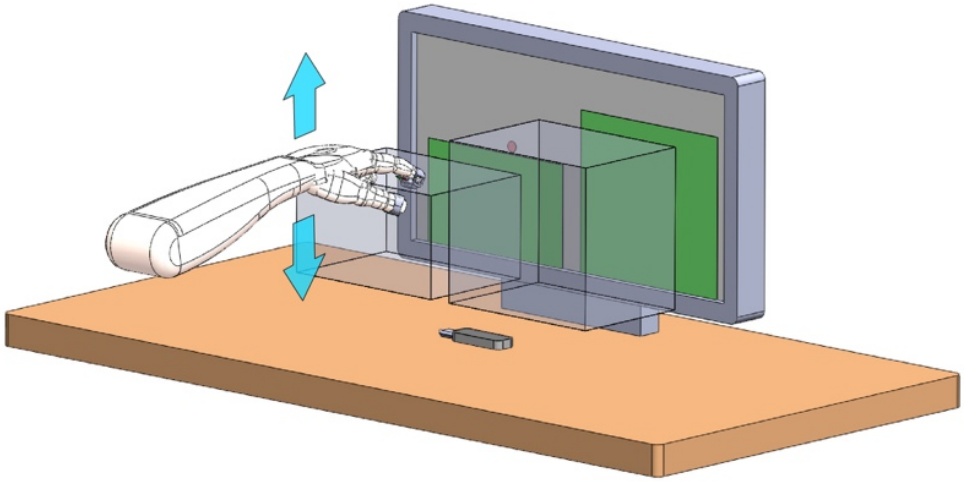

Figure 7-8 schematic highlighting the palpation motion on a virtual soft object (displayed by the transparent grey boxes).

Again, five equally spaced reference values are tested. In this test, these reference values correspond to 20, 40, 60, 80 and 100mm. These values were selected as to maximise tracking accuracy from the tracking system used. Figure 7-9 shows the force applied to the participant's fingers at different object penetrations, for the five different reference values.

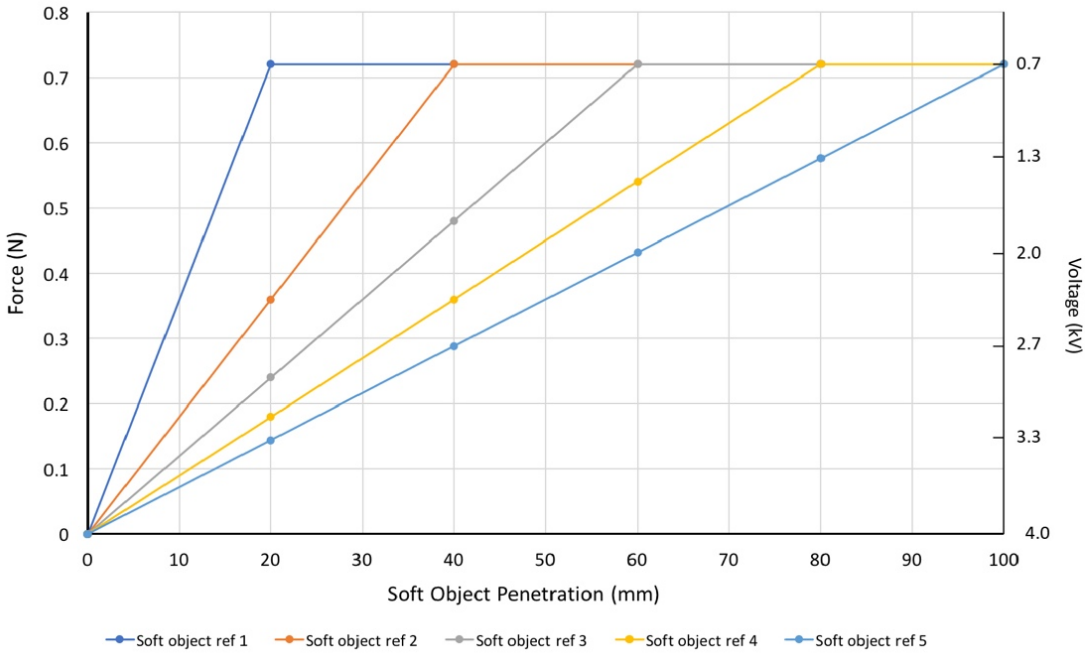

Figure 7-9 Force/ Voltage profiles of the five reference values to be tested. Soft object ref 1 is harder than soft object ref 5, as maximal force is applied over a smaller object penetration distance.

Similarly, to the previously described JND tests, one soft object would represent the reference stimuli, and the other would be the comparator stimuli. The left-right positions of these boxes would be random as with the other JND test methods. Participants at the start of the test would palpate both boxes as shown in fig 88. Initially, they are both set to the reference value being tested. For example, a reference value of 60 would correspond to the maximal force, 0.72N, at a 60mm palpation distance. Forces are linearly ramped due to object penetrations as shown in fig 89. Once the user has familiarized themselves with this palpation, the distance in which the force is applied over the palpation range would then be shortened by the experimenter for one of the boxes. When the participant perceives a difference between palpating the two boxes, the participant indicates this to the experimenter. The participant then has to inform the experimenter which box feels “harder” or “softer”. If the correct box is selected, the difference in palpation distances of the two boxes is recorded, and this is value represents the JND for that reference value. The test repeated for the five other reference values.

7.2 Psychophysical testing results

The results of the Psychophysical testing are presented here. The single finger and multi-finger tests were performed in an alternating order between participants to mitigate training effects, but the active pinch and single finger soft palpation tasks were performed after these tasks as the interaction required training, in order for participants to get used to the hand tracking system.

For each of these tests, 15 volunteer participants were enlisted, 9 males and 6 females. None reported any issues that would affect their cutaneous sensitivity or motor functions. The tests on average took around 20 minutes for each participant. Ethical approval was granted by Queen Mary University, see appendix. Only 8 participants completed the active pinch test, as this test appeared to have limitations which will be discussed later.

It was also noted that actuators could fail during testing. This could be due to over stretching of the HC-DEA or perhaps excess thinning of the active membrane due to the viscoelastic behaviour of the VHB film used. Failure is instantly perceivable due to the actuator going from a state of full actuation, where no force is applied; to zero actuation, where full force is applied. If at the start of each test, when the maximum voltage is applied across the actuator, and the passive surface of the actuator fails to move away from the fingertip, the actuator is therefore broken and has to be changed. If an actuator fails during testing, that specific JND test is repeated for the new actuator.

It is important to note that six of the triple layers, 12.5mm, 300% prestretch actuators were constructed and used for these tests; and therefore, there is an expected variance in the mechanical performance of actuators as concluded in section 6.

7.2.1 Single and multi-finger Just Noticeable Difference test results

The figure 7-10 (next page) shows the JND performance of the device placed on the index finger of the dominant hand of the 15 participants involved. The JND values are determined as the delta between the original stimulus, and the point where the participant notices a change to the reference stimulus as described in the method in 7.1.3. When the user indicates that they can perceive a difference between the stimuli

zones, the delta is recorded and the next reference stimuli are tested. Tests are presented in a random order of the 5 reference stimuli.

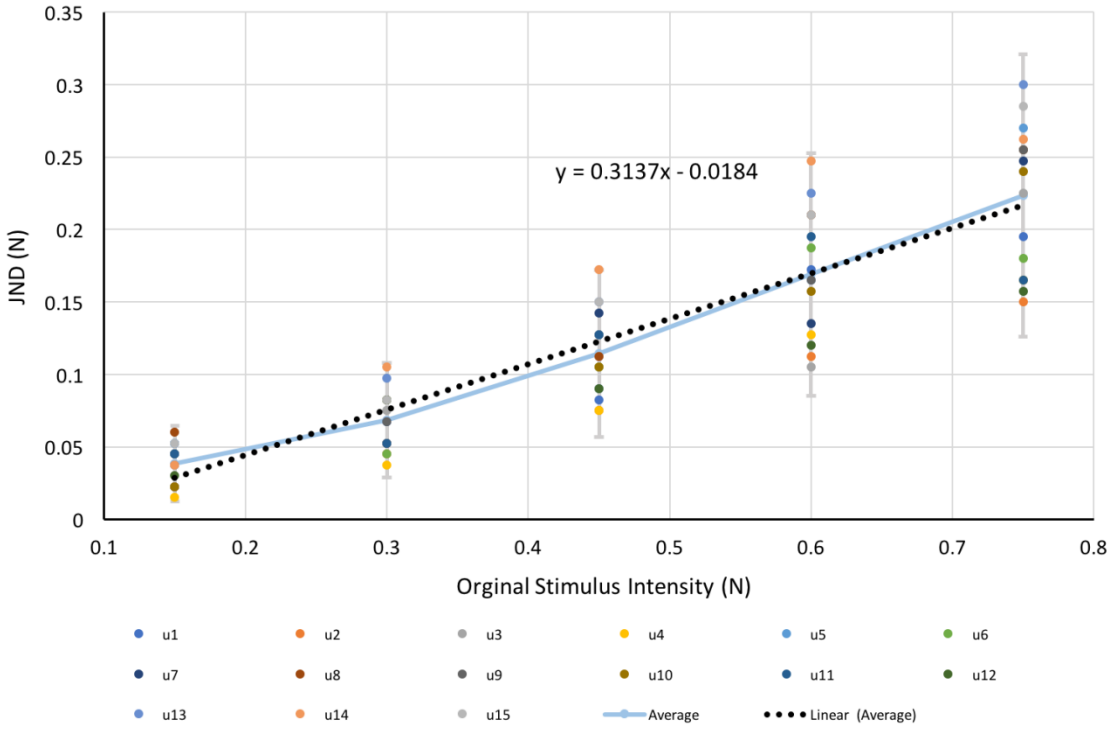

Figure 7-10 **Single finger JND test results from the method described in 7.1.1. Error bars represent a 95% degree of confidence, and the fitting line is drawn based around the average JND for each of the JND intensities.**

Creating an average performance for the 15 participants and using the least squares method gives an average K value (gradient of linear fitting line in fig 80) of 0.31 with a standard deviation of 0.07. Figure 7-5 shows the performance of the same 15 participants conducting the test with the device placed on both the index finger and thumb simultaneously.

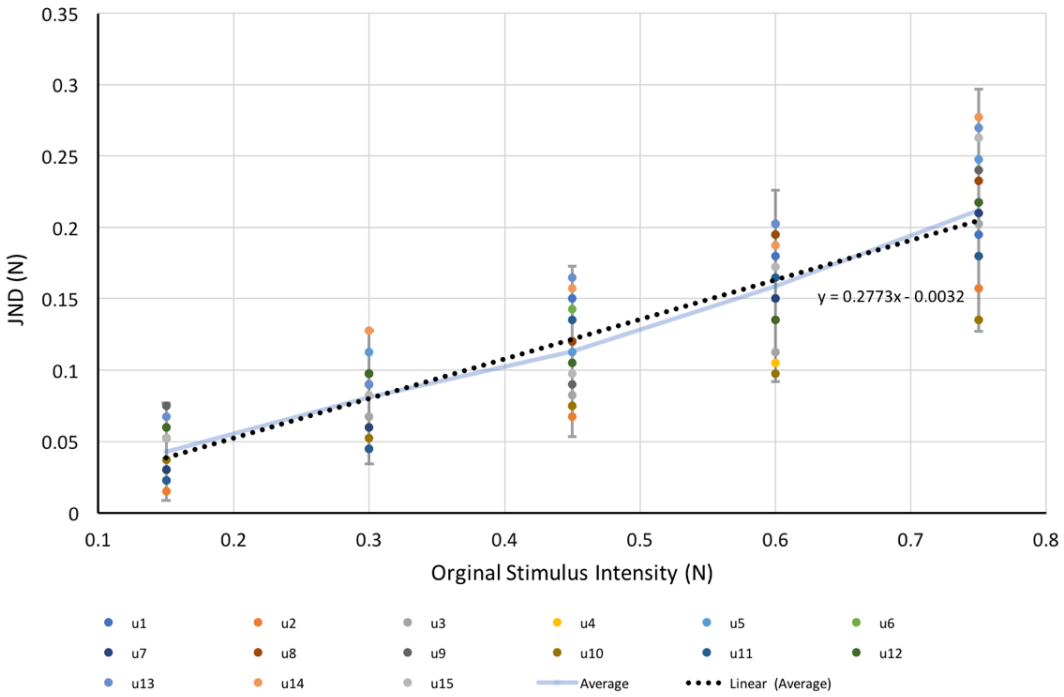

Figure 7-11 Multi-finger JND test results from the method described in 7.1.2. Error bars represent a 95% degree of confidence, and the fitting line is drawn based around the average JND for each of the JND intensities.

For the multi-finger version of the JND test outlined in 7.1.4, an average K value was calculated to be 0.28 with a standard deviation of 0.05.

Comparing the K values of the participants in each of the tests using a two tailed T-test, we derive a P value of 0.036. Suggesting that there is a significant K value performance increase between the two tests (assuming a 0.05 level of significance). This is discussed further at the end of this chapter.

7.2.2 Active pinch Just Noticeable Difference test results

The test was then repeated for the active pinch method described in 7.1.6. It is worth mentioning that only 8 out of the 15 volunteers were able to complete this experiment. Indeed, they required training to ensure that the pinch motion occurred in a plane parallel to the surface of the hand tracking sensor, which was necessary to prevent optical occlusion of the thumb and index fingertips from the other fingers.

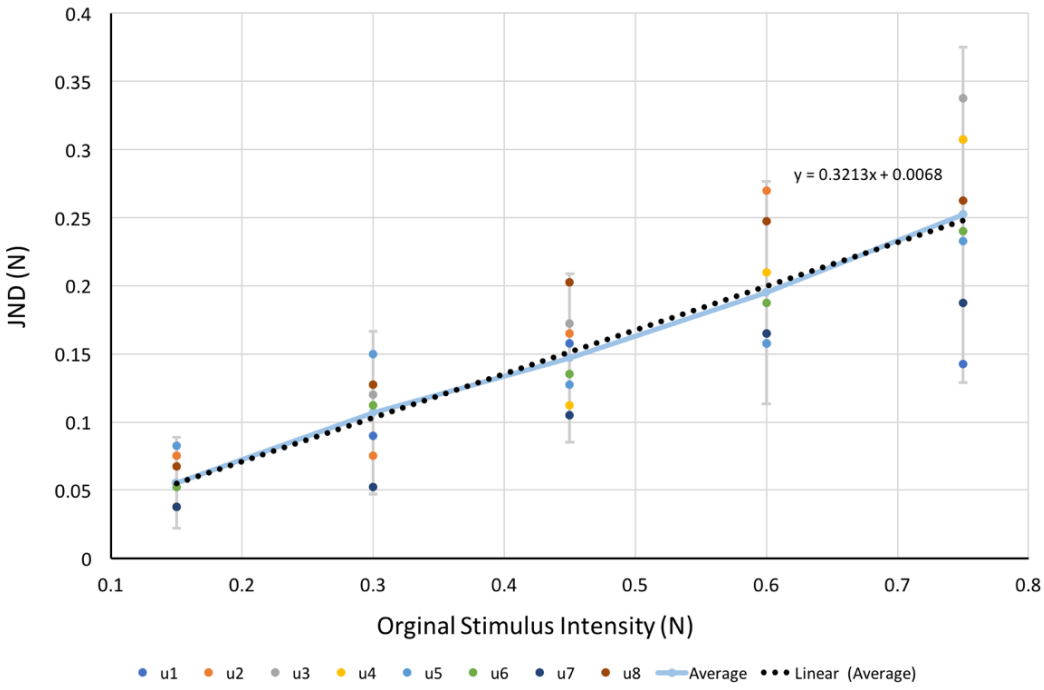

Figure 7-12 Active JND test results from the method described in 7.1.6. Error bars represent a 95% degree of confidence, and the fitting line is drawn based around the average JND for each of the JND intensities.

For the active pinch force discrimination JND tests, the K value was calculated to be 0.32 with a standard deviation of 0.09.

The higher K value and variance between the participants could be due to the increased difficulty of the test. It was found to be common for the tracking system to not accurately track the positions of the thumb and index finger simultaneously, typically due to occlusion by the other fingers. This led to an inconsistent haptic experience for some users. A possible way to mitigate this effect could be to locate the optical tracking above the participant's hands, as to have a top-down perspective of the scene, instead of a bottom-up perspective from the desktop position.

7.2.3 Comparison of force discrimination tests

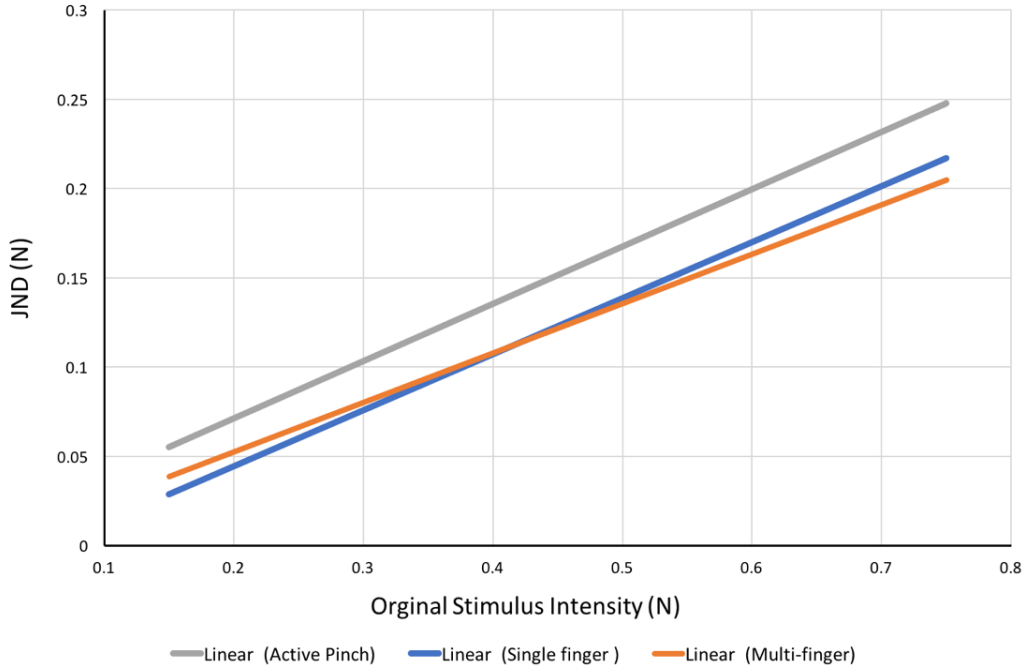

Figure 7-13 Comparison of average results for each of the force discrimination tasks described in 7.1

The above figure presents the average line of best fit for each of the force discrimination JND tests. It is noticeable that there is not a dramatic variance between the three types of interactions. This is confirmed by performing a one-way ANOVA test across the K values collected for the single, multi and active pinch force discrimination tasks. According to the test, there is no statistically significant difference in JND performance between these interaction types ($F = 1.36$, $P = 0.27$, $Fcrit = 3.3$).

7.2.4 Palpation Just Noticeable Difference test results

The last test in the series is the palpation task. For this test, all 15 participants could complete the task as per the method described in 7.1.7.

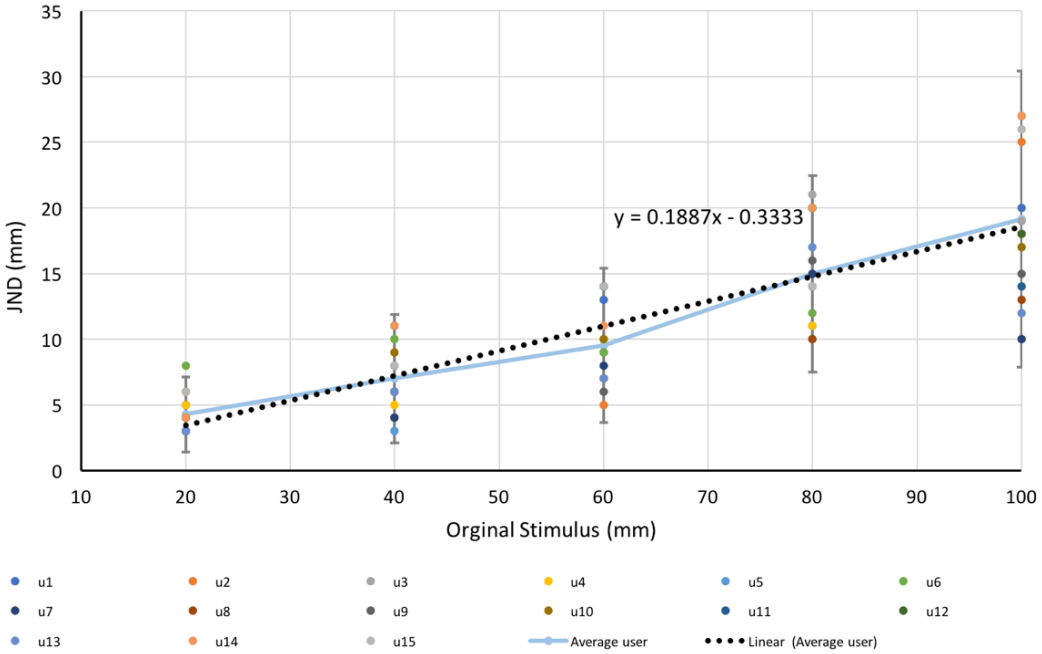

Figure 7-14 Results of soft object palpation JND test as described in the methodology in 7.1.7. Error bars represent a 95% degree of confidence, and the fitting line is drawn based around the average JND for each of the JND intensities.

It is important to note that for the soft object palpation task, JND and original stimulus units is measured in millimetres instead of Newton's, as the maximum force applied is the same in each of the tests (0.72N at 0.7kV), the only variable is the distance the finger has to travel for that force to be applied. For this test, the K value was calculated to be 0.19 with a standard deviation of 0.05.

7.2.5 Comparison table of K values collected in each JND psychophysical test

Table 7-2 K values of the different JND tests outlined in 7.1 for each of the different users.

Participant	Single Finger K Value	Multi-finger K Value	Active pinch K Value	Palpation test K Value
U1	0.26	0.28	0.19	0.17
U2	0.22	0.25	0.44	0.24
U3	0.27	0.27	0.41	0.23
U4	0.26	0.17	0.42	0.24
U5	0.37	0.31	0.21	0.27
U6	0.28	0.28	0.30	0.11
U7	0.31	0.30	0.28	0.13
U8	0.37	0.31	0.34	0.11
U9	0.38	0.30	-	0.17
U10	0.34	0.16	-	0.16
U11	0.26	0.29	-	0.16
U12	0.20	0.24	-	0.22
U13	0.44	0.35	-	0.15
U14	0.40	0.34	-	0.28
U15	0.40	0.34	-	0.23
Average	0.31	0.28	0.32	0.19
Standard Dev	0.07	0.05	0.09	0.05

7.3 Psychophysical testing conclusion and discussion

Through the psychophysical tests performed, it has been found that participants can use the system presented to distinguish between soft haptic stimuli rendered by the device in the four different test conditions. Furthermore, it has been shown that the device can be worn on multiple fingertips to facilitate multi-finger interaction with virtual soft body objects.

From the single finger and multi-finger JND force discrimination tests performed, it is calculated that the average participant generated a K value of 0.31 and 0.28 respectively. Using a two-tailed T-test, a P value of 0.036 is derived. Suggesting that there is a significant K value performance increase between the two tests (assuming a 0.05 level of significance). Although this suggests that there is a slight increase in ability for the participant to distinguish between stimuli that are closer in intensity using the multi-finger approach, further tests should be conducted to confirm this result.

Performing a one-way ANOVA test across the K values collected for the single, multi and active pinch JND force discrimination tasks suggests that there is no statistically significant difference in JND performance between these interaction types with the system proposed ($F = 1.36$, $P = 0.27$, $Fcrit = 3.3$).

The JND K values found in this work are comparable to those of other JND force discrimination studies performed on the index finger and within index and thumb pinch tasks, 0.19 – 0.31 (B. Färber., 2006; Brewer et al., 2005; Di Luca, 2011; Scilingo et al., 2010).

Performing the same one-way ANOVA test across the K values collected for all tests, including the single finger palpation task, there is a statistically significant difference in JND performance ($F = 10.8$ $P = 1.15E-05$, $Fcrit = 2.79$). This is due to the typically lower K value calculated from the performance of users in the single finger palpation task. These JND's are not directly comparable though, due to the nature of distinguishing between different forces and the same force but applied over varying object penetration distance.

The average K value for the single finger palpation task, 0.19 ±0.05, is comparable, although slightly higher to the results collected by Kocak et al of 0.13 ±0.07 (Koçak et al., 2011) and Genecov 0.14 ±0.03 (Genecov et al., 2014) for a similar soft object palpation task. Although the methods are not directly comparable, due to soft forces being generated by a fixed desktop device, rather than wearable tactile fingertip attachment. This could explain the slightly higher K value, possibly due to a lack of kinaesthetic sensation delivered by the system proposed in this work.

One issue that could affect the data collected is the variance in actuator performance. This is particularly so, as during testing, four actuators failed and had to be replaced. Failure of the actuators typically occurred between participants when the device was being placed on the fingertip of the new user. Although during this fitting phase there is no voltage applied across the actuator, it is possible that overstretching of the active membrane could occur, and therefore fails when a voltage is applied at the start of the perceptual tests. Further investigation needs to be conducted to confirm this.

Another issue was the tracking capability of the optical tracking sensor used. This particularly affected the active pinch task, as it was common for index and thumb

pinch gesture to be occluded by the other fingers. This too has been found by other groups, who suggests that the optical motion tracking controller is placed perpendicular to the motion of the fingers for optimal tracking (Okazaki et al., 2017). As suggested, moving the optical tracking system as to have a top-down perspective of the scene might improve the tracking consistency in the active pinch task. Issues pertaining to the tracking consistency, especially in dynamic scenarios, have also been highlighted in previous studies (Guna et al., 2014; Niechwiej-Szwedo et al., 2018; Weichert et al., 2013).

8 Conclusions and future developments

This thesis has developed and investigated the performance of a new tactile haptic display for the purpose rendering soft forces to multiple fingertips simultaneously. It is believed that such an approach could have a significant impact on improving human computer interaction for purposes of medical simulation, teleoperation and virtual environment immersion.

To do this, various actuation techniques in fingertip tactile rendering were investigated. From this, dielectric elastomer actuators were selected as the most suitable candidate, although they also presented several problems affecting their adoption in a compact, lightweight and multi-fingertip system. The problems that were addressed are as follows: ability of a compact HC-DEA to generate significant forces, ability of a system to be placed on multiple fingers simultaneously, ability to be used in conjunction with a low cost optical tracking device, ability to control multiple DEA tactile devices simultaneously, ability for the tactile display to render varying types of touch interactions with virtual soft objects. This led to following investigations and results.

A new multilayer configuration of HC-DEA is proposed. This design has delivered a significantly smaller encumbrance to the device (20x23x12mm) as compared to the initial approaches in HC-DEA design(30x45x20mm). The smaller encumbrance of the device enables placement on multiple fingertips simultaneously whilst minimising impedance to fingertip dexterity. The design also makes it possible to increase the number of layers used in the formation of the active membrane. The new approach can achieve uniaxial forces of up to 1N as compared to 0.6N (Frediani et al., 2014b) and is driven by a maximum voltage of 4kV as opposed to 5kV. The containment of the HC-DEA on a rigid support frame also enables greater control of the actuators' dimensional properties, as well as providing a robust method in which to attach penetrating electrodes. The penetrating electrode design proposed appears to be a robust method in order to connect the corresponding electrode layers of the multi-layered HC-DEAs. The movement of the low-to-high voltage circuitry from the fingertip reduces significant bulk from the fingertip, minimising weight and size of the device on the fingertip. The device with the silicone strap weighs a total of 6g. This shows significant improvement over previous wearable systems, such as a single

finger HC-DEA approach at ~20g (Frediani et al., 2014b), A ring mounted SMA approach at 7.2g (Hwang et al., 2017) and is comparable to a uniaxial brushless DC motor version at 4.8g (Kawasaki et al., 2010).

Through the psychophysical performance tests conducted in this work, validation of the system's use in force discrimination tasks has been presented; as well as within more active virtual object interaction scenarios, such as soft object pinching and palpation tasks. It has been shown that the system can be used to differentiate between virtual "soft" objects of programmable tactile properties. The performance of the device is consistent with other investigations of psychophysical perceptual tasks.

8.1 Key contributions

The core contributions of this work primarily concern system design, manufacturing methodologies and testing in terms mechanical characterisation and user interaction. With this new system, it has been demonstrated that a significantly improved electroactive polymer actuator, in terms of mechanical performance and size, can be used to render multi-finger tactile interactions with virtual objects of programmable haptic properties for a variety of touch interaction types. Further to this, a number of research papers are now possible, to show how the system proposed in the thesis can be used to solve real-world problems. With this novel system, there are a number of possible future avenues of exploration which hopefully shine a light on the possible applications for electroactive polymers.

8.2 Future developments

This section describes ongoing research based upon the initial work presented in this thesis. The ultimate aim is to create a device a that can be turned into a robust development kit, in order to enable other software developers and designers to identify future use cases of such a soft tactile display. For this aim to be met, a number of areas are discussed. In summary, methods of improving the following issues are discussed: actuation cycle life, driving voltages, dense arrays, multiplexing of HV driving signals, mass manufacture techniques and integration into existing VR/AR development platforms.

8.2.1 Silicone elastomer construction

One of the primary issues with the device proposed in this work is the use of VHB Acrylic membranes. To mitigate the viscoelastic performance drop-off of this material, initial experiments are being conducted with silicone based elastomers, more specifically Elastosil (Wacker, Germany). The issues involved with this material approach is the difficulty in bonding layers of the thin silicone film together and a general reduced Arial stain of ~10% compared to <100% for VHB films.

Initial experiments with oxygen plasma bonding techniques have proved to be a robust way to bond layers of silicone films together, making the multilayer approach proposed in this work possible. Adhesion of the Elastosil silicone membranes to the rigid acrylic support frames (Plexiglas, Evonik, Germany) is adequate with double sided Kapton (DuPont, USA) tape method outlined in chapter 4.

To compensate for the drop in aerial strain, an Asymmetric ratio between the bottom active membrane and the top passive membrane has been proposed. To achieve this diameter of the hole in the centre of the rigid support frame on the top passive layer has been made smaller than that of the bottom frame. Performance characteristics of this approach are currently under evaluation.

8.2.2 Simultaneous HC-DEA construction

A limitation found in this work consists of the time to fabricate each multilayer HC-DEA. Currently, it takes around four hours to prepare eight triple layer actuators. For each actuator, six elastomer membranes have to be stretched to the correct pre-strain amount. To these means, a process has been developed that allows multiple actuators to be formed simultaneously. In the current prototype version of the system, a specialised frame system allows for the fabrication of four triple layer actuators with only six pre-stretched membranes. Significantly reducing manufacture time.

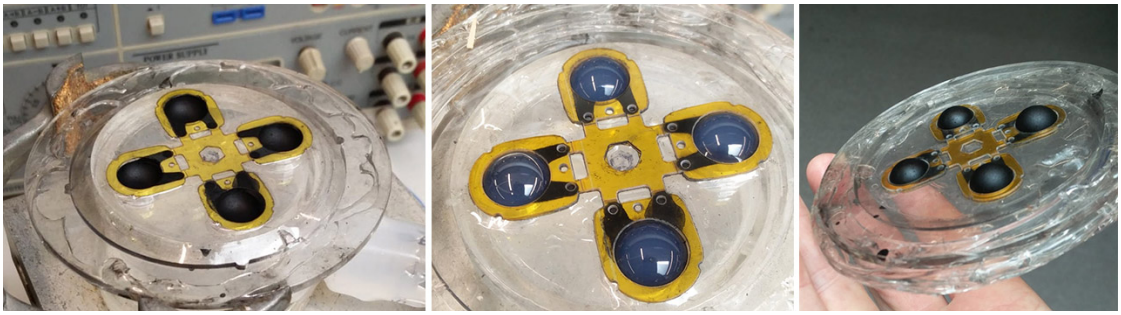

Figure 8-1 Fabrication of multiple actuators simultaneously using a modified vacuum chamber (left) and modified support frames.

8.2.3 Dense arrays of HC-DEA

HC-DEAs have been identified as possible candidates for Braille displays (Runyan and Carpi, 2011). To these means there have been a number of designs presented that show that it possible to create dense arrays of DEAs for tactile actuation purposes (Choon Koo et al., 2008; Koo et al., 2006; Lee et al., 2004). But so far none of these approaches has been demonstrated in VR/AR scenarios. To these means, a prototype dense array of HC-DEAs has been developed based upon the method developed in this thesis to create four individually controllable HC-DEA driven tactors. Each actuator has a 4mm diameter with a separation of 1mm arranged in a square configuration. The actuation stroke of each tactor is ~2mm, and the device fits within a width of 16mm. Further investigation into the mechanical and psychophysical performance of the device is currently being conducted, as well as adaption into a wearable system.

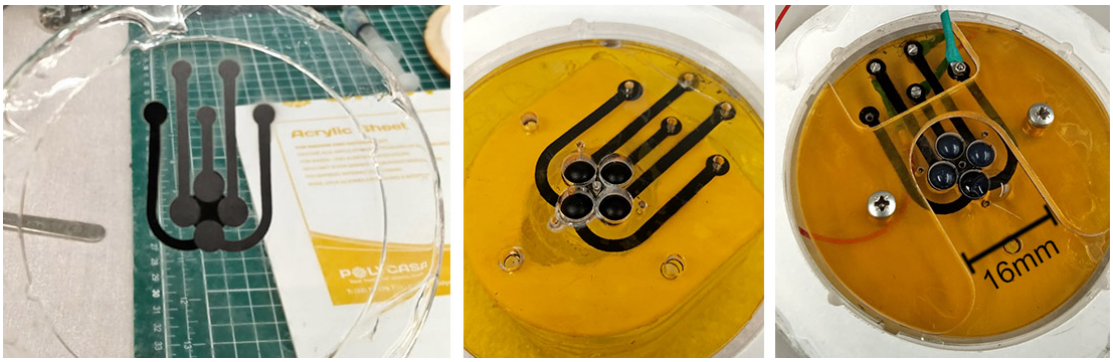

Figure 8-2 Left, an electrode pattern for a denser array of individually controllable 4mm HC-DEAs. Middle, shows the cavity formation process similar to the method presented in this work. Right, final configuration.

8.2.4 Multiplexing of HV driving signals

As discussed in the conclusion of chapter 4, being able to multiplex a single low-to-high voltage converter could dramatically decrease the cost of the system. One such

method to do this is multiplex the HV supply with the use of low-cost HV transistors. To these means, initial experiments with IXTF02N450 (IXYS, USA) HV transistor have shown that gates can be driven using an unmodified 5v 490 Hz PWM signal from an Arduino microcontroller.

Such an approach could also have a significant effect on the power consumption of the device. The low-to-high voltage converting unit used in this work can consume a maximum of 4A at 5V, leading to a maximal power consumption of 2W. Considering the output HV signal is at maximum 5kV at 100μA, corresponding to 0.5W output, the converting unit only has a power conversion rate of 25% when driven by the maximum voltage. Therefore, the use of multiple low-to-high voltage units could compound the power loss.

8.2.5 Integration with VR/AR software development environments

Once a robust consistently performing display has been constructed, ideally able to perform over a million plus actuation cycles. It should be possible to create a development pack that allows for the developers and researchers to explore the use of soft tactile displays within different contexts. To these means, work is being conducted to create a plugin for a prominent VR/AR software development platform called Unity ("Unity," 2018). This should enable rapid development of software that can be integrated with the soft tactile display system proposed in this work.

9 References

Anderson, I.A., Gisby, T.A., McKay, T.G., O'Brien, B.M., Calius, E.P., 2012. Multi-functional dielectric elastomer artificial muscles for soft and smart machines. Journal of Applied Physics 112, 041101. https://doi.org/10.1063/1.4740023

Araromi, O.A., Conn, A.T., Ling, C.S., Rossiter, J.M., Vaidyanathan, R., Burgess, S.C., 2011. Spray deposited multilayered dielectric elastomer actuators. Sensors and Actuators A: Physical, Solid-State Sensors, Actuators and Microsystems Workshop 167, pp. 459–467. https://doi.org/10.1016/j.sna.2011.03.004

Arduino - ArduinoBoardUno [WWW Document], 2018 URL https://www.arduino.cc/en/Main/arduinoBoardUno (accessed 2.23.17).

Arduino Micro [WWW Document], 2018 URL https://store.arduino.cc/arduino-micro (accessed 9.30.17).

ATmega328 - Microcontrollers and Processors [WWW Document], 2018 URL http://www.microchip.com/wwwproducts/en/ATmega328 (accessed 2.23.17).

ATmega328P - 8-bit AVR Microcontrollers - Microcontrollers and Processors [WWW Document], 2018 URL http://www.microchip.com/wwwproducts/en/atmega328p#datasheet-toggle (accessed 4.12.18).

B. Färber., F., F.K., 2006. Compliance discrimination of deformable objects by squeezing with one and two fingers. EuroHaptics.

Bach-Y-Rita, P., Collins, C.C., Saunders, F.A., White, B., Scadden, L., 1969. Vision Substitution by Tactile Image Projection. Nature 221, pp. 963–964. https://doi.org/10.1038/221963a0

Bach-y-Rita, P., Kaczmarek, K.A., Tyler, M.E., Garcia-Lara, J., 1998. Form perception with a 49-point electrotactile stimulus array on the tongue: a technical note. J Rehabil Res Dev 35, pp. 427–430.

Banggood.com, 2018. DC 3.7-6V To 400KV Boost Step Up Power Module High Voltage Generator [WWW Document]. www.banggood.com. URL https://www.banggood.com/DC-3_7V-6V-To-400KV-Boost-Step-Up-Power-Module-High-Voltage-Generator-p-915426.html (accessed 4.15.18).

Bial, D., Kern, D., Alt, F., Schmidt, A., 2011. Enhancing Outdoor Navigation Systems Through Vibrotactile Feedback, in: CHI '11 Extended Abstracts on Human Factors in Computing Systems, CHI EA '11. ACM, New York, NY, USA, pp. 1273–1278. https://doi.org/10.1145/1979742.1979760

Blum, M., Büeler, M., Grätzel, C., Giger, J., Aschwanden, M., 2012. Optotune focus tunable lenses and laser speckle reduction based on electroactive polymers, in: MOEMS and Miniaturized Systems XI. Presented at the MOEMS and Miniaturized Systems XI, International Society for Optics and Photonics, pp. 207. https://doi.org/10.1117/12.902631

Brewer, B.R., Fagan, M., Klatzky, R.L., Matsuoka, Y., 2005. Perceptual limits for a robotic rehabilitation environment using visual feedback distortion. IEEE Transactions on Neural Systems and Rehabilitation Engineering 13, pp. 1–11. https://doi.org/10.1109/TNSRE.2005.843443

Brochu, P., Pei, Q., 2010. Advances in dielectric elastomers for actuators and artificial muscles. Macromol Rapid Commun 31, pp. 10–36. https://doi.org/10.1002/marc.200900425

Carpi, F., Anderson, I., Bauer, S., Frediani, G., Gallone, G., Massimiliano Gei, Graaf, C., Jean-Mistral, C., Kaal, W., Kofod, G., Kollosche, M., Roy Kornbluh,

Lassen, B., Matysek, M., Michel, S., Nowak, S., O'Brien, B., Pei, Q., Ron Pelrine, Rechenbach, B., Rosset, S., Shea, H., 2015. Standards for dielectric elastomer transducers. Smart Mater. Struct. 24, 105025. https://doi.org/10.1088/0964-1726/24/10/105025

Carpi, F., De Rossi, D., Kornbluh, R., Pelrine, R., Sommer-Larsen, P., 2008. Fundamentals, Materials, Devices, Models and Applications of an Emerging Electroactive Polymer Technology, in: Dielectric Elastomers as Electromechanical Transducers. Elsevier, Amsterdam, pp. ix. https://doi.org/10.1016/B978-0-08-047488-5.00033-2

Carpi, Federico, Frediani, G., De Rossi, D., 2012. Bioinspired Tunable Lens Driven by Electroactive Polymer Artificial Muscles, in: Prescott, T.J., Lepora, N.F., Mura, A., Verschure, P.F.M.J. (Eds.), Biomimetic and Biohybrid Systems, Lecture Notes in Computer Science. Springer Berlin Heidelberg, pp. 74–82.

Carpi, F., Frediani, G., Rossi, D.D., 2012. Contractile Hydrostatically Coupled Dielectric Elastomer Actuators. IEEE/ASME Transactions on Mechatronics 17, pp. 987–994. https://doi.org/10.1109/TMECH.2011.2141145

Carpi, F., Frediani, G., Rossi, D.D., 2010. Hydrostatically Coupled Dielectric Elastomer Actuators. IEEE/ASME Transactions on Mechatronics 15, pp. 308–315. https://doi.org/10.1109/TMECH.2009.2021651

Carpi, F., Salaris, C., Rossi, D.D., 2007. Folded dielectric elastomer actuators. Smart Mater. Struct. 16, S300. https://doi.org/10.1088/0964-1726/16/2/S15

Cheng, L.-T., Kazman, R., Robinson, J., 1996. Vibrotactile Feedback in Delicate Virtual Reality Operations, in: Proceedings of the Fourth ACM International Conference on Multimedia, MULTIMEDIA '96. ACM, New York, NY, USA, pp. 243–251. https://doi.org/10.1145/244130.244220

Chinello, F., Malvezzi, M., Pacchierotti, C., Prattichizzo, D., 2015. Design and development of a 3RRS wearable fingertip cutaneous device, in: 2015 IEEE International Conference on Advanced Intelligent Mechatronics (AIM). Presented at the 2015 IEEE International Conference on Advanced Intelligent Mechatronics (AIM), pp. 293–298. https://doi.org/10.1109/AIM.2015.7222547

Choi, H.R., Jung, K., Chuc, N.H., Jung, M., Koo, I., Koo, J., Lee, Joonho, Lee, Jonghoon, Nam, J., Cho, M., Lee, Y., 2005. Effects of prestrain on behavior of dielectric elastomer actuator, in: Bar-Cohen, Y. (Ed.), . Presented at the Smart Structures and Materials, San Diego, CA, pp. 283. https://doi.org/10.1117/12.599363

Choon Koo, J., Ryeol Choi, H., Jung, K., Nam, J., Lee, Y. kwan, Lee, S., 2008. Chapter 23 - A NEW BRAILLE DISPLAY SYSTEM DESIGN USING A POLYMER-BASED SOFT ACTUATOR TACTILE DISPLAY, in: Dielectric Elastomers as Electromechanical Transducers. Elsevier, Amsterdam, pp. 239–248. https://doi.org/10.1016/B978-0-08-047488-5.00023-X

Clark, F.J., Larwood, K.J., Davis, M.E., Deffenbacher, K.A., 1995. A metric for assessing acuity in positioning joints and limbs. Exp Brain Res 107, pp. 73–79.

Coles, T.R., John, N.W., Gould, D., Caldwell, D.G., 2011. Integrating Haptics with Augmented Reality in a Femoral Palpation and Needle Insertion Training Simulation. IEEE Transactions on Haptics 4, pp. 199–209. https://doi.org/10.1109/TOH.2011.32

Conn, A.T., Rossiter, J., 2012. Towards holonomic electro-elastomer actuators with six degrees of freedom. Smart Mater. Struct. 21, 035012. https://doi.org/10.1088/0964-1726/21/3/035012

Culjat, M.O., King, C.-H., Franco, M.L., Lewis, C.E., Bisley, J.W., Dutson, E.P., Grundfest, W.S., 2008. A tactile feedback system for robotic surgery. Conf Proc IEEE Eng Med Biol Soc 2008, pp. 1930–1934. https://doi.org/10.1109/IEMBS.2008.4649565

CyberGrasp [WWW Document], 2017. . CyberGlove Systems LLC. URL http://www.cyberglovesystems.com/cybergrasp/ (accessed 2.23.17).

CyberTouch [WWW Document], 2017. . CyberGlove Systems LLC. URL http://www.cyberglovesystems.com/cybertouch/ (accessed 2.23.17).

da Vinci Surgery - Minimally Invasive Robotic Surgery with the da Vinci Surgical System [WWW Document], 2018 URL http://www.davincisurgery.com/da-vinci-surgery/da-vinci-surgical-system/ (accessed 4.11.18).

Dexta Robotics [WWW Document], 2017. URL http://www.dextarobotics.com/ (accessed 2.23.17).

Di Luca, M., 2011. Perceived compliance in a pinch. Vision Res. 51, pp. 961–967. https://doi.org/10.1016/j.visres.2011.02.021

Erp, J.B.F. van, Dobbelsteen, J.J. van den, 1998. On the Design of Tactile Displays. TNO Human Factors.

Faimagne, J., 1986. Psychophysical measurements and theory, in: Handbook of Perception and Human Performance. Handbook of Perception and Human Performance.

Fan, R.E., Wottawa, C., Mulgaonkar, A., Boryk, R.J., Sander, T.C., Wyatt, M.P., Dutson, E., Grundfest, W.S., Culjat, M.O., 2009. Pilot testing of a haptic feedback rehabilitation system on a lower-limb amputee, in: 2009 ICME International Conference on Complex Medical Engineering. Presented at the 2009 ICME International Conference on Complex Medical Engineering, pp. 1–4. https://doi.org/10.1109/ICCME.2009.4906637

Fasolt, B., Hodgins, M., Rizzello, G., Seelecke, S., 2017. Effect of screen printing parameters on sensor and actuator performance of dielectric elastomer (DE) membranes. Sensors and Actuators A: Physical 265, pp. 10–19. https://doi.org/10.1016/j.sna.2017.08.028

Fechner, G., 1860. Elemente der Psychophysik. Breitkopf und Hrtel.

firmata/arduino [WWW Document], 2018 . GitHub. URL https://github.com/firmata/arduino (accessed 9.30.17).

Force Dimension [WWW Document], 2018. URL http://www.forcedimension.com/products/omega-7/overview (accessed 8.31.18).

Frediani, G., Boys, H., Poslad, S., Carpi, F., 2016. Enabling Wearable Soft Tactile Displays with Electroactive Smart Elastomers, in: Haptics: Perception, Devices, Control, and Applications. Presented at the International Conference on Human Haptic Sensing and Touch Enabled Computer Applications, Springer, Cham, pp. 326–334. https://doi.org/10.1007/978-3-319-42324-1_32

Frediani, G., Mazzei, D., Rossi, D.E.D., Carpi, F., 2014. Wearable Wireless Tactile Display for Virtual Interactions with Soft Bodies. Frontiers in Bioengineering and Biotechnology 2. https://doi.org/10.3389/fbioe.2014.00031

Gabardi, M., Solazzi, M., Leonardis, D., Frisoli, A., 2016. A new wearable fingertip haptic interface for the rendering of virtual shapes and surface features, in: 2016 IEEE Haptics Symposium (HAPTICS). Presented at the 2016 IEEE

Haptics Symposium (HAPTICS), pp. 140–146. https://doi.org/10.1109/HAPTICS.2016.7463168
Genecov, A.M., Stanley, A.A., Okamura, A.M., 2014. Perception of a Haptic Jamming display: Just noticeable differences in stiffness and geometry, in: 2014 IEEE Haptics Symposium (HAPTICS). Presented at the 2014 IEEE Haptics Symposium (HAPTICS), pp. 333–338. https://doi.org/10.1109/HAPTICS.2014.6775477
Geomagic Touch [WWW Document], 2017. URL http://www.geomagic.com/en/products/phantom-omni/overview (accessed 2.23.17).
Ghilardi, M., Busfield, J.J.C., Carpi, F., 2017. Electrical breakdown detection system for dielectric elastomer actuators, in: Bar-Cohen, Y. (Ed.). pp. 101632B. https://doi.org/10.1117/12.2258617
Giousouf, M., Kovacs, G., 2013. Dielectric elastomer actuators used for pneumatic valve technology. Smart Mater. Struct. 22, 104010. https://doi.org/10.1088/0964-1726/22/10/104010
Guna, J., Jakus, G., Pogačnik, M., Tomažič, S., Sodnik, J., 2014. An analysis of the precision and reliability of the leap motion sensor and its suitability for static and dynamic tracking. Sensors (Basel) 14, pp. 3702–3720. https://doi.org/10.3390/s140203702
Hale, K.S., Stanney, K.M., 2004. Deriving haptic design guidelines from human physiological, psychophysical, and neurological foundations. IEEE Computer Graphics and Applications 24, pp. 33–39. https://doi.org/10.1109/MCG.2004.1274059
HaptX | Haptic gloves for VR training, simulation, and design [WWW Document], 2018 URL https://haptx.com/ (accessed 9.12.18).
Huang, J., Li, T., Chiang Foo, C., Zhu, J., Clarke, D.R., Suo, Z., 2012. Giant, voltage-actuated deformation of a dielectric elastomer under dead load. Appl. Phys. Lett. 100, 041911. https://doi.org/10.1063/1.3680591
Hurmuzlu, Y., Ephanov, A., Stoianovici, D., 1998. Effect of a Pneumatically Driven Haptic Interface on the Perceptional Capabilities of Human Operators. Presence: Teleoper. Virtual Environ. 7, pp. 290–307. https://doi.org/10.1162/105474698565721
Hwang, D., Lee, J., Kim, K., 2017. On the design of a miniature haptic ring for cutaneous force feedback using shape memory alloy actuators. Smart Mater. Struct. 26, 105002. https://doi.org/10.1088/1361-665X/aa860d
Hyun, W.J., Secor, E.B., Hersam, M.C., Frisbie, C.D., Francis, L.F., 2015. High-Resolution Patterning of Graphene by Screen Printing with a Silicon Stencil for Highly Flexible Printed Electronics. Advanced Materials 27, pp. 109–115. https://doi.org/10.1002/adma.201404133
IXTF02N450 IXYS [WWW Document], 2018. Mouser Electronics. URL https://eu.mouser.com/ProductDetail/747-IXTF02N450 (accessed 4.15.18).
Jaaoh, D., Jarawae, R., Intan, M., Chaidana, H., 2018. Electrostriction of Dielectric Elastomer Based on Natural Rubber/Graphene Composites for Actuator Applications [WWW Document]. Applied Mechanics and Materials. https://doi.org/10.4028/www.scientific.net/AMM.879.32
Jia, Z., Li, J., Chen, C., 2015. Design and Evaluation of a Thermal Tactile Display for Colour Rendering. International Journal of Advanced Robotic Systems pp. 12, 162. https://doi.org/10.5772/61741

Johansson, R.S., 1978. Tactile sensibility in the human hand: receptive field characteristics of mechanoreceptive units in the glabrous skin area. J Physiol 281, pp. 101–125.
Johansson, R.S., Birznieks, I., 2004. First spikes in ensembles of human tactile afferents code complex spatial fingertip events. Nature Neuroscience 7, pp. 170–177. https://doi.org/10.1038/nn1177
Johansson, R.S., Vallbo, Å.B., 1983. Tactile sensory coding in the glabrous skin of the human hand. Trends in Neurosciences 6, pp. 27–32. https://doi.org/10.1016/0166-2236(83)90011-5
Jones, L.A., 2000. Kinesthetic Sensing. Human and Machine Haptics, MIT Press.
Jones, L.A., Lederman, S.J., 2006. Active Haptic Sensing. Oxford University Press.
Kaczmarek, K.A., Webster, J.G., Bach-y-Rita, P., Tompkins, W.J., 1991. Electrotactile and vibrotactile displays for sensory substitution systems. IEEE Trans Biomed Eng 38, pp. 1–16. https://doi.org/10.1109/10.68204
Kawasaki, H., Koide, S., Mouri, T., Endo, T., 2010. Finger pad force display for hand haptic interface, in: 2010 IEEE International Conference on Automation Science and Engineering. Presented at the 2010 IEEE International Conference on Automation Science and Engineering, pp. 374–379. https://doi.org/10.1109/COASE.2010.5584147
Kim, M., Jang, I., Lee, Y., Lee, Y., Lee, D., 2016. Wearable 3-DOF cutaneous haptic device with integrated IMU-based finger tracking, in: 2016 13th International Conference on Ubiquitous Robots and Ambient Intelligence (URAI). Presented at the 2016 13th International Conference on Ubiquitous Robots and Ambient Intelligence (URAI), pp. 649–649. https://doi.org/10.1109/URAI.2016.7733974
Kim, M., Jeon, C., Kim, J., 2017. A Study on Immersion and Presence of a Portable Hand Haptic System for Immersive Virtual Reality. Sensors (Basel) 17. https://doi.org/10.3390/s17051141
Kim, Y., Oakley, I., Ryu, J., 2006. Design and Psychophysical Evaluation of Pneumatic Tactile Display, in: 2006 SICE-ICASE International Joint Conference. Presented at the 2006 SICE-ICASE International Joint Conference, pp. 1933–1938. https://doi.org/10.1109/SICE.2006.315347
Knoop, E., Rossiter, J., 2015. A compliant soft-actuator laterotactile display. Smart Mater. Struct. 24, pp. 34-45. https://doi.org/10.1088/0964-1726/24/4/045034
Koçak, U., Palmerius, K.L., Forsell, C., Ynnerman, A., Cooper, M., 2011. Analysis of the JND of Stiffness in Three Modes of Comparison, in: Haptic and Audio Interaction Design, Lecture Notes in Computer Science. Presented at the International Workshop on Haptic and Audio Interaction Design, Springer, Berlin, Heidelberg, pp. 22–31. https://doi.org/10.1007/978-3-642-22950-3_3
Kofod, G., Sommer-Larsen, P., Kornbluh, R., Pelrine, R., 2003. Actuation Response of Polyacrylate Dielectric Elastomers. Journal of Intelligent Material Systems and Structures 14, pp. 787–793. https://doi.org/10.1177/104538903039260
Koh, S.J.A., Li, T., Zhou, J., Zhao, X., Hong, W., Zhu, J., Suo, Z., 2011a. Mechanisms of large actuation strain in dielectric elastomers. Journal of Polymer Science Part B: Polymer Physics 49, pp. 504–515. https://doi.org/10.1002/polb.22223
Koh, S.J.A., Li, T., Zhou, J., Zhao, X., Hong, W., Zhu, J., Suo, Z., 2011b. Mechanisms of large actuation strain in dielectric elastomers. J. Polym. Sci. B Polym. Phys. 49, pp. 504–515. https://doi.org/10.1002/polb.22223

Kong, K.W., Lau, W.M., Wong, K.S., Chan, H.Y., Lee, F.C.S., Shen, J., Wong, V.T.C.W., Li, W.J., 2016. A pulse-sensing robotic hand for tactile arterial palpation, in: 2016 IEEE International Conference on Cyber Technology in Automation, Control, and Intelligent Systems (CYBER). Presented at the 2016 IEEE International Conference on Cyber Technology in Automation, Control, and Intelligent Systems (CYBER), pp. 141–145. https://doi.org/10.1109/CYBER.2016.7574811

Koo, I., Jung, K., Koo, J., Nam, J., Lee, Y., Choi, H.R., 2006. Wearable tactile display based on soft actuator, in: Proceedings 2006 IEEE International Conference on Robotics and Automation, 2006. ICRA 2006. Presented at the Proceedings 2006 IEEE International Conference on Robotics and Automation, 2006. ICRA 2006., pp. 2220–2225. https://doi.org/10.1109/ROBOT.2006.1642033

Koo, I.M., Jung, K., Koo, J.C., Nam, J.D., Lee, Y.K., Choi, H.R., 2008. Development of Soft-Actuator-Based Wearable Tactile Display. IEEE Transactions on Robotics 24, pp. 549–558. https://doi.org/10.1109/TRO.2008.921561

Kornbluh, R.D., Pelrine, R., Pei, Q., Heydt, R., Stanford, S., Oh, S., Eckerle, J., 2002. Electroelastomers: applications of dielectric elastomer transducers for actuation, generation, and smart structures, in: McGowan, A.-M.R. (Ed.). pp. 254–270. https://doi.org/10.1117/12.475072

Kornbluh, R.D., Pelrine, R., Pei, Q., Oh, S., Joseph, J., 2000. Ultrahigh strain response of field-actuated elastomeric polymers, in: Smart Structures and Materials 2000: Electroactive Polymer Actuators and Devices (EAPAD). Presented at the Smart Structures and Materials 2000: Electroactive Polymer Actuators and Devices (EAPAD), International Society for Optics and Photonics, pp. 51–65. https://doi.org/10.1117/12.387763

Kovacs, G., Düring, L., 2009. Contractive tension force stack actuator based on soft dielectric EAP, in: Bar-Cohen, Y., Wallmersperger, T. (Eds.). Presented at the SPIE Smart Structures and Materials + Nondestructive Evaluation and Health Monitoring, San Diego, California, USA, p. 72870A. https://doi.org/10.1117/12.815195

Kovacs, G., Lochmatter, P., Wissler, M., 2007. An arm wrestling robot driven by dielectric elastomer actuators. Smart Mater. Struct. 16, S306. https://doi.org/10.1088/0964-1726/16/2/S16

Lau, G.-K., Goh, S.C.-K., Shiau, L.-L., 2011. Dielectric elastomer unimorph using flexible electrodes of electrolessly deposited (ELD) silver. Sensors and Actuators A: Physical 169, 234–241. https://doi.org/10.1016/j.sna.2011.04.037

Leap Motion [WWW Document], 2017. . Leap Motion. URL http://leapmotion.com/ (accessed 2.23.17).

Lee, Sangwon, Jung, K., Koo, J., Lee, Sungil, Choi, Hoogon, Jeon, J., Nam, J., Choi, Hyoukryeol, 2004. Braille display device using soft actuator, in: Smart Structures and Materials 2004: Electroactive Polymer Actuators and Devices (EAPAD). Presented at the Smart Structures and Materials 2004: Electroactive Polymer Actuators and Devices (EAPAD), International Society for Optics and Photonics, pp. 368–380. https://doi.org/10.1117/12.539739

Li, M., Luo, S., Seneviratne, L.D., Nanayakkara, T., Althoefer, K., Dasgupta, P., 2013. Haptics for Multi-fingered Palpation, in: 2013 IEEE International Conference on Systems, Man, and Cybernetics. Presented at the 2013 IEEE International Conference on Systems, Man, and Cybernetics, pp. 4184–4189. https://doi.org/10.1109/SMC.2013.713

Liu, L., Chen, H., Sheng, J., Zhang, J., Wang, Y., Jia, S., 2014. Experimental study on the dynamic response of in-plane deformation of dielectric elastomer under alternating electric load. Smart Materials and Structures 23, pp. 25-37.

Maffli, L., Rosset, S., Ghilardi, M., Carpi, F., Shea, H., 2015. Ultrafast All-Polymer Electrically Tunable Silicone Lenses. Advanced Functional Materials 25, pp. 1656–1665. https://doi.org/10.1002/adfm.201403942

Massie, T.H., Salisbury, J.K., 1994. The PHANToM haptic interface: A device for probing virtual objects, in: Proceedings of the ASME Dynamic Systems and Control Division. pp. 295–301.

Matysek, M., Lotz, P., Winterstein, T., Schlaak, H.F., 2009. Dielectric elastomer actuators for tactile displays, in: World Haptics 2009 - Third Joint EuroHaptics Conference and Symposium on Haptic Interfaces for Virtual Environment and Teleoperator Systems. Presented at the World Haptics 2009 - Third Joint EuroHaptics conference and Symposium on Haptic Interfaces for Virtual Environment and Teleoperator Systems, pp. 290–295. https://doi.org/10.1109/WHC.2009.4810822

Mazzoni, A., Bryan-Kinns, N., 2016. Mood Glove: A haptic wearable prototype system to enhance mood music in film. Entertainment Computing 17, pp. 9–17. https://doi.org/10.1016/j.entcom.2016.06.002

Michel, S., Zhang, X.Q., Wissler, M., Löwe, C., Kovacs, G., 2010. A comparison between silicone and acrylic elastomers as dielectric materials in electroactive polymer actuators. Polymer International 59, pp. 391–399. https://doi.org/10.1002/pi.2751

Minamizawa, K., Fukamachi, S., Kajimoto, H., Kawakami, N., Tachi, S., 2007. Gravity Grabber: Wearable Haptic Display to Present Virtual Mass Sensation, in: ACM SIGGRAPH 2007 Emerging Technologies, SIGGRAPH '07. ACM, New York, NY, USA. https://doi.org/10.1145/1278280.1278289

Moy, G., Wagner, C., Fearing, R.S., 2000. A compliant tactile display for teletaction, in: Proceedings 2000 ICRA. Millennium Conference. IEEE International Conference on Robotics and Automation. Symposia Proceedings (Cat. No.00CH37065). Presented at the Proceedings 2000 ICRA. Millennium Conference. IEEE International Conference on Robotics and Automation. Symposia Proceedings (Cat. No.00CH37065), pp. 3409–3415 vol.4. https://doi.org/10.1109/ROBOT.2000.845247

Murray, A.M., Klatzky, R.L., Khosla, P.K., 2003. Psychophysical Characterization and Testbed Validation of a Wearable Vibrotactile Glove for Telemanipulation. Presence 12, pp. 156–182. https://doi.org/10.1162/105474603321640923

Niechwiej-Szwedo, E., Gonzalez, D., Nouredanesh, M., Tung, J., 2018. Evaluation of the Leap Motion Controller during the performance of visually-guided upper limb movements. PLoS One 13. https://doi.org/10.1371/journal.pone.0193639

Ninomiya, T., Osawa, K., Okayama, Y., Matsumoto, Y., Miki, N., 2009. MEMS Tactile Display with Hydraulic Displacement Amplification Mechanism, in: 2009 IEEE 22nd International Conference on Micro Electro Mechanical Systems. Presented at the 2009 IEEE 22nd International Conference on Micro Electro Mechanical Systems, pp. 467–470. https://doi.org/10.1109/MEMSYS.2009.4805420

O'Brien, B., Thode, J., Anderson, I., Calius, E., Haemmerle, E., Xie, S., 2007. Integrated extension sensor based on resistance and voltage measurement for a dielectric elastomer, in: Bar-Cohen, Y. (Ed.), . Presented at the 14th

International Symposium on: Smart Structures and Materials & Nondestructive Evaluation and Health Monitoring, San Diego, California, p. 652415. https://doi.org/10.1117/12.715823

Okazaki, S., Muraoka, Y., Suzuki, R., 2017. Validity and reliability of Leap Motion Controller for assessing grasping and releasing finger movements. Journal of Ergonomic Technology 17, pp. 32–42.

Pacchierotti, C., Sinclair, S., Solazzi, M., Frisoli, A., Hayward, V., Prattichizzo, D., 2017. Wearable Haptic Systems for the Fingertip and the Hand: Taxonomy, Review, and Perspectives. IEEE Transactions on Haptics PP. 1–1. https://doi.org/10.1109/TOH.2017.2689006

Palakodeti, R., Kessler, M.R., 2006. Influence of frequency and prestrain on the mechanical efficiency of dielectric electroactive polymer actuators. Materials Letters 60, 3437–3440. https://doi.org/10.1016/j.matlet.2006.03.053

Pei, Q., Rosenthal, M.A., Pelrine, R., Stanford, S., Kornbluh, R.D., 2003. Multifunctional electroelastomer roll actuators and their application for biomimetic walking robots, in: Bar-Cohen, Y. (Ed.), . Presented at the Smart Structures and Materials, San Diego, CA, pp. 281. https://doi.org/10.1117/12.484392

Pelrine, R., Kornbluh, R., 2008. Chapter 1 - ELECTROMECHANICAL TRANSDUCTION EFFECTS IN DIELECTRIC ELASTOMERS: ACTUATION, SENSING, STIFFNESS MODULATION AND ELECTRIC ENERGY GENERATION, in: Dielectric Elastomers as Electromechanical Transducers. Elsevier, Amsterdam, pp. 3–12. https://doi.org/10.1016/B978-0-08-047488-5.00001-0

Pelrine, R., Kornbluh, R., Joseph, J., Heydt, R., Pei, Q., Chiba, S., 2000a. High-field deformation of elastomeric dielectrics for actuators. Materials Science and Engineering: C 11, 89–100. https://doi.org/10.1016/S0928-4931(00)00128-4

Pelrine, R., Kornbluh, R., Pei, Q., Joseph, J., 2000b. High-Speed Electrically Actuated Elastomers with Strain Greater Than 100%. Science 287, pp. 836–839. https://doi.org/10.1126/science.287.5454.836

Pelrine, R.E., Kornbluh, R.D., Joseph, J.P., 1998. Electrostriction of polymer dielectrics with compliant electrodes as a means of actuation. Sensors and Actuators A: Physical, Tenth IEEE International Workshop on Micro Electro Mechanical Systems 64, pp. 77–85. https://doi.org/10.1016/S0924-4247(97)01657-9

Plante, J.-S., Dubowsky, S., 2006. Large-scale failure modes of dielectric elastomer actuators. International Journal of Solids and Structures 43, pp. 7727–7751. https://doi.org/10.1016/j.ijsolstr.2006.03.026

Poulin, A., Rosset, S., Shea, H.R., 2015. Printing low-voltage dielectric elastomer actuators. Appl. Phys. Lett. 107, 244104. https://doi.org/10.1063/1.4937735

Processing.org [WWW Document], 2017. URL https://processing.org/ (accessed 9.30.17).

Raitor, M., Walker, J.M., Okamura, A.M., Culbertson, H., 2017. WRAP: Wearable, restricted-aperture pneumatics for haptic guidance, in: 2017 IEEE International Conference on Robotics and Automation (ICRA). Presented at the 2017 IEEE International Conference on Robotics and Automation (ICRA), pp. 427–432. https://doi.org/10.1109/ICRA.2017.7989055

Ramsamy, P., Haffegee, A., Jamieson, R., Alexandrov, V., 2006. Using Haptics to Improve Immersion in Virtual Environments, in: Alexandrov, V.N., van Albada, G.D., Sloot, P.M.A., Dongarra, J. (Eds.), Computational Science –

ICCS 2006, Lecture Notes in Computer Science. Springer Berlin Heidelberg, pp. 603–609.
Rosset, S., Shea, H.R., 2013. Flexible and stretchable electrodes for dielectric elastomer actuators. Appl. Phys. A 110, pp. 281–307. https://doi.org/10.1007/s00339-012-7402-8
Runyan, N.H., Carpi, F., 2011. Seeking the “holy Braille” display: might electromechanically active polymers be the solution? Expert Rev Med Devices 8, 529–532. https://doi.org/10.1586/erd.11.47
Saint-Aubin, C.A. de, Rosset, S., Schlatter, S., Shea, H., 2018. High-cycle electromechanical aging of dielectric elastomer actuators with carbon-based electrodes. Smart Mater. Struct. 27, 074002. https://doi.org/10.1088/1361-665X/aa9f45
Salisbury, K., Conti, F., Barbagli, F., 2004. Haptic rendering: introductory concepts. IEEE Computer Graphics and Applications 24, pp. 24–32. https://doi.org/10.1109/MCG.2004.1274058
Sarakoglou, I., Garcia-Hernandez, N., Tsagarakis, N.G., Caldwell, D.G., 2012. A High Performance Tactile Feedback Display and Its Integration in Teleoperation. IEEE Transactions on Haptics 5, pp. 252–263. https://doi.org/10.1109/TOH.2012.20
Scilingo, E.P., Bianchi, M., Grioli, G., Bicchi, A., 2010. Rendering Softness: Integration of Kinesthetic and Cutaneous Information in a Haptic Device. IEEE Transactions on Haptics 3, pp. 109–118. https://doi.org/10.1109/TOH.2010.2
Sonar, H.A., Paik, J., 2016. Soft Pneumatic Actuator Skin with Piezoelectric Sensors for Vibrotactile Feedback. Front. Robot. AI 2. https://doi.org/10.3389/frobt.2015.00038
Summary of MIDI Messages [WWW Document], 2018 URL https://www.midi.org/specifications/item/table-1-summary-of-midi-message (accessed 4.12.18).
Tan, H.Z., Eberman, B., Srinivasan, M.A., Cheng, B., 1994. Human Factors for the Design of Force-reflecting Haptic Interfaces.
Tsetserukou, D., Hosokawa, S., Terashima, K., 2014. LinkTouch: A wearable haptic device with five-bar linkage mechanism for presentation of two-DOF force feedback at the fingerpad, in: 2014 IEEE Haptics Symposium (HAPTICS). Presented at the 2014 IEEE Haptics Symposium (HAPTICS), pp. 307–312. https://doi.org/10.1109/HAPTICS.2014.6775473
Uchiyama, H., Covington, M.A., Potter, W.D., 2008. Vibrotactile Glove Guidance for Semi-autonomous Wheelchair Operations, in: Proceedings of the 46th Annual Southeast Regional Conference on XX, ACM-SE 46. ACM, New York, NY, USA, pp. 336–339. https://doi.org/10.1145/1593105.1593195
Unity [WWW Document], 2018. . Unity. URL https://unity3d.com (accessed 9.18.18).
Vallbo, A.B., Johansson, R.S., 1984. Properties of cutaneous mechanoreceptors in the human hand related to touch sensation. Hum Neurobiol 3, 3–14.
van Jan, B.F., 2006. The Multi-Dimensional Nature of Encoding Tactile and Haptic Interactions: From Psychophysics to Design Guidelines. Proceedings of the Human Factors and Ergonomics Society Annual Meeting 50, pp. 685–688. https://doi.org/10.1177/154193120605000515

Weichert, F., Bachmann, D., Rudak, B., Fisseler, D., 2013. Analysis of the Accuracy and Robustness of the Leap Motion Controller. Sensors (Basel) 13, 6380–6393. https://doi.org/10.3390/s130506380

Yousefzadeh, M., 2017. Modeling and simulation of the electrospinning process, in: Electrospun Nanofibers. Elsevier, pp. 277–301. https://doi.org/10.1016/B978-0-08-100907-9.00012-X

Yuan, W., Hu, L.B., Yu, Z.B., Lam, T., Biggs, J., Ha, S.M., Xi, D.J., Chen, B., Senesky, M.K., Grüner, G., Pei, Q., 2008. Fault-Tolerant Dielectric Elastomer Actuators using Single-Walled Carbon Nanotube Electrodes. Advanced Materials 20, pp. 621–625. https://doi.org/10.1002/adma.200701018

Yuan, W., Lam, T., Biggs, J., Hu, L., Yu, Z., Ha, S., Xi, D., Senesky, M.K., Grüner, G., Pei, Q., 2007. New electrode materials for dielectric elastomer actuators, in: Electroactive Polymer Actuators and Devices (EAPAD) 2007. Presented at the Electroactive Polymer Actuators and Devices (EAPAD) 2007, International Society for Optics and Photonics, p. 65240N. https://doi.org/10.1117/12.715383

Zhang, R., Kunz, A., Lochmatter, P., Kovacs, G., 2006. Dielectric Elastomer Spring Roll Actuators for a Portable Force Feedback Device, in: 2006 14th Symposium on Haptic Interfaces for Virtual Environment and Teleoperator Systems. Presented at the 2006 14th Symposium on Haptic Interfaces for Virtual Environment and Teleoperator Systems, pp. 347–353. https://doi.org/10.1109/HAPTIC.2006.1627137

Zhao, X., Suo, Z., 2010. Theory of Dielectric Elastomers Capable of Giant Deformation of Actuation. Phys. Rev. Lett. 104, 178302. https://doi.org/10.1103/PhysRevLett.104.178302

10 Appendix

10.1 Ethical approval

Queen Mary
University of London

Queen Mary, University of London
Room W117
Queen's Building
Queen Mary University of London
Mile End Road
London E1 4NS

Queen Mary Ethics of Research Committee
Hazel Covill
Research Ethics Administrator
Tel: +44 (0) 20 7882 7915
Email: h.covill@qmul.ac.uk

c/o Dr Stefan Poslad
Eng E306
Department of Electronic Engineering
Queen Mary University of London
Mile End Road
London

2nd May 2017

To Whom It May Concern:

Re: QMREC1567 – Psychophysical characterization of a wearable tactile display.

I can confirm that Hugh Boys has completed a Research Ethics Questionnaire with regard to the above research.

The result of which was the conclusion that his proposed work does not present any ethical concerns; is extremely low risk; and thus does not require the scrutiny of the full Research Ethics Committee.

Yours faithfully

Ms Hazel Covill – QMERC Administrator

Queen Mary
University of London

Information sheet

Electroactive Polymer Soft Tactile Display study: information for participants

We would like to invite you to be part of this research project, if you would like to. You should only agree to take part if you want to, it is entirely up to you. If you choose not to take part there won't be any disadvantages for you and you will hear no more about it.

Please read the following information carefully before you decide to take part; this will tell you why the research is being done and what you will be asked to do if you take part. Please ask if there is anything that is not clear or if you would like more information.

If you decide to take part you will be asked to sign the attached form to say that you agree.

You are still free to withdraw at any time and without giving a reason.

For this study, we are examining the effectiveness of a new type of tactile display. Tactile displays are devices aimed at creating touch sensations within computing environments, and we envisage that our new type of device will hopefully be used one day to simulate interactions with soft body objects for the purpose medical simulations.

But within this study, you will be asked to use the device, which will be placed upon your fingertips, to deduce between different soft touch sensations. These soft touch sensations will be created by electronically controlled soft bubble, that will move up and down to render small soft forces against the tips of your thumb and index finger.

In the first part of the test we will be trying to work out if you can discriminate between different levels force created by the bubble. The forces created by the bubble are very low, up to about one Newton (1N), or approximately the weight of one apple being place upon your fingertip. We will then move on to a test to see if you can use the device, in conjunction with an optical hand tracking device (Leap Motion), to interact with virtual objects, also displayed on a monitor, that will render varying soft forces against your thumb and index fingertip.

The study should take no longer than 15 minuets, and if at any stage of the test you feel any signs of discomfort or apprehension, you are more than welcome to discontinue the test at any time without having to give a reason.

It is up to you to decide whether or not to take part. If you do decide to take part you will be given this information sheet to keep and be asked to sign a consent form.

If you have any questions or concerns about the manner in which the study was conducted please, in the first instance, contact the researcher responsible for the study. If this is unsuccessful, or not appropriate, please contact the Secretary at the Queen Mary Ethics of Research Committee, Room W104, Queen's Building, Mile End Campus, Mile End Road, London or research-ethics@qmul.ac.uk.

Queen Mary
University of London

Consent form

Please complete this form after you have read the Information Sheet and/or listened to an explanation about the research.

Title of Study: **Electroactive Polymer Soft Tactile Display study**
Queen Mary Ethics of Research Committee Ref: **QMREC1567**

. • Thank you for considering taking part in this research. The person organizing the research must explain the project to you before you agree to take part.

. • If you have any questions arising from the Information Sheet or explanation already given to you, please ask the researcher before you decide whether to join in. You will be given a copy of this Consent Form to keep and refer to at any time.

. • *I understand that if I decide at any other time during the research that I no longer wish to participate in this project, I can notify the researchers involved and be withdrawn from it immediately.*

. • *I consent to the processing of my personal information for the purposes of this research study. I understand that such information will be treated as strictly confidential and handled in accordance with the provisions of the Data Protection Act 1998.*

Participant's Statement:

I _____ agree that the research project named above has been explained to me to my satisfaction and I agree to take part in the study. I have read both the notes written above and the Information Sheet about the project, and understand what the research study involves.

Signed: Date:

Investigator's Statement:

I Hugh Boys confirm that I have carefully explained the nature, demands and any foreseeable risks (where applicable) of the proposed research to the volunteer.